"MECHANICAL PROPERTIES OF SINTERED LOW ALLOY STEELS"

RUSSELL JOHN FARROW

A thesis submitted for the degree

MASTER OF PHILOSOPHY

THE UNIVERSITY OF ASTON IN BIRMINGHAM

OCTOBER 1981

SUMMARY

"MECHANICAL PROPERTIES OF

SINTERED LOW ALLOY STEELS"

by

Russell John Farrow

A thesis presented for the degree of Master of Philosophy, in the University of Aston in Birmingham, 1981.

Published literature relating to the mechanical properties of sintered low alloy steels, is reviewed. The relationship between processing schedule and mechanical properties, in particular, fracture toughness, of a sintered, commercially available, low alloy steel was investigated. Three sintering treatments were compared, namely :

1). Reducing atmosphere sinter in a laboratory tube furnace
2). Vacuum sinter in a laboratory furnace
3). Reducing atmosphere sinter in an industrial mesh belt furnace.

A number of test pieces were examined in the fully heat treated condition.

The application of the potential drop technique in COD testing for determining the onset of fracture in the material was investigated and was also found to be reliable for monitoring the crack length during fatigue pre-cracking of the test pieces. This enabled some fatigue data to be obtained. This data, however, proved to be of limited use due to the comparatively short length of fatigue crack produced for the subsequent fracture toughness test.

The results presented and discussed include fracture toughness and fatigue properties, tensile tests, hardness, metallography and fractography. The applicability of Linear Elastic Fracture Mechanics, and the subsequent use of the J integral concept, as a means of assessing fracture toughness is also discussed.

Fracture toughness values ranged from 14.5 to 32$MNm^{-3/2}$ which compare with the results of other workers, and, for comparison, are of the same order as published values for flake graphite cast irons. Fracture toughness was found to be directly related to yield stress. Vacuum sintering produced improved tensile properties, with a corresponding effect on fracture toughness at the higher densities only. Test procedures used by previous workers created several anomalies, and the investigation has resulted in recommendations on test procedures for sintered materials. No physico-chemical differences between laboratory and industrial reducing atmosphere sintering were revealed.

Key words : powder metallurgy, fracture mechanics, sintering, porosity.

Acknowledgements

The author would like to express his sincere thanks to Mr.L.W. Crane for his most valuable assistance in the preparation of this thesis. Thanks are also due to Professor J.T. Barnby for helpful discussion on the interpretation of results.
The author would also like to express his gratitude to the Technicians of the Department of Metallurgy and Materials for their technical advice, and to Miss. Karen Ensor for all typing.

CONTENTS

LIST OF FIGURES

LIST OF TABLES

1. INTRODUCTION

The relationships between mechanical properties, such as yield or proof stress and elongation, when dealing with conventionally processed components (cast, wrought, machined), is well understood. In the case of sintered components the mechanical properties determined in a laboratory from specially produced test pieces, may be of limited value in the design of a component, and the decision to use a sintered low alloy steel component, the subsequent design and selection of a composition and processing schedule, is still based mainly on experience. Structural peculiarities such as inherent porosity, micro-inhomogeneity and macro-density variations present in sintered low alloy steel components are the main causes of small scale i.e. laboratory investigations having a limited value, but changes in attitude are taking place. There is growing interest in relating mechanical properties to service performance, which will in turn allow more flexibility in design. The mechanical properties of most significance in the application of structural low alloy steel components are fracture toughness and fatigue resistance, but as yet little systematic work has been carried out in investigating the fracture behaviour of sintered materials.

Fracture mechanics presupposes the existance of minute cracks or defects in the majority of components, and the quantity known as fracture toughness relates these defects to the applied stresses which can cause fracture. The inherent porosity effectively contributes to the overall size and proportion of defects present in a sintered component.

These defects may be characterised by a parameter called the "stress intensity factor", denoted by the symbol K. If, under stress, a defect such as a notch or crack extended, energy would be consumed in creating the new surfaces formed and may also be

consumed in plastic deformation of the metal near the crack tip. This energy is supplied from the elastic strain energy stored in that stressed body. The energy available for propagation of the crack is proportional to the square of the stress intensity factor. If the stress at the tip of a stable crack was gradually increased, the crack would begin to propagate at a critical value of the stress intensity factor, K_c, provided the energy required was available. The magnitude of this critical stress intensity factor, K_c, represents the quantity fracture toughness, which is a material property and must be determined experimentally. The testing techniques which have been developed are based on a quantitative assessment of the conditions necessary to cause a defect to propogate, and these techniques are now well established for the determination of fracture toughness under linear elastic conditions (L.E.F.M.). In some cases however, where linear elastic behaviour is not experienced, due to effects of plasticity and crack extension preceding fracture, the application of elastic-plastic fracture mechanics (E.P.F.M.) to the analysis of fracture is required. In such cases the concept of J integral analysis is introduced, which relates the applied stress, crack length and material toughness when fracture has occured after general yielding.

Reviews on the powder metallurgy (P/M) industry have shown[1,2] that this industry has maintained a steady level of output since the early 1970's in terms of weight production of ferrous and non-ferrous parts in the United Kingdom up to 1980. The world wide decline of industrial output and the P/M industry's apparently static position can be viewed as a success for the P/M industry in the present climate. There has also been a steady decline in the United Kingdom production of motorcars, traditionally a market for P/M component manufacturers, but areas of new application have

allowed the market for P/M components to grow at a faster rate than the market for the finished commodity. With the prospect of many potential users, appraisal of acceptable stress levels and defect size is necessary and the best tool available for determining these is fracture mechanics.

The main production of ferrous structural components by P/M is well established[3], plain iron and carbon steels being widely used. The range of alloy steels which can be used in structural applications is limited by processing constraints mainly associated with sintering. The choice of alloying elements are made to take advantage of the fact that some alloying elements cause shrinkage and some expansion, to produce alloys in which the overall shrinkage/expansion of the alloying elements is balanced to retain dimensional stability during the sintering process. The large surface areas of powders cause them to be very susceptible to surface contamination, particularly oxidation, and those elements which have a high affinity for oxygen cause particular difficulty because their oxides are not readily reducible. This again limits the number of alloying elements which can be used in conventional powder metallurgy.

Alloy steels are produced by several routes which differ mainly in the type of powder used, and these are:

1). Fully pre-alloyed (atomised)

2). Elemental mixture

3). Pre-alloyed master alloy addition to iron

4). Diffusion alloyed, where, minute particles of the alloying element are diffusion bonded onto iron powder particles.

In the first method individual particles are already alloyed, while in the last three, alloying takes place by the diffusion of the alloying element into the iron particles during sintering. Thus only the fully pre-alloyed powders give a homogenous distribution of the alloying elements with practicable sintering times (considered to be up to two hours), but are not popular due to their poor compressibility. "Master alloys" are ideal for homogenisation in the sense that the particle size of alloying elements should be fine to give a large number of contact points with the iron powder, but again have poor compressibility and are mainly used for the alloying of oxidisable elements. Elemental mixes have the advantage that the composition of the mixes can be readily adjusted, they can be compacted more easily and work-harden less rapidly. However, there can be problems in ensuring homogenous distribution of the alloying elements and this is largely overcome by the use of partially pre-alloyed powders, such as diffusion alloyed powders. It has been shown[4] that the strength of a steel made from partially pre-alloyed powder is generally greater by about 100 MPa than one of identical composition made from an elemental mix, and this is attributed to a better distribution of the alloying elements, as was shown to be the case in an earlier work[5]. There is a certain amount of information available concerning the fracture toughness of plain iron and iron-carbon steels[6,7,8,9] and on certain types of pre-alloyed powder,[7,8,9,10,11,12] which in the main had been sinter forged. Thus information on a popular commercial as sintered pre-alloyed steel would be valuable.

Industrially, sintering treatments are applied in a reducing (endothermic) atmosphere in a mesh belt furnace. In laboratory work sintering is often carried out in a flow of gas in a tube furnace, offering greater control over the process. The question

then arises "are there any differences which would invalidate laboratory simulation of industrial practise?", and this question does not appear to have been answered in the literature.

Vacuum sintering is viewed as the ultimate in striving for maximum mechanical properties in a given compact, but its application is naturally very limited in industry for economic reasons, and, as yet, there is no standard vacuum sintering process. The types of vacuum furnaces used for sintering have been broadly described as 'various'[13], but vacuum technology is being increasingly applied in industry and costs are gradually reducing. Thus there is the possibility of introducing vacuum sintering into 'low-cost' processing routes, and vacuum processing of powders in current usage is worthy of examination.

2. LITERATURE REVIEW

2.1 Mechanical Properties

2.1.1 General

The mechanical properties of a sintered compact are controlled by a number of factors, the most prominent of which is the porosity. The strength of a compact will be directly related to the density and can be expected to reach a maximum at 100% of the theoretical maximum density (0% porosity) . Very high densities are of interest to the powder metallurgist involved in recently developed processes such as sinter forging or strip production from powder. The highest practical densities are therefore aimed for in the mass production of components, the first stage being to compact to as high a density as possible. Currently in industry this is about 90% of the theoretical maximum. With tooling made from tool steels wear becomes a problem and special carbide die sets are required which will increase the overall cost of a component. Commercial sintering treatments impart the required mechanical strength to a compact but only increase the density by a small amount during the short time (typically 40 minutes) at the temperatures employed. Mesh belt furnaces which are widely used for mass production are limited to about 1125°C, since the working life of the belt is drastically reduced at higher temperatures. The density and strength of a compact can be further increased by sintering at higher temperatures than normal (in the region of 1250-1300°C for ferrous based materials) and for longer times (over two hours) requiring special furnaces e.g. 'walking beam' which are expensive to install and maintain. Thus the use of these furnaces is limited by economic factors, which affect the final cost of a compact.

Post-sintering treatments such as repressing and sintering

and coining are widely practiced, coining being carried out with the principal object of improving dimensional accuracy,but again considerably adds to the cost. By incorporating in the mix a powder which has a melting point lower than the sintering temperature, liquid phase sintering is achieved. This mainly improves particle bonding but also assists densification. Another technique involves a positive attempt to fill the pores by melting and infiltrating a low melting point metal into a sintered 'skeleton' . In ferrous materials copper is used in each of these techniques, generally 1-4% powder addition for liquid phase sintering and about 15% melted solid for infiltration.

The composition and processing route of the powder, as discussed in Section 1, will also affect the strength of a compact. The matrix strength is determined by the composition, the alloying elements chosen such that they will impart the desired properties to a compact during sintering and/or subsequent heat treatment. The strength of the bonds between particles is another important feature which will affect the strength of a sintered compact. Initially bonds are formed between particles during compaction by pressure welding and these welds are consolidated and extended during sintering, unless hindered by surface contamination, in particular oxide films to which powders are very susceptible. Thus the sintering atmosphere is important and in general a reducing atmosphere is used not only to prevent oxidation of the compacts at the sintering temperatures used, but also to help break down any oxide films which may be present in the first place.

The major structural feature which influences the mechanical properties is the porosity and for this reason many workers have aimed to express the properties of sintered materials as a function

of their total porosity. Most attention has hitherto been devoted to the determination of the relationship between maximum stress, as the principal strength property, and porosity, resulting in the formulation of many equations[14-31] . A detailed discussion of the merits and limitations of the relationships introduced in the individual papers is not within the scope of the present work, but they are briefly discussed below. Overall, the data for the relationships has been obtained by differing means; some by means of test models, others by means of experimentation with real materials and a limited number of test pieces, and some have been derived theoretically. Several papers consider the occurence of stress concentrations around pores as being the basic factor, whilst others consider the shape of the pores and open as well as closed porosity. Some papers take into consideration the size distribution of pores, mean pore intercept, decrease in effective cross-section of a sample due to the pores as well as for the existence of micro-cracks within non-porous grains. Many of the equations formulated resulted in the same type of curve, which showed an exponential relationship between porosity and the property considered, but none of them encompassed all or most of the above mentioned factors. They all strived towards a better understanding of the strength contolling parameters of sintered materials and many of them reviewed previous findings with a view to checking the validity of quoted relationships. For this reason Salak et al[28] used the relationships proposed by a number of workers[14-19,21,23-26] to compute values of maximum stress , elongation and hardness using what was considered to be a large amount of data. They used mainly their own results but included evaluated properties from published literature on Hoganas sponge iron and Mannesmann atomised

iron powder and some (unspecified) individual data. They summarised that when determining the relationship between porosity and the maximum stress , elongation or hardness the influence of the origin and quality of the iron powder, the H_2-loss, select size fractions and sintering time and temperature will all be reflected in the results as a wide scatter and that only the mean values can be characterised by porosity content. This relationship between property values and porosity is well established showing the general trend of an increase in value with a decrease in porosity.

Other properties which have been related to porosity include electrical conductivity, Young's Modulus and toughness. Two well known relationships between Young' modulus and porosity are those obtained empirically by Pohl[32] and McAdam[33]. Pohl obtained the relationship:

$$E = 1 - k\varepsilon \qquad (1)$$

where E = Young's modulus, ε = fractional porosity and k is a factor which is related in some way to the stress distributions in the matrix. Despite this equation describing the experimental data reasonably, values of k have to be derived from curve fits and their precise physical meaning is obscure. The work of McAdam showed that the elasticity ratio E_n / E was related to the porosity by the expression:

$$E_n = E\,(1-\varepsilon)^{3.4} \qquad (2)$$

where E_n = elastic modulus of sintered steels and iron base alloys,

E = elastic modulus of steel and ε = fractional porosity. As with the maximum stress , the results from equations (1) and (2) show a degree of scatter and are "best fit" relationships from computed data. Leheup and Moon[34] investigated the relationship between porosity and Young's modulus, as well as toughness and electrical conductivity, and obtained scatter bands in the data which were considered to be not much wider than might be expected for individual errors of measurement, and the results were generally in accord with the results of other workers[32,33] . With reference to Young' modulus, they state that any relationship between porosity and this material property must depend on pore shape, size, spacing and orientation with respect to stress which are features not reflected in the density value.

Within any one system, relationships between porosity and a given property may be determined with the accuracy to be expected from any practical determination, and applied to that system with confidence. However, caution must be exercised when applying an expression to another system due to the influence of other factors mentioned previously, such as shape, size and distribution of pores. Many workers have obtained results which generally agree with those of others working with different materials produced under various conditions, but it would appear that to relate two properties, individual determination of each may be required in order to achieve greatest accuracy, and it cannot be assumed that one system will behave identically to another.

Comparisons have been made between the properties of P/M components and cast irons[35,36] and it is useful to discuss them here. The comparison arises from work where graphite is compared with voids in a steel matrix when investigating the internal

deformation of cast irons. For this purpose Meyersberg[37] extended the work of Thum and Ude[38,39], concluding that graphite flakes transmit no tensile stresses and were equivalent to voids, a conclusion made by Schwartz and Junge[40] on investigating the density/modulus ratio. The latter workers determined that the modulus was proportional to the volume of the metallic phase present when the matrix contained graphite in the form of approximate spheres (nodules) and that graphite in the form of flakes caused the modulus to be lower than an equivalent proportion of graphite nodules. This effect was due to the stress concentrations associated with flakes being greater than those associated with nodules, this being analogous to the increased notch effect of irregularly shaped pores over spherical pores[29].

Research was furthered by Gilbert[41,42] who examined the distribution of graphite flakes and found that the cross-section interrupted by the graphite in this form could not account for the resultant reduction in modulus. By examination of the way in which stress was transmitted through the matrix, being forced to deviate from the stress axis around the graphite flakes, it was possible to show that this was equivalent to a reduction in cross-section and as such reduced the modulus. The work also demonstrated the notch effect of graphite flakes, where plastic deformation occured at the ends of flakes due to high local stress causing deviations from linearity of the stress/strain curve, again demonstrating the similarity with sintered materials[29].

The above comparison serves as a demonstration that useful information may be gleaned from materials which behave in a similar manner to sintered materials in order to develop an understanding of the internal deformation of sintered components.

2.1.2 Distaloy SA

Comprehensive details of the properties of the powder and sintered and heat treated material properties are supplied by the manufacturer, Hoganas A.B. .

The data[43] shows, in graphical form, the effects of sintering time and temperature on the dimensional stability, ultimate tensile strength, elongation and hardness as well as the variation of these properties with density in both the as sintered and heat treated conditions.

Other workers[7,12] have investigated the mechanical properties of Distaloy SA, and a comparison between the results of these workers and the manufacturers, with respect to ultimate tensile strength and yield strength, is given below in Table 2.1 (the values are quoted at two densities, namely 6.7 and 6.9Mgm^{-3}, on the basis that these represent common densities for all three investigations):

	DENSITY Mgm^{-3}				
Source	6.7		6.9		
	YS(MPa)	MS (MPa)	YS(MPa)	MS (MPa)	
Hoganas[43]	360	490	390	560	As sintered(A/s)
	830	880	950	1000	Heat treated(H/T)
	0.5				%C
Ghosh[12]	-	427	-	471	A/s
	-	658	-	733	H/T
	0.65				%C
Andrews[7]	280	320	310	360	A/s
	400	440	440	480	H/T
	0.4				%C

Table 2.1 : Comparison of maximum stress and yield stress of Distaloy SA from various sources.

As can be seen from Table 2.1 the values quoted by Ghosh and Andrews differ from tnose of the manufacturer, Hoganas. One obvious explanation for this is the different carbon content of the alloy

used in the investigations. Increasing the carbon content of this alloy will affect the properties two ways, viz. the ferrite content is reduced and the hardness of the martensite is increased, whereas the content of martensite and bainite is only moderately affected. Another explanation is that the alloy is influenced by the cooling rate from the sintering temperature which has been shown[44] to have a decisive effect on the properties of the material. Lindskog and Thornblad[44] determined the maximum stress of Distaloy SA as a function of cooling rate between 800 and 250°C after sintering at 1120°C . The compacts had a sintered density of $6.95 Mgm^{-3}$ and a combined carbon content of 0.45% . They found that increasing the cooling rate from 0.2 degree centigrade per second to $6^{\circ}Cs^{-1}$ increased the tensile strength from 500MPa to 700MPa . It is thought likely that the combined effects of differing carbon contents and cooling rates from the sintering temperature is the cause of the large variation in the values given in Table 2.1 between the three investigators.

Investigation into the transformation characteristics of Distaloy SA has been carried out by Tunstall and Haynes[45] . They concluded that the distribution of the alloying elements, especially nickel, was very heterogeneous, causing the steel to transform in an extremely complex manner. Typical microstructures were shown indicating which areas contain the various transformation products, which were stated as being pro-eutectoid ferrite and pearlite together with a bainite-like transformation product, probably carbide-free bainite. These workers make no mention of the presence of any martensite, a transformation product indicated on the micrographs presented by Hoganas, as a light etching area with diffuse boundaries.

2.2 The Mechanics of Fracture

2.2.1 Linear Elastic Fracture Mechanics (LEFM)

Fracture mechanics pre-supposes the existance, in a material body, of a crack like defect that will lead to fracture, and theory is then used to develop parameters which characterise the crack tip stress intensity factor, K . The importance of fracture mechanics is that it enables quantitative relationships to be obtained between the applied stress which leads to failure and the size of any defect or crack which may be present in a structure or test piece. The study of fracture properties of materials was first undertaken by Griffith[46], who considered a crack of length 2a contained within a plane elastic body, of infinite width, in tension. The premise taken was that unstable crack propagation would take place if an increment of crack growth resulted in more stored energy being released than is absorbed by the formation of the new crack surface. Griffith carried out a series of experiments on hard glass and found a relationship between the fracture stress, σ_F, and crack length, a , and the resultant simple formula obtained was:

$$\sigma_F = \sqrt{\frac{2E\gamma}{\pi a}} \qquad (3)$$

where E = Young's modulus, γ = specific surface energy and a = half crack length.

This work, however, limited the application to materials where linear effects only, prior to fracture, were present. Irwin[47] and Orowan[48] suggested a modification to the Griffith fracture criteria so that limited plastic deformation prior to fracture could be accommodated by replacing the term 2γ (the surface energy) by a term γ_p which represented the energy of plastic

distortion, thus:

$$\sigma_F = \sqrt{\frac{2E(\gamma + \gamma_p)}{\pi a}} \qquad (4)$$

Since the term γ_p is of the order of three times the term γ this latter term may be negelcted:

$$\sigma_F = \sqrt{\frac{2\gamma_p E}{\pi a}} \qquad (5)$$

Irwin[49] reviewed the theories of crack tip stresses in an elastic body and by applying the analyses of Sneddon[50] and Westergaard[51] noted that the local stress distribution was always of the same form, described by:

$$\sigma_L = K/\sqrt{2\pi x} \qquad (6)$$

where K = constant determining the level of stress distribution, σ_L = local tensile stress, x = distance ahead of the crack tip, (see Figure 2.1) . In the region ahead of the crack tip the distribution is always of the same form, and thus the criterion for fracture to commence can be taken as the attainment of a sufficiently high level of stress distribution and so the constant K is defined as the stress intensity factor.

Irwin proved, by the principle of virtual work, that the attainment of a critical value of K, namely K_C , was equivalent to the Griffith approach, which required a level of a critical stored elastic strain energy, G_c, and that a relationship existed between K_C and G_c, which was:

$$K_C^2 = E'G_c \qquad (7)$$

where E' = relevant extensional modulus (equal to Young's Modulus E for plane stress and $E/1-\nu^2$ for plane strain, ν being Poisson's Ratio) .

The term G is defined as the total energy absorbed during cracking per unit increase in crack length, per unit thickness and is equivalent to 2δ when the creation of new surface energy is required at the new crack surfaces, and G_c also includes energy consumed in plastic deformation at the crack tip.

The Griffith's solution may then be rewritten:

$$\sigma_F = \sqrt{\frac{E'G_c}{\pi a}} \qquad (8)$$

and by further substitution of equation (7):

$$\sigma_F = \frac{K_C}{\sqrt{\pi a}} \qquad (9)$$

The terms G_c and K_C are material properties and represent the material's resistance to fracture at the fracture stress σ_F . Use of K_C instead of G_c to represent fracture toughness is more generally made since it allows direct comparison of the fracture resistance of different materials without having to first include the relevant values of E' .

The preceeding relationships between fracture stress and crack length take into account limited plastic deformation, as stated previously, and this plastic deformation is characterised by a plastic zone within which micro-structural damage is initiated, preparing the way for fracture. If the plastic zone size is small in comparison to the dimensions of the body, the behaviour approx-

imates to the theories of linear elastic fracture mechanics which can then be applied to design problems. Thus the size of the plastic zone is an important feature, and the radius is given by:

$$r_y = \frac{1}{2\pi} \left(\frac{K_C}{\sigma_{YS}} \right)^2 \quad \text{for plane stress} \quad (10)$$

$$\text{and } r_y = \frac{1}{4\sqrt{2\pi}} \left(\frac{K_C}{\sigma_{YS}} \right)^2 \quad \text{for plane strain} \quad (11)$$

The size of the plastic zone generated is very dependent upon the state of stress at the crack tip. In thin sheets in tension containing through cracks, the conditions are those of plane stress, where the crack tip stresses lie in the plane of the sheet and in the thickness direction stress is virtually zero. Within the plastic zone the tensile stress is the uniaxial yield stress and fracture will occur on 45° shear planes. Increases in sheet thickness give rise to tensile constraint in the thickness and width directions, Figure 2.2 . The region very close to the crack tip undergoes a large plastic stretch, the surrounding material resisting the resulting need for a Poissons contraction in the directions perpendicular to the applied stress, thus producing this tensile constraint. The resolved shear components of the local stress, σ_L , are reduced and yielding cannot take place until the local stress reaches a value of about three times the uniaxial yield stress, resulting in a smaller plastic zone size as shown in Figure 2.3. This gives rise to a flat fracture whose faces are normal to the applied stress under these plane strain conditions.

At free surfaces no constraint in the thickness direction may exist and the plastic zone size is that for plane stress, the size decreasing along 45° shear lines into the thickness until a

size corresponding to plane strain conditions is reached. In thin sheets the extent of the plane stress region is limited by the actual dimensions, giving rise to 45° shear failure, but as thickness is increased the plane strain region occupies a larger and larger proportion of the thickness. Since the plane strain region consumes less energy than the plane stress region, the value of G_C or K_C will decrease with this increase in thickness of material as shown in Figure 2.4 . The value of K_C at the minimum plateau value is termed the plane strain fracture toughness. The possible modes of cracking are shown in Figure 2.5 , and brittle fracture in engineering structures is usually assumed to occur with Mode I crack surface displacements, with fractures under strictly Mode II or Mode III conditions being rare in practice. Since only the opening mode is generally considered, the plane strain fracture toughness in this mode is referred to as K_{IC} (and as K_{IIC} and K_{IIIC} for Modes II and III respectively).

In order to take into account different specimen geometries, such as bend specimens and tension specimens, in the calculation of stress intensity, K , equation (9) may be rewritten thus:

$$K_C = Y\sigma_F\sqrt{a} = Y'\sigma_F \qquad (12)$$

where Y is the geometrical constant, (with a value of $\sqrt{\pi}$ in the Griffith's analysis) and Y' a similar constant which incorporates $\sqrt{a}$. For a given class of geometry Y is dependent upon the ratio of crack length, a , to specimen width, W . The value of Y is obtained from a 'K-calibration curve', which is a plot of Y vs. a/W. Different classes of geometry will naturally require different calibration curves and the various modes of cracking have equally

applicable K-calibrations. The variation of K with specimen dimensions for standard test pieces is often described by a polynomial series, which are "best-fit" relationships over a limited range. Considerable effort has been directed towards establishing K-calibration curves for the different geometries, and these are published in the form of tables of Y values.

2.2.2 Fracture Toughness Measurement

The material property K_{IC} characterises the resistance of a material to fracture in the presence of a sharp crack, and a K_{IC} value represents a lower limiting value of fracture toughness.

The details of testing procedure to obtain plane strain fracture toughness values are laid down in two very similar documents, namely the American Society for Testing and Materials(ASTM) E399-78[52] and the British Standards Institition(BSI) BS 5447: 1977[53] . The development of these test methods is mainly given in various ASTM Special Technical Publications(STP)[54-57]. It is relevant to give a description of the related standards for plane strain fracture toughness testing, and since the work described in this report concerned the use of single edge notch bend(SENB) specimens only, the test procedure for this type of specimen alone will be given.

The nominal dimensions for the SENB specimen are shown in Figure 2.6 , and the most important dimensions are given in Table 2.2 and 2.3 , which summarise the two standards E399 and BS 5447 , respectively. The main difference and possibly most important in respect of powder metallurgical test pieces, between the two standards is that the minimum thickness allowed by BS 5447 is 13mm, whereas E399 allows specimens of a minimum of 6.4mm thick to be tested. Both standards require that during

testing the load and crack opening displacement be monitored on an autographic recorder. The linearity of this record must be checked to assess the validity of the K_I values at the onset of measurable crack extension, which is defined as a maximum of 2% crack growth. This is determined by a specific deviation from linearity of the load/displacement trace. With reference to Figure 2.7 , a typical load displacement trace, the point P_Q corresponds to a 2% crack growth, which is found to correspond to a line having a 5% decrease in slope than the elastic slope of the initial trace. The validity check for linearity from BS 5447 (for which there is no corresponding check in ASTM E399) , is that a horizontal line representing a force of $0.8P_Q$ is drawn and v_1 is the distance along this line between OA and OP_Q . If this distance is greater than one quarter of the corresponding deviation v at P_Q , then excessive non-linearity is deemed to be present and the curve is invalid. In both standards, the ratio P_{max}/P_Q (where P_{max} is the maximum force sustained by the test piece) is calculated and if this ratio exceeds 1.10 then the curve is rejected as it is possible that K_Q , a provisional value of K_{IC} which may be calculated from the test data, bears insufficient or no relationship to K_{IC} .

The value of K_Q is calculated from the relationship:

$$K_Q = \frac{P_Q L}{BW^{3/2}} \; f(a/w) \qquad (13)$$

It can be seen from Tables 2.2 and 2.3 that different K calibrations are used in the two standards. However, within the specified range of the value of the ratio crack length, a , to specimen width, W , that is $0.45 \leqslant a/W \leqslant 0.55$, the values of f(a/W) according to E399 are within 1% of those according to BS 5447.

A general requirement which gives rise to the basic test piece size is :

$$\text{crack length, a, and thickness, B, } > 2.5\left(\frac{K_Q}{\sigma_{YS}}\right)^2 \qquad (14)$$

where σ_{YS} is the 0.2% proof stress. The above equation is a formal statement that a and B have to be greater than approximately 50 times the radius of the plastic zone, r , ahead of the crack tip, thus ensuring plane strain conditions. The justification for the limitation of the crack size can be demonstrated by comparing the distribution of the σ_{YY} stresses (Figure 2.8) in the plane of the crack ahead of the crack tip in test pieces of different geometry. Wilson[58] showed that there are errors in characterising the stress at a finite distance ahead of the crack tip, shown for four geometries in Figure 2.9 , and it can be seen that the implied ratio of $a = 50r$ or $r/a = 0.02$ from (14) corresponds to an error in using K to characterise stresses, of 8.5% between the extreme curves for the infinite plate and the compact tension (CT) test piece. Thus inherent errors are present when using laboratory test pieces to represent large structures, which are better represented by an infinite plate. Recent analysis of experimental data by Kaufmann[59] suggests that for some materials the crack size validity requirements in equation (14)

should be increased to give:

$$a > 5\left(\frac{K_{IC}}{\sigma_{YS}}\right)^2 \qquad (15)$$

This implies that the differences in K values for different geometries may be even larger than those differences indicated by Figure 2.9 . BS 5447 recommends that, if possible, larger test pieces be used such that a and $B > 4(K_{IC}/\sigma_{YS})^2$ in order to take account of "uncertainties such as underestimation of the K_{IC} value and the possibility of the test not meeting some of the other validity criteria". If the conditions required of tne standard test method are met, then K_Q can be recorded as K_{IC}.

As can be seen from the above outline of the standards for plane strain fracture toughness testing, the main feature is to ensure that Linear Elastic conditions exist and in many situations LEFM analyses are invalidated by significant amounts of plastic deformation. These situations are described by Elastic-Plastic Fracture Mechanics (EPFM) .

2.2.3 Elastic-Plastic Fracture Mechanics (EPFM)

EPFM, like LEFM, seeks to find a relationship between applied stress, crack size and material toughness, except that EPFM is extended to include cases of plastic behaviour to a degree where the LEFM approach becomes inappropriate as a testing method. The crack opening displacement (COD), δ , and the J contour integral are two methods which may be used as a failure parameter in this instance.

There are difficulties with the COD characterisation of fracture toughness, both theoretically and experimentally.

Experimental observation shows that critical values of δ for a given material, section thickness and temperature, appear to be approximately the same regardless of whether crack growth commences from a pre-yield or post-yield state. Eftis and Liebowitz[60] have critically analysed the alternative methods of assessing the fracture toughness of materials exhibiting 'semi-brittle' fracture. They state that critical values of δ may, perhaps, appear the same because they are generally quite small (of the order of 2.5×10^{-4}m), and large differences in local crack tip stress and strain patterns may be reflected by very small differences in δ . This is then made problematical since precise measurement of COD is not always possible, particularly in the case of fatigue induced cracks.

Precise measurement of COD values was found to be very difficult and consequently, since no values of δ are quoted for the material in question in this work, a review of literature related to COD measurement was not undertaken.

2.2.4 The J Contour Integral

This integral was derived by Rice[61] for non-linear elastic materials as an expression for the rate of change of potential energy per unit thickness with respect to an increment of crack extension. The integral was shown to be independent of the choice of path for a crack with stress free faces, and defined to be:

$$-\frac{1}{B}\frac{dP}{da} = J = \int_{\Gamma}\left(Wdy - T\frac{du}{dx}ds\right) \qquad (16)$$

where P is the potential energy and Γ the contour surrounding the crack tip (described in an anticlockwise direction from the bottom crack surface to the top) as in Figure 2.10 , W is the strain energy density given by:

$$W = \int_0^{\varepsilon} \sigma_{ij} \, d\varepsilon_{ij} \qquad (17)$$

where σ_{ij} and ε_{ij} are stress and strain tensors, T is the traction vector, u the displacement vector and ds an increment of arc length. For a material which behaves elastically equation (16) can be integrated on substitution of the stress, strain and displacements associated with the singular region of a sharp crack to give:

$$J = K_I^2 \Big/ E' = G \quad \text{(c.f. equation (7))} \qquad (18)$$

which suggests a failure criterion J_{IC}, which may be equated with the linear elastic fracture toughness K_{IC} thus:

$$J_{IC} = K_{IC}^2 \Big/ E' \qquad (19)$$

The Rice formulation of the usage of J as a failure parameter stems from the stress analysis solutions, in the small scale yielding regime, of Rice and Rosengren[62] and Hutchinson[63], from which M^{c}Clintock[64] combined the results to express the stress and strain ahead of a sharp crack. The equations obtained stated that for a given material, i.e. a specific hardening law, modulus and limit of linearity, the stress and strain ahead of a crack tip are a function of J.

Experimental work in support of the use of J as a fracture parameter has been produced by Landes and Begley[65,66]. Load-displacement records for specimens of varying crack lengths were obtained and, by evaluating the area under these curves up to

specific displacements, they were able to construct graphs of energy/unit thickness vs. crack length for varying displacements. The gradients of these curves represented the change in potential energy per change in crack length on a unit thickness basis and were equivalent to J . To estimate J_{IC} , the critical value of J, J was plotted against displacement, and the point at which the average displacement cut the curve, corresponded to J_{IC} . This method is obviously costly and time consuming and the possibility of obtaining J_C from a single specimen was extremely attractive, as was pointed out in an estimation proceedure based on elastic compliance and slip line field theory[67] . Subsequent work[68] focused on the use of the correlation between J and absorbed energy, and the following relationship has emerged for three point bend specimens:

$$J = 2U_{crack} \Big/ (B(W-a)) \qquad (20)$$

where U_{crack} denotes the component of energy absorbtion due to the presence of a crack. For a deeply cracked bend specimen, the component of energy absorbtion for the uncracked ligament is small, equation (20) may be simplified to:

$$J = 2U/B(W-a) \qquad (21)$$

where U becomes the total area as measured under the load/load point displacement curve. Empirical evaluations of equation (21) have shown[69] more accurate values of J over greater ranges of crack length when the total area, that is, due to both the cracked and uncracked contributions, is taken. However, it has been

pointed out[69] that there will be a discrepancy between equations (20) and (21) when the energy due to uncracked ligament is significant, as in the standard three-point bend geometry, and therefore the portion of the energy contributed by an uncracked ligament should be subtracted in this instance.

Aspects of materials testing and the methods of evaluating J have been discussed by a number of researchers[69-73] and experimental techniques for the laboratory determination of J have also been reviewed, including proposed methods for the calculation of J_{IC} which may lead to a standard testing procedure [69,70]. Recommended procedure for J-integral testing has been proposed[74] and a more recent version of the procedure has now emerged[75]. The methods of measuring fracture toughness values, with emphasis on their practical limitations, has been assessed by Scarlin and Shakeshaft[76]. They conclude that the J integral technique has the advantage of possessing a sound theoretical basis, whereas equivalent energy and COD methods contain considerable empiricism. They also conclude that a disadvantage of the J integral technique is that a number of specimens are required when the recommended practice of heat tinting is used. As stated previously, the possibility of obtaining J_C from a single specimen is therefore very attractive and the determination of the point of first crack growth is of prime importance in fracture-toughness measurement. Various methods can be employed, one of which is the electrical potential method in which crack length is directly determined. This method was one of those suggested by Scarlin and Shakeshaft and also by Landes and Begley in an earlier review[70], and was the method employed by the author.

As with LEFM, specimen size limitations are imposed when determining J_{IC} values in order that certain crack-tip field conditions are preserved. This is expressed by:

$$(W-a) \text{ and } B > \alpha \frac{J}{\sigma_{YS}} \qquad (22)$$

where $\alpha = 25$ in the recommended proceedure, and is in the range suggested by Landes and Begley[70], who state that the value of the dimensionless constant α may vary from one material to another, but is taken to be somewhere in the order of 25 to 50 . The specimen thickness and crack length requirements for different materials are still the subject of investigation by many researchers.

The J integral approach offers promising applications in elastic-plastic fracture analysis, and at present is able to give a quantitative guide to the acceptance or rejection of flaws and defects in engineering components.

2.2.5 The Fracture Toughness of Sintered Materials

The use of the plane strain fracture toughness, K_{IC} , and more recently the J contour integral as a design parameter is becoming widespread and has effectively increased the choice of available materials. Once a material has been 'put on the map' its use need not be restricted to particular applications. However, the lack of information regarding the fracture toughness of sintered materials will only serve to maintain the 'status quo' and restrict the use of this type of material to relatively low stressed applications. Increasing interest is being shown in the study of fracture toughness of sintered materials and the published results should increase the field of application.

Barnby et al[6], investigated the fracture resistance of Fe-Cu, Fe-C and Fe-Cu-C alloys and reported K_C values between 10 (Fe-Cu, Fe-C at a density of $6.4Mgm^{-3}$) and $25MNm^{-3/2}$ (Fe-Cu-C, $7.2Mgm^{-3}$) using pre-fatigue cracked SENB test pieces. Fracture toughness was found to be related to both the density and percentage addition of copper, but the increase in toughness due to the copper additions was only noticeable at the higher densities. A significant point to arise from this work was that a linear increase in toughness was observed with an increase in yield stress for all materials tested, the reverse of the trend observed in wrought and cast materials. Extrapolation of this trend would suggest the possibility of high strength, highly alloyed, sintered steels being able to compete with high strength wrought steels, titanium alloys and aluminium alloys. A second series of toughness values was determined by Barnby et al using the same materials but the test pieces had notches with a machined root radius of 0.1mm and no fatigue crack was introduced. Within experimental error the results were found to be identical with those for the standard fatigue cracked specimens. This finding indicates the possible controlling factor for fracture in a sintered material, since it can be assumed that there has to be a defect present which has a root radius equivalent to, or smaller than that of a fatigue crack. Examination of irregularly shaped pores by scanning electron microscopy would make it possible to measure the minimum radii of curvature present in complex shaped pores, which would, if the radii were small enough, effectively sharpen the notch tip so long as the final machining operation on the notch is performed delicately so as not to produce a heavily deformed region below the cutting tool. Investigations into the fracture toughness of a copper infiltrated

alloy sintered steel by Trunick and Queeney[10] showed that the fracture resistance was improved beyond rule-of-mixtures expectations. It was stated that this was to be expected since the infiltration process would reduce the diameter of the stress concentrators or local sharp flaws present in the form of pores, by either eliminating or partially filling the sharp corners of pores. It was also made clear by this work that the degree of infiltration was critical since the inherent porosity would eventually reach a size which is close to the critical defect size and thus lower the fracture resistance.

The defect size, a_c, that can be sustained at a given working stress is calculated by use of the simple formula:

$$a_c = \left(\frac{K_{IC}}{\sigma_{YS}} \right)^2 \left(\frac{1}{Y} \right)^2 \qquad (23)$$

and it has been highlighted by Barnby et al[6] that the value of Y, which is the geometrical term that varies with the shape of the component and geometry of load application, increases as the ratio of defect size to gross specimen dimensions increases, such that the smaller the component the smaller the tolerable defect size. This indicates that the 'brittleness' of sintered metal components arises partly from the shape and small scale of the components and is not simply an inherent material property.

Ingelstrom and Nordberg[8] carried out fracture toughness tests on a pre-alloyed atomised powder (Hoganas ATST-A) compacted to two different densities namely 6.83 and 7.83Mgm^{-3}, the latter being achieved by hot forging after sintering. The purpose was to investigate whether the fracture toughness of sintered steels could be determined using specimens of realistic size at practical

testing temperatures. Using compact tension type specimens they concluded that it was possible to evaluate the toughness of sintered steels using specimens of ordinary size. It has to be assumed that by ordinary size it is meant that the size can conform to that laid down by the relevent standard used (ASTM annual book of standards 1972, Volume 31) and that the criterion for obtaining valid results is that testing be carried out at a reduced temperature, since only at -73°C were valid K_{IC} values obtained for all the tested materials, only the fully dense (hot forged) steel providing a valid determination at room temperature.

Inglestrom and Ustimenko[9] also investigated the fracture toughness of Hoganas ATST-A low alloy steel at the same densities as the previous workers i.e. 6.8 and 7.8Mgm^{-3} (powder forged), as well as the effect of varying the carbon content on the fracture toughness of a sponge iron powder with a 2% copper addition, using the round compact tension (RCT) test piece which allowed a greater thickness to be used than the compact tension (CT) type. Valid results were obtained for the low alloy steel and for the sponge iron powder with 0.6 and 0.8% carbon content, the specimen with 0 and 0.3% carbon being too small to provide a valid K_{IC} determination owing to their high toughness. They reported values ranging from 23.9 to 80.3$MNm^{-3/2}$ for the fracture toughness of the low alloy steel, the values being dependent upon density and tempering temperature, and a value of 34$MNm^{-3/2}$ for the sponge iron with both 0.6 and 0.8% carbon. It was concluded from this work that fracture toughness of the porous materials showed a strong, almost linear dependence on yield stress and that fracture toughness decreases with increasing porosity.

Andrews[7] and Ghosh[12] both investigated the fracture

resistance of a range of sintered steels which included Distaloy SA. Andrews showed that the fracture toughness varied from 11.5 to 25.8$MNm^{-3/2}$ over the density range 5.95 to 7.00Mgm^{-3} for as sintered Distaloy SA of 0.4% carbon content. At the same carbon content and over the same density range toughness varied from 18.0 to 33.9$MNm^{-3/2}$ for the material in the heat treated condition. Increasing the carbon content from 0 to 0.65% was shown to give rise to an approximate linear increase in toughness from 14.9 to 26.4$MNm^{-3/2}$ for as sintered material of 6.70Mgm^{-3} density. Ghosh investigated two densities with this material, namely 6.7 and 6.9Mgm^{-3} and reported toughness values of 24.9 and 28.5$MNm^{-3/2}$ in the as sintered condition and 25.8 and 29.6$MNm^{-3/2}$ in the heat treated condition. The material had a combined carbon content of 0.65% . Both workers reported a linear increase in toughness with increasing yield strength and that a comparison between test pieces with notches and with fatigue cracks yielded toughness values which were identical within the limits of experimental error.

Examination of the fracture faces in all the above investigations showed that the fractures of bonded areas between pores were apparently of the ductile dimple type for all porous materials tested at room temperature, only fully dense (sinter forged or hot pressed) material or that tested at low temperatures,showing cleavage fracture together with ductile dimples. The micromechanism of ductile fracture is one of the enlargement and coalescence of voids which are often clearly associated with inclusions. In porous materials the voids are an inherent feature which can contain acuities which will concentrate the plastic strain causing local damage to carbides or inclusions, opening up a void sheet. The attainment of local shear stresses for

plastic deformation, resulting in ductile dimple failure, occurs when appreciable porosity is present because of the relaxation of strict plane strain conditions on a micro scale.

In a similar way to other mechanical properties, a comparison has been made between graphitic cast irons and sintered material in respect of fracture toughness. Work carried out on a flake grey cast irons[77] reported toughness values of the order of $20MNm^{-3/2}$ for as cast material, and demonstrated that it was unnecessary to introduce a fatigue crack prior to testing since the graphite flakes provided "atomically sharp cracks within the material".

The work carried out to date on the fracture toughness of sintered materials indicates that the testing proceedure could perhaps be modified by substitution of the standard fatigue pre-cracked specimen by a simple notched specimen of small root radius, avoiding the need for expensive ancilliary equipment in the form of fatigue machines and also reducing time, and hence cost, of carrying out a test.

The correlation between yield stress and fracture toughness has been shown to exist and ultimately it may be possible to carry out a tensile test in lieu of a fracture toughness test once the 'ground work' has been done.

2.3 Fatigue

2.3.1 Theoretical Aspects

The phenomenon of the failure of metals under alternating loads has been a subject of study for many years, and has consequently produced a large quantity of research literature. The realisation that fatigue failure could occur at stresses below the elastic limit came about when experimental work was carried out on the subject in the 1930's. It also became apparent that there existed a fatigue limit, below which an infinite amount of cyclic loading could be endured. Traditionally, fatigue data is represented in the form of an S/N curve, where the stress amplitude, S, is plotted against the logarithmic value of the number of cycles to failure, N.

Knowledge of the process known as metal fatigue has been growing for many years and is now recognised as a three stage process: a fatigue crack initiates in the metal, often at the surface, and propagates until the remaining ligament is reduced to a size which cannot sustain the working load and fracture ensues. It is now realised that most structures contain crack like defects or flaws introduced during their manufacture, so that virtually the whole fatigue process in a structure is concerned with the propagation of a fatigue crack. Thus it is desirable to be able to predict fatigue crack growth rates from a knowledge of working stresses and flaw size in the engineering service of a component in order to predict its residual life. Also it is useful to have a knowledge of the type of microstructure which will give the best resistance to crack growth and hence be able to state which is the most suitable for a particular application. The traditional approach is of limited value in these instances since

information on the contributions of crack initiation and crack growth is not found from determined S/N curves. Consequently, the application of fracture mechanics concepts to fatigue crack growth for the solution of practical engineering problems has become widespread.

2.3.2 Mechanisms of Fatigue Failure

The development of the scanning and transmission electron microscopes has enabled fracture surfaces to be studied in relation to the causes and basic mechanisms of fracture. Fatigue is a complex phenomenon which involves the processes of microscopic flow and macroscopic crack extension. It has long been recognised[78] that the development of slipbands due to localised plasticity is a feature of the process. On investigating slip-bands produced in different materials under cyclic loading, Forsyth[79] observed that extrusions and intrusions were formed within the bands, the latter developing into micro cracks which then propagated in a direction 45° to the stress axis, mainly on crystallographic directions. This stage of fatigue crack growth was termed Stage I by Forsyth. In the case of brittle materials, fatigue cracks were found to initiate at inclusion or precipitate sites. The micro cracks formed in Stage I eventually link up to form dominant cracks which propagate on a plane which is normal to the applied stress, and this marks the end of Stage I fatigue crack growth. Stage II fatigue crack growth is generally characterised by progressive markings, parallel to each other and normal to the direction of crack growth. Each striation corresponds to one stress cycle, and the formation of these striations is caused by alternate blunting and resharpening of the crack tip. This process, as proposed by Laird[80], comprises a double notch at the end of

the sharp crack which causes the deformation to be concentrated along planes at 45° to the plane of the sharp crack when a tensile load is applied. At its maximum opening, the crack grows by plastic shearing, and blunting of the tip occurs due to broadening of the slip bands. On reversal of the load, slip occurs in the opposite direction and the newly created crack surface at the crack tip is folded back slightly as the crack closes, forming another double notch. This process is shown diagramatically in Figure 2.11 . Two types of striation marks were noted by Forsyth et al[81], these being Type A or ductile striations of light and dark bands lying on non-crystallographic plateau and Type B or brittle striations lying on fan shaped crystal facets. The latter type show river markings which are normal to the striations and in the direction of crack propagation.

Finally, at high rates of crack growth, the striations tend to give way to ductile dimples or cleavage facets depending on the ductility of the material, and the fatigue fracture surfaces are sometimes indistinguishable from those produced by monotonic loading.

The formation of a fatigue crack, outlined above, has indicated that only a free surface is required, where local plasticity and slip band formation give way to initiation and Stage I of a fatigue crack. However, initiation has been reported to occur at sub-surface sites and, in brittle materials, around inclusions and precipitates.

2.3.3 Fatigue Crack Initiation and Propagation from Notches

The traditional approach to obtaining fatigue data by determining the number of cycles to failure N at stress amplitudes S shows the importance of the surface finish of the material in

relation to 'fatigue strength'. A reduction in fatigue strength accompanies a worsening in surface finish, as shown in Figure 2.12. Stress concentration is invariably present in engineering components due to design, in the form of changes in section, keyways, bolt holes etc. and pre-existing defects introduced in metallurgical processes during material production, such as shrinkage porosity in castings and laminations in wrought products. Thus fatigue failure assessment needs to take into account these stress concentrations and fatigue failure is extended to that which occurs from notches.

Description of the initiation and propagation of a crack from a notch requires knowledge of the stress-strain region ahead of the notch and that this region can be related to the applied load. To this end, the use of the fracture mechanics approach is valuable as a means of characterising the stress-strain region and it is also nearly independent of material and takes geometry into account. This approach uses the concept of the stress intensity factor K_I, which describes the stress field at a crack tip. Values of K_I are known for a wide range of cracked configurations[82-84] and in view of its success in dealing with static problems, its use has been extended to analyse fatigue crack growth data.

2.3.4 Fracture Mechanics approach to Fatigue Crack Propagation

Numerous laws of fatigue crack growth have been described, a number of which are based upon stress intensity factors. All can be used to predict crack growth rates in situations similar to those used to collect the data, but to be able to predict growth rates for any cracked body configuration is more valuable to a designer. Hence, stress intensity factors provide a convenient means of correlating fatigue crack growth rate and range of stress

intensity factors, by describing the stress conditions at a crack tip by a single parameter[85]. The stress intensity factor in the opening mode is given by:

$$K_I = \sigma \sqrt{a}\, Y \qquad (24)$$

where σ is the applied stress, a is the crack length, and Y is a geometrical coefficient. The fatigue stress intensity during the fatigue cycle is usually described by ΔK, where $\Delta K = K_{max} - K_{min}$, K_{max} and K_{min} being the values of the stress intensity factor calculated from the maximum and minimum stress during the fatigue cycle. The most widely accepted law from a practical point of view, in that it has the most general applicability and is the simplest to use, is the Paris-Erdogan law[86]:

$$\frac{da}{dN} = C(\Delta K)^n \qquad (25)$$

where da/dN = the crack growth rate, ΔK = fatigue stress intensity, C,n = material constant. This formula is purely an empirical one and cannot be derived. The values of C and n are determined experimentally and it is suggested[86] that, due to their empirical nature, these values should not be determined from one plot alone. The growth rate is proportional to the square of the plastic zone size, according to the approach described by M^{c}Clintock[87], and this is given by equations (10) and (11) (see Section 2.2.1). Thus the value of n in equation (25) should be equal to 4. Where a linear proportionality exists between growth rate and plastic zone size, n is equal to 2. The value of n has been determined experimentally for a wide variety of materials and has been shown

to lie mainly between 2 and 4 , with some values as high as 19 being reported[88] . Criticisms of the stress intensity approach are that material properties and microstructural effects on growth rate are not included. It is clear however, that such effects will be reflected in the value of the exponent n .

The form of equation (25) indicates that a logarithmic plot of da/dN vs. ΔK would result in a straight line, but it has been demonstrated that crack propagation behaviour gives rise to a fatigue crack growth curve which is sigmoidal in shape, Figure 2.13. This curve can be divided into three regions, indicated as 1, 2, and 3 in the diagram. It is region 2 to which the fatigue crack propagation law, as in equation (25), applies. Region 1 is characterised by a steep variation of da/dN with ΔK and is in the vicinity of the 'threshold' level of ΔK below which fatigue crack growth does not take place. Region 3 corresponds to the occurence of occasional brittle fracture and a contribution from monotonic failure modes leading to static failure due to a single load.

Attempts have been made to incorporate the mean stress, in the form of a stress ratio, $R = \sigma_{min} / \sigma_{max}$, in growth laws where high crack growth rates are utilised. The formulae advanced attempts to relate the crack growth rate to the fracture toughness of the material, since at high crack growth rates K_{max} approaches K_{IC} . For thin specimens Forman et al[89] proposed:

$$\frac{da}{dN} = \frac{C(\Delta K)^n}{(1-R)K_C - \Delta K} \qquad (26)$$

where C and n are material constants, K_C = critical stress intensity and R = stress ratio.

Investigations into the effect of mean stress by Pearson[90], showed that specimens of increased thickness required the use of plane strain value of K_c, namely K_{IC}, in equation (26) and a modification to account for high values of ΔK . The formula obtained by Pearson was:

$$\frac{da}{dN} = \frac{C(\Delta K)^n}{\left[(1-R)K_{IC}-\Delta K\right]^{1/2}} \qquad (27)$$

Comparison of the influence of mean stress over a range of stress intensity, ΔK, for materials of high and low toughness values was provided by Maddox[91], in which the predicted magnifications in da/dN for given values of R, K_{IC} and ΔK were redefined relative to the values of $R = 0$. The magnifications were plotted against ΔK for various stress ratios. The resultant factors for a low toughness material differed widely when comparing Pearsons and Formans equations, especially at high values, over the entire range of ΔK and R values.

Fatigue crack growth is dependent upon many uncontrollable variables, and in practice a large scatter in results has to be expected. Any empirical expression will have some merit and when applied to the data and materials from which it was derived it will obviously be valid, but therefore limited. From this point of view fracture mechanics and the Paris Law give the widest application for representation of crack growth and remain the best to date.

2.3.5 The Fatigue Properties of Sintered Materials

Previous investigations of the fatigue characteristics of sintered materials have been primarily concerned with fatigue strength as determined from standard S-N curves[92-98], and limited information is available concerning fatigue under cyclic loading. A comprehensive review of published data is made by Haynes[95] who compared sintered materials with equivalent wrought materials, and concluded that the notch sensitivity of sintered materials was less than that of the wrought materials. It was proposed that this could be explained by the fact that the pores exerted a stress concentration effect which reduced the significance of an external notch, this notch insensitivity, as with other properties discussed earlier, showing a marked similarity to cast irons. Overall, the fatigue behaviour of sintered materials is not unlike that of conventional materials and would prove no more hazardous in fatigue situations by sensible use of available data. The results in the form of S-N data from copper, iron and iron based sintered materials have indicated that the curves are similar to those for fully dense material and that an endurance limit exists which decreases with decreasing density. The fatigue ratio S_f / S_u, where S_f is the fully reversed fatigue limit and S_u is the maximum stress, normally lies within the range 0.3-0.5, and is lower than that for equivalent wrought materials, but exhibits the same decrease in value with increasing maximum stress[94-96].

Porosity is the most important factor controlling the mechanical properties of sintered materials, as outlined in Section 2.1.1. A reduction in the porosity will raise the fatigue limit, although fatigue ratios appear to be independent of the amount of porosity[94].

The notch sensitivity of sintered, low alloy, nickel steels is increased by hardening[99], showing that the structure plays a role in the fatigue process and that porosity alone is not the contolling factor. The interaction between porosity and microstructure is also prominent in the fatigue behaviour of cast irons[92].

It is generally accepted that a fatigue crack initiates most readily at a free surface, but since pores act as sites of stress concentration it is by no means certain that this is the case with regard to sintered materials. Wheatley and Smith[94] attempted to remove the effects of accumulated fatigue damage by removing the surface layers from sintered iron test pieces after each 5000 stress reversals, but the results were inconclusive. The nucleation of microcracks at pores has been observed by Bankowski and Feilbach[100], these microcracks occuring at sharp corners of the pores, but their growth may be inhibited by the structure of the matrix, although they may well eventually become part of the macrocrack, assisting the overall fatigue crack propagation process. These microcracks were observed to grow in a mixed intergranular-transgranular mode and it was argued that this occured due to the microcrack nuclei being located within grains as well as along grain boundaries. Williams and Haynes[96] found the fatigue cracks in sintered nickel to be essentially intergranular and that the presence of a film-like porosity would halt a propagating crack and the stress transferred to the leading edge of the pore. This effectively allowed the crack to advance but at the same time become 'blunt' and a crack would have to be reformed at the leading edge before it could advance further. Franklin and Davies[97] observed fracture paths to pass through the sintered necks between

adjacent particles and to pass around the particles themselves, their observations having more in common with the theory of Williams and Haynes than with that of Bankowski and Feilbach. This same fracture path was also observed by Rodzinak and Slesar[98], who concluded that two types of intergranular neck failure were possible, depending on the stress amplitudes and the size of the connection between the grains. They found that the fracture surface showed a ductile dimpled fracture when high stress levels were employed, and at low stress levels a fatigue like failure occured, having a mixed morphology of striations combined with dimples. Fatigue striae together with fracture modes charcteristic of ductile fracture were also apparent in the fractographs present by the earlier investigations[96,97].

Information regarding crack growth rates in sintered materials is sparse. That which is available, represents data as determined from the Paris-Erdogan law (see Section 2.3.4). Ghosh[12], testing a range of sintered maraging steels, found that the growth rate decreased with decreasing porosity, quoting values of the growth exponent, n, in the Paris-Erdogan equation in the range 2.26 to 4.50, depending upon the composition and density of the material. The micromechanism of fracture was of the ductile type in all cases, and no striation markings were observed on the fracture surfaces. Andrews[7], investigating low alloy sintered steels, also obtained a trend of decreasing growth rate with decreasing porosity, and quoted growth exponent values in the range 3.65-5.90 , these values being dependent upon density and carbon content. The exponent was found to be lower in heat treated samples than in their sintered counterparts. Again, the ductile dimple type of fracture was observed in all cases.

There is an obvious need for extensive research in the field of fatigue in sintered materials as information is notably lacking, and there will be continued reticence on behalf of engineers in using sintered materials in relatively highly stressed situations involving dynamic loading until there is a clearer understanding in the area of the fatigue properties related to microstructure and porosity.

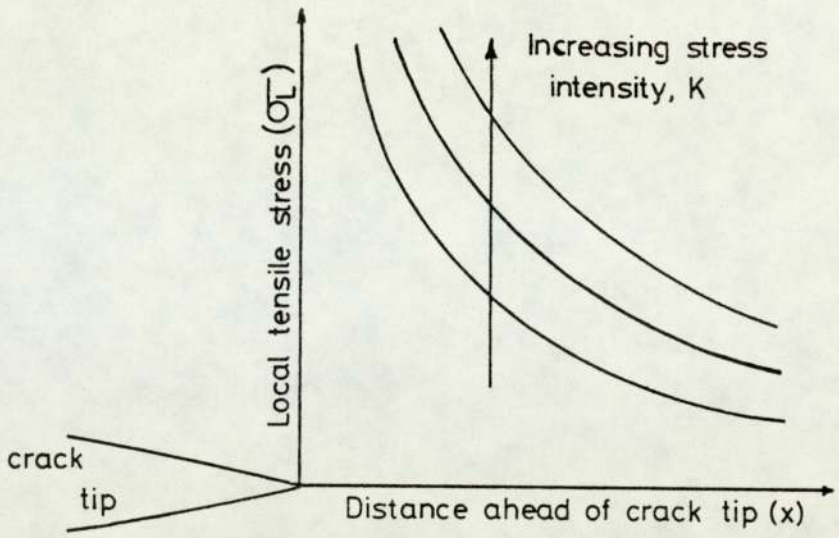

Figure 2.1 : Distribution of tensile stresses ahead of the crack tip.

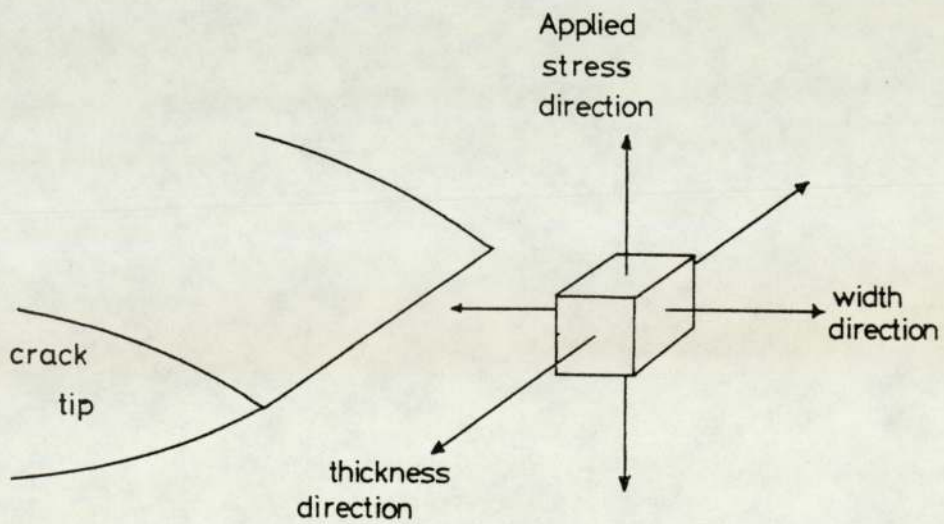

Figure 2.2 : Directions of tensile constraint.

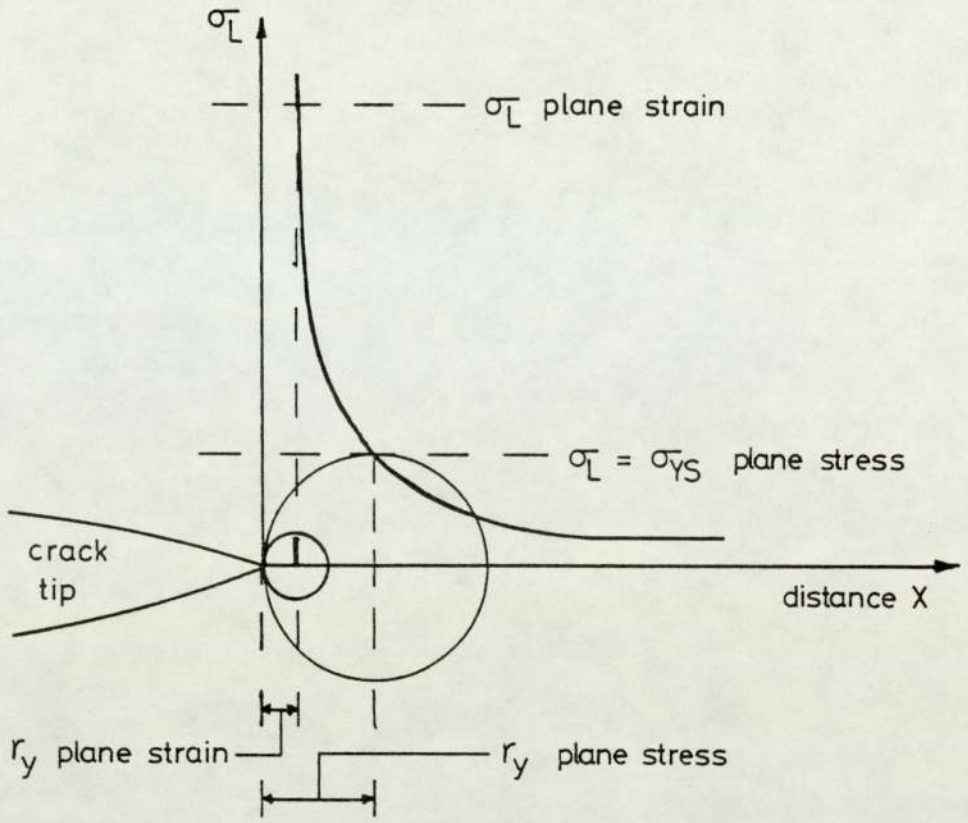

Figure 2.3 : Plane stress and plane strain plastic zones.

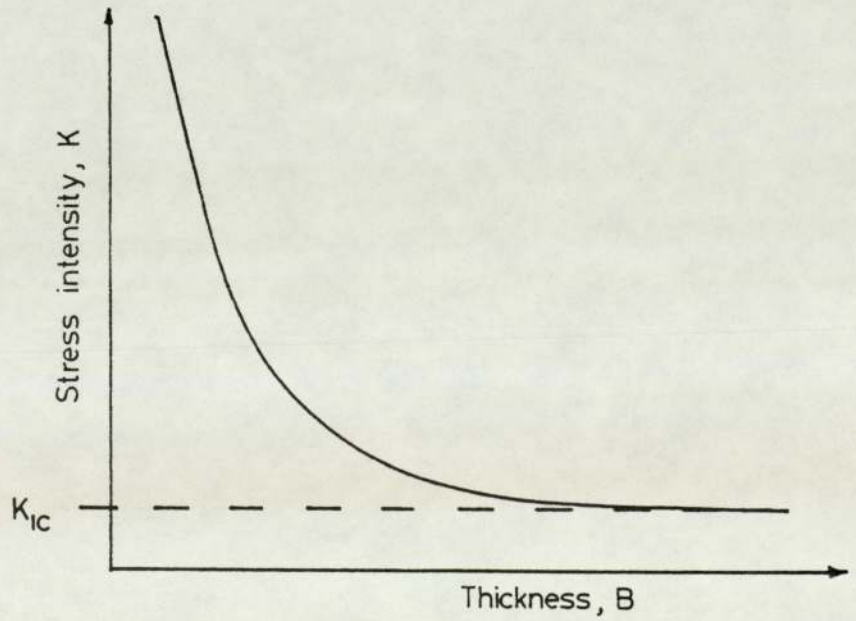

Figure 2.4 : Variation of stress intensity with thickness.

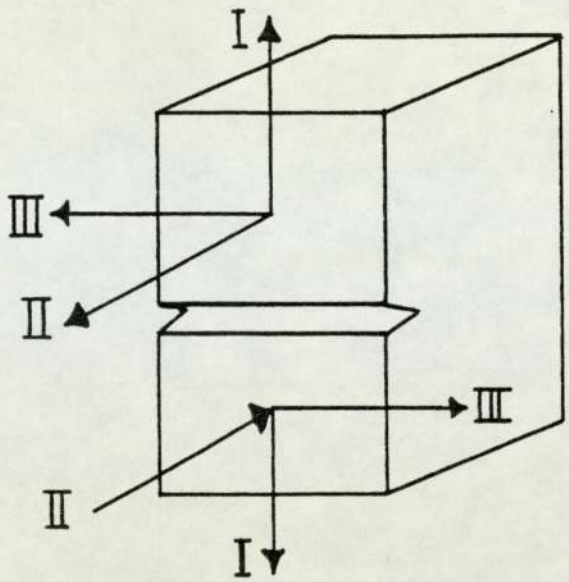

MODE I: the opening mode

MODE II: the forward shear mode

MODE III: the anti-plane shear mode

Figure 2.5 : Modes of crack displacement.

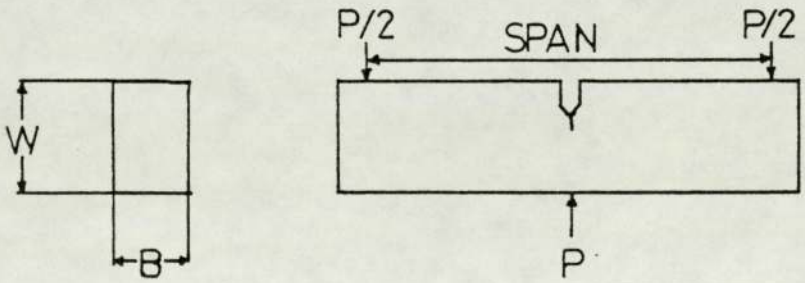

Figure 2.6 : Nominal dimensions for the SENB specimen.

Specimen dimensions	K calibration
Thickness, $B \geq 6.4$mm $B = 0.5W$ Alternative thickness: $B = 0.25 - 1.0W$ Loading span, $S = 4W$ Crack length, $a = 0.45\text{-}0.55W$	$K = \frac{PS}{BW^{3/2}} f(a/W)$ where $f(a/W) = 3(a/W)^{1/2}$ $\times \left[1.99-(a/W)(1-a/W)(2.15-3.99a/W+2.7(a/W)^2)\right] \times \left[2(1\ 2a/W)(1-a/W)^{3/2}\right]^{-1}$

Table 2.2 : Summary of Standard Test Method for Plane Strain Fracture Toughness testing, E3999-78a[52], for Three-point SENB test piece.

Specimen dimensions	K calibration
Thickness, $B \geq 13$mm $B = 0.5W$ Alternative thickness: $B = 0.25 - 1.0W$ Loading span, $L = 4W$ Crack length, $a = 0.45\text{-}0.55W$	$K = \frac{PL}{BW^{3/2}} \left[1.93(a/W)^{1/2}-3.07(a/W)^{3/2}\right.$ $+14.53(a/W)^{5/2}-25.11(a/W)^{7/2}$ $\left.+25.80(a/W)^{9/2}\right]$

Table 2.3 : Summary of Standard Methods of Test for Plane Strain Fracture Toughness (K_{IC}), BS 5447:1977[53], for Three-point SENB test piece.

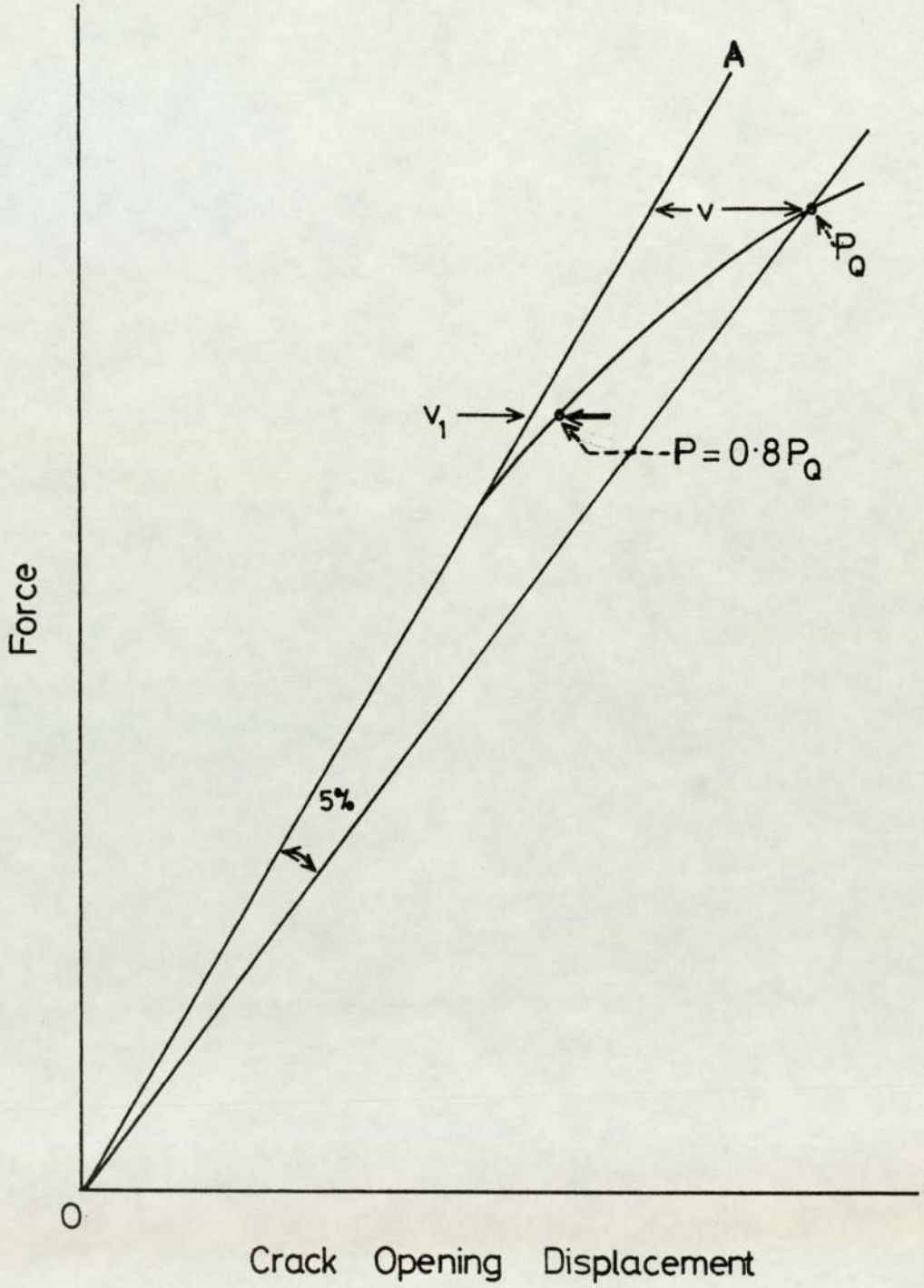

Figure 2.7 : Typical load/crack opening displacement trace

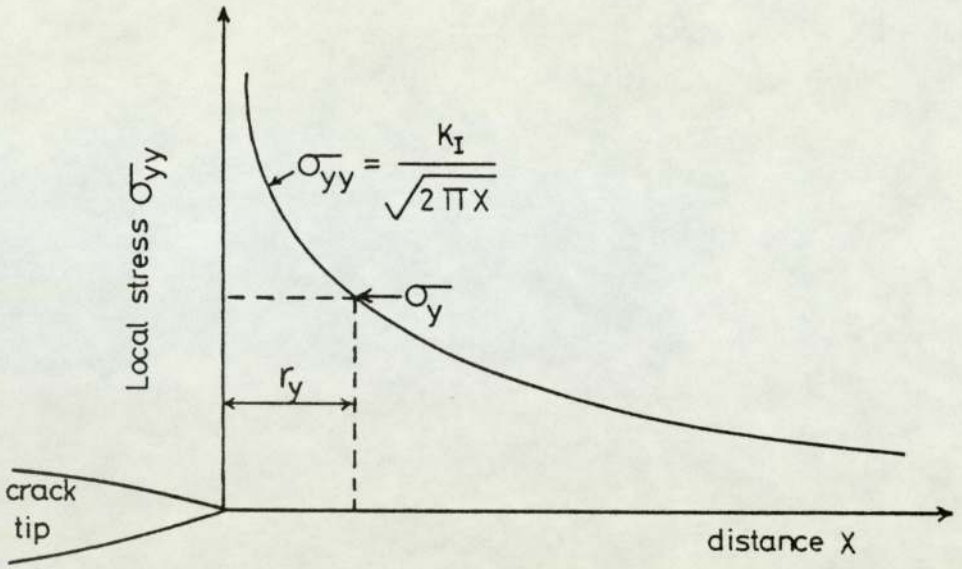

Figure 2.8 : Crack plane elastic stress field

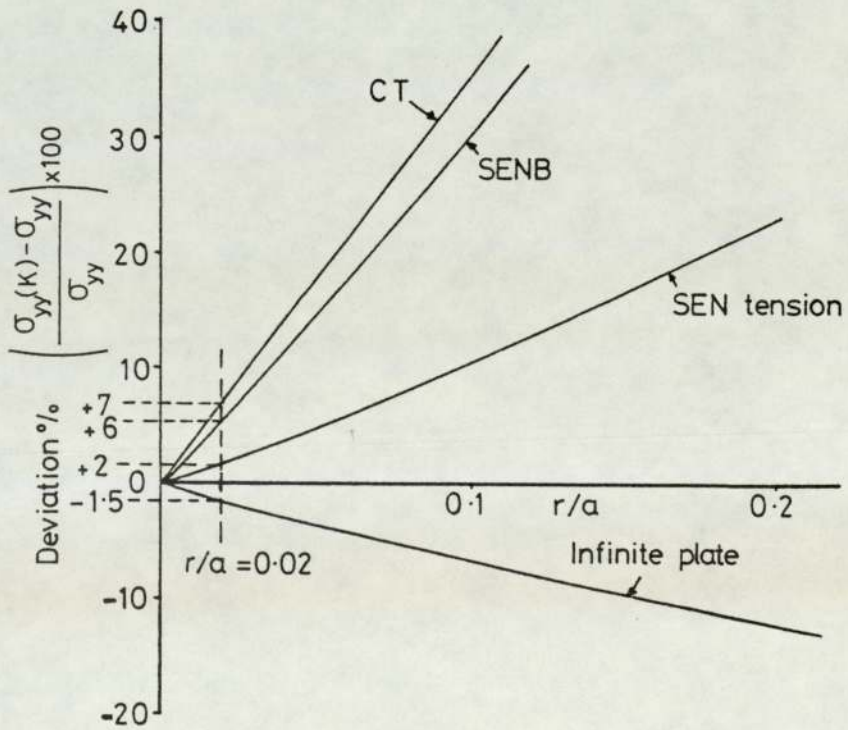

Figure 2.9 : Deviation of crack tip stress, σ_{yy} (K), ahead of crack tip.

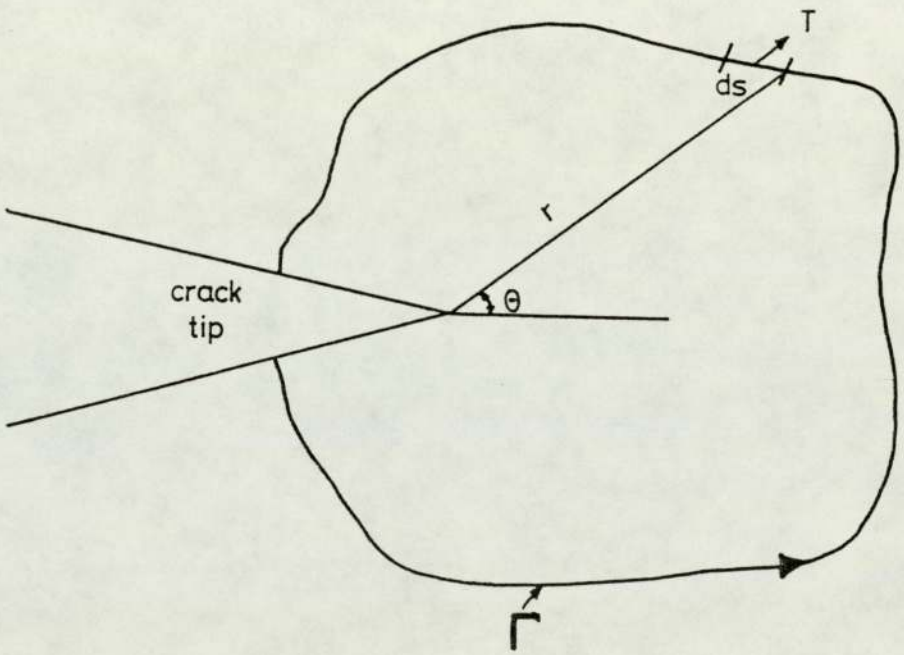

Figure 2.10 : A possible path Γ for the calculation of the J integral

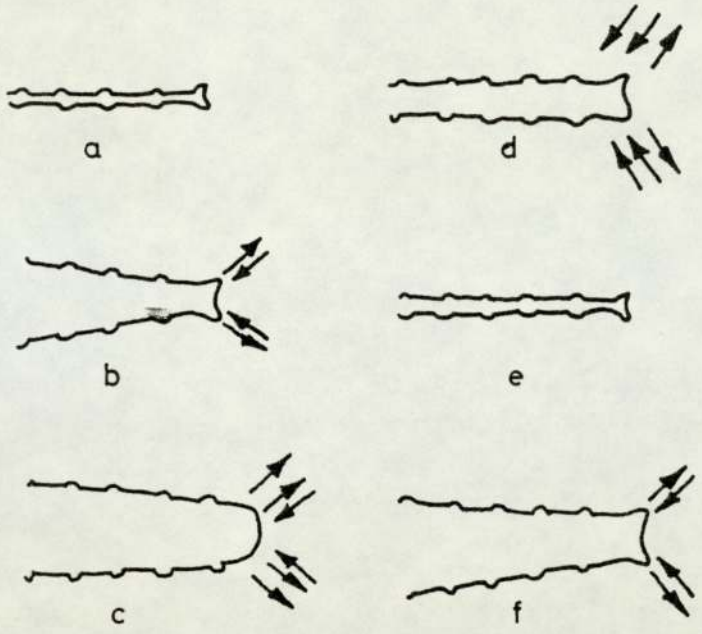

Figure 2.11 : Mechanism of striation formation by a process of plastic blunting

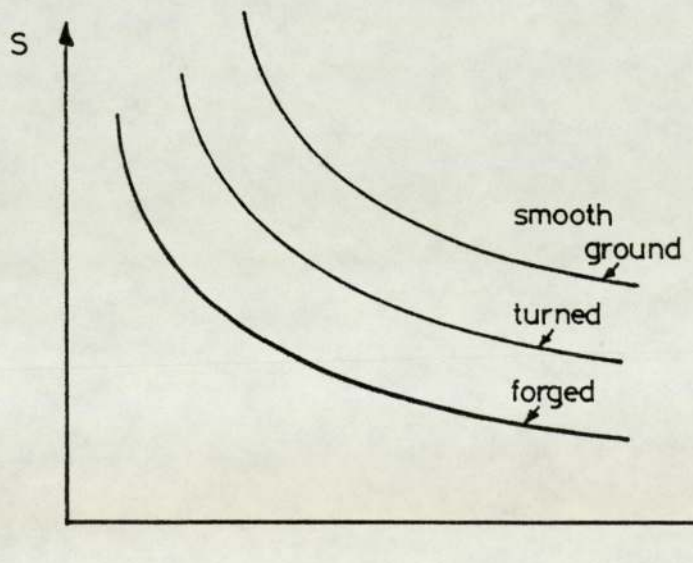

Figure 2.12 : Effect of surface finish on fatigue strength

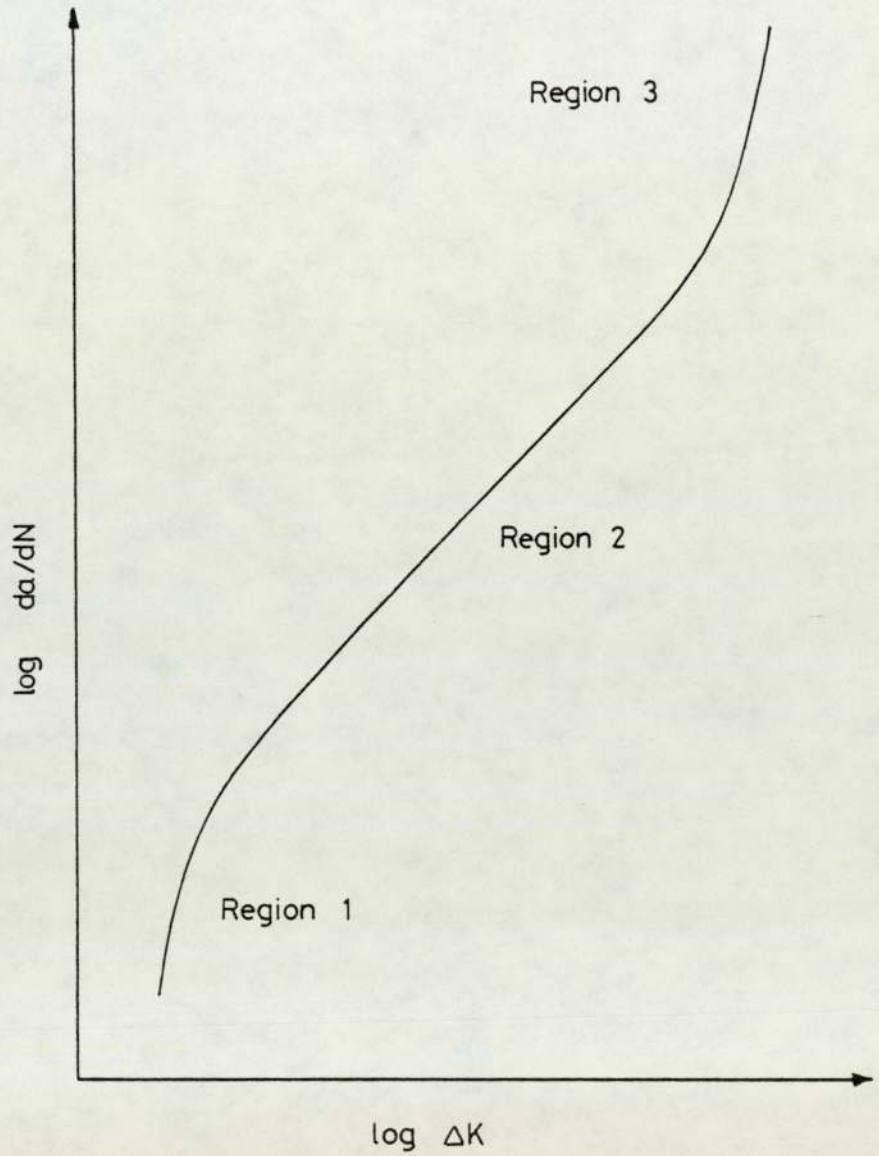

Figure 2.13 : Schematic plot of fatigue crack growth data

3. EXPERIMENTAL PROCEDURE

3.1 Materials

The material chosen for this investigation was a commercially available pre-alloyed powder manufactured by Hoganas AB, designated Distaloy SA. This powder, previously marketed as Ancoloy SA, is manufactured by the reduction of high grade magnetite concentrates with admixed coke and lime in tunnel kilns. The metal powder, or 'sponge', produced, undergoes a hydrogen reduction treatment to form iron powder of high quality. Finely divided alloying elements, that is, copper, nickel and molybdenum, are then diffusion bonded onto the surface of the iron powder, resulting in irregularly shaped particles with many aspirities on the surface. Scanning electron micrographs in Figure 3.1, together with X-ray maps, show a typical powder particle and the alloying elements being distinguishable by reference to the relevent X-ray map.

The powder has good compressibility, and a high green strength of the compacted component. The form of the alloy powder, that is, diffusion bonded alloying elements, eliminates the risk of segregation of the alloying elements and aids rapid diffusion into the iron powder during sintering. The additions of copper and nickel are balanced such that little dimensional change will take place during sintering and heat treatment. The use of molybdenum raises the hardenability of the alloy, and all three alloying elements have less affinity for oxygen than iron, allowing the same atmosphere as for normal iron powder to be used for sintering operations.

The manufacturers recommendations[43] are that Distaloy SA is primarily for use in the sintered condition, sintering temperatures being preferably of the order of 1120°C to achieve dimensional stability. It is also for use in the heat-treated condition,

and is suitable for case hardening applications.

Carbon additions to the alloy powder were made in the form of synthetic graphite powder. This extremely fine powder was readily available in the required form from laboratory chemical suppliers and was found to be more consistent than the 'natural graphite' form which can contain fairly high levels of impurities. As with the graphite, zinc stearate lubricant of high purity was used as supplied, in the form of fine powder.

3.2 Preparation of Test Pieces

3.2.1 Compacting

Carbon additions were made to Hoganas Distaloy SA powder by adding the powdered graphite. Additions of 0.65 wt% zinc stearate were made prior to mixing to reduce die wall friction and facilitate compact ejection. Blending of the powder, graphite and zinc stearate in 5kgm batches was carried out by tumbling in a ceramic container for ten minutes and the blended powders were then brushed through a 75 mesh sieve. Any agglomerated powder was brushed through the sieve and the powders blended again by tumbling, for a further ten minutes. This mixing procedure was found to be the optimum for mixing under laboratory conditions by a previous worker[101].

The required load for compaction was read from a previously determined pressure/density curve, Figure 3.2, and the powder charge to the die was weighed accurately (the required weight being calculated from the density of the compact to be produced). The powder was gradually added to the die cavity which was progressively increased until all the powder had been added. The die cavity was varied by the use of spacing blocks which allowed compression of the springs which supported the die block- see Figure 3.3 .

The powder was "strickled" to the level of the upper surface of the die block, the spacing blocks removed and the top punch inserted. The load was applied slowly up to the required load, held for about ten seconds and then released. Ejection of the compact was achieved by inserting the spacing blocks which caused the die block to move down when load was applied, the bottom punch forcing the compact out from the cavity.

After compaction the test piece must be dewaxed under controlled conditions, otherwise the compacts would break up when introduced into the hot zone of a furnace at sintering temperatures due to the sudden volatilization of the zinc stearate lubricant. This treatment was carried out for one hour at 450°C in a tube furnace with a flowing gas mixture of 90% N_2 : 10% H_2.

3.2.2 Sintering

Three sintering treatments were carried out on the compacts, namely:

1) reducing atmosphere sinter in laboratory
2) vacuum sinter in laboratory
3) reducing atmosphere sinter in industry.

The reducing atmosphere sinter in the laboratory was achieved by using a laboratory tube furnace consisting of a nichrome tube externally heated by crucilite elements, the whole encased in refractory bricks, Figure 3.4 . The reducing atmosphere used was 90% N_2 : 10% H_2 gas mixture dried in a three stage drying train prior to entry to the furnace. The first stage of the drying train contained a hydrogen catalyst to remove oxygen, the second silica gel and the third magnesium perchlorate, the latter two substances being drying agents. An added precaution, to prevent sucking back of moisture into the furnace via the exit line, was

a drying tower containing silica gel. This preceeded a further tower containing water through which spent gas was bubbled. Gas flow was controlled by means of a flow meter, and although no quantitative control was applied, the flow was maintained at the same level for all sintering operations. The furnace was flushed out with the gas mixture by means of a high flow rate for a minimum of ten minutes before charging green compacts to the hot zone by drawing a boat containing the compacts along the tube by means of an attached wire (see Figure 3.4) . After sintering for one hour at 1120°C, the compacts were cooled to room temperature by drawing the boat to the water cooled zone of the furnace tube. The cooling period was forty five minutes, which enabled the sintered compacts to be removed from the furnace without any oxidation of the surface. A "good" sintering treatment was determined visually as one which yielded compacts with a bright surface finish and no discolouration.

The vacuum sinter in laboratory was carried out in a Scot-Vac vacuum furnace consisting of a water jacketed vacuum chamber lined with insulating material and heated by means of graphite elements. The compacts were placed vertically in an alumina crucible in the centre of the furnace on a graphite support. The furnace was evacuated by use of a rotary and diffusion pump until a vacuum of 0.133 Pa(10^{-4}Torr) was achieved and the heating was then turned on. A constant rate of heating was maintained up to the sintering temperature of 1120°C, and at no time did the vacuum fall below 1.067 Pa($8x10^{-4}$Torr) . After one hour at temperature the heating was switched off and the compacts were furnace cooled under vacuum. As with the reducing atmosphere sinter a "good" sinter was determined visually.

An industrial mesh belt furnace at a local company was used

to give the industrial reducing atmosphere sinter. The furnace used was a standard industrial type consisting of a pre-heating or "burn-off" zone held at 450-500°C, a sintering zone at 1120°C and a cooling zone. The compacts were loaded in a 'boat' and placed on the continuously moving mesh belt which took them through the furnace at a pre-determined rate, which was twenty minutes in the "burn-off" zone, forty minutes in the sintering zone and forty minutes in the cooling zone. Dewaxing of the compacts, prior to sending them to industry, was not necessary since this was carried out in the industrial furnace as part of the standard treatment. The atmosphere was endothermic gas produced by cracking methane gas over a nickel catalyst with air to give carbon monoxide and carbon dioxide, hydrogen and water. The carbon potential was controlled by controlling the CO : CO_2 ratio.

3.2.3 Post-sintering Treatment

Selected sintered compacts were heat-treated by austenitising for thirty minutes at 850°C in an argon atmosphere to prevent any decarburisation, followed by an oil quench, the oil being heated to 50°C. Tempering was carried out in an air circulating furnace for one hour at 200°C.

All compacts were then surface ground to a nominal thickness of 12.5mm and width of 25mm. Slight variations in these dimensions were sometimes necessary due to distortion of the compacts either during sintering or heat-treatment.

The specimens were then notched by milling, the notch depth being 8.5mm for specimens which were to be fatigue pre-cracked. A notch depth of 12.5mm was milled in some specimens used at the beginning of the programme in which a fatigue pre-crack was not used in order to determine the comparison in toughness between

milled notch and fatigue pre-cracked specimens. The milling cutter used had a cutting radius of 0.127mm.

The quantity of lubricant, sintering temperature and heat-treatment used throughout the work was chosen on the basis of the recommendations of the powder manufacturers.[43] Carbon additions were made in the first instance such that the content of the sintered or heat-treated compacts was 0.5%C. Since equipment was not available for carbon control during sintering, the proportion of graphite added to the Distaloy SA powder was 0.65%C to account for any loss incurred during processing of the powder, including any 'dusting' which may have occured during sieving due to the very fine nature of the graphite powder.

3.3 Fracture Toughness Testing

3.3.1 Outline of Test Proceedure

Documents consulted were A.S.T.M.E-399[52], B.S.D.D.3[102], B.S.5447[53] and B.S.2590[103].

The test piece blanks were surface ground to remove any distortion which may have occured during sintering or subsequent heat-treatment. A notch was then milled in the test piece and a fatigue crack introduced under three point bending with a controlled alternating load on an Amsler Vibrophore machine. When a crack of the desired length had been produced, knife edges were attached either side of the notch with adhesive. A clip guage was located on the knife edges and the test piece loaded in three point bending on an Instron universal testing machine. The outputs from both the clip guage and testing machine load cell were fed to an X-Y recorder to give a trace load vs. crack opening displacement (C.O.D.) . Adjustments to the sensitivity of the recorder were made so that the slope of the trace fell within

specified limits. After completion of the test, the fatigue crack length was measured accurately by inspection of the fracture faces using a travelling microscope.

The initial tests included tests on specimens without fatigue pre-cracking in which a notch was machined to a depth which represented the notch plus fatigue crack depth in other specimens. These test pieces were then tested in the same manner as outlined on the previous page.

The approach taken initially to the fracture toughness testing of sintered material was based on previous experience gained by other workers in this field[4,12]. Thus, experiments were carried out using the Linear Elastic Fracture Mechanics approach for fracture toughness testing. The use of the potential drop technique was well established by other research workers specialising in fatigue properties of various materials and this technique had been adopted for use with sintered materials successfully[7], despite difficulty encountered in the measurement of fatigue crack lengths due to the extremely rough nature of the crack faces. The method was to produce a number of specimens and fatigue pre-crack them to various lengths so that a calibration curve could be determined. The time consuming process of producing a number of specimens was circumvented in this work by the use of the method known as heat-tinting. The criteria laid down for a valid determination of fracture toughness was not met in all cases during initial testing of the sintered material investigated, although the invalid results were considered to be "borderline" between valid and invalid results or at worst, not far from the specifications. For this reason, reservations were held regarding the application of L.E.F.M. in

this work for the production of consistent results. Continual contact with other research workers specialising in fracture toughness investigations led to the adoption of the J-integral concept as a means of assessing the fracture toughness, a method now receiving much attention in the field of fracture mechanics to such an extent that it is considered it will be the one standardised method to be used for failure assessment in the near future. Consequently, the test proceedure was expanded and the displacement of the loading point was measured to give a load vs. load point displacement trace, in addition to the load vs. crack opening displacement trace, such that values of J could be calculated.

A small tensile test piece (dimensions as per B.S.2590) was machined from one half of the broken fracture toughness test piece and from this the yield and ultimate tensile strengths of the material were determined. The remaining half was available for examination of the fracture face, hardness determination and microstructural analysis.

3.3.2 Fatigue Pre-cracking

A test piece with a machined notch was set up in a three point bending in an Amsler Vibrophore fatigue machine, as shown in Figure 3.5 . When in operation this machine produces a loading frequency resonant with the natural frequency of the test piece. Measurement and display of both the static and dynamic loads occurs through an optical dynamometer system. The loads were set by lowering the upper part of the bending jig onto the specimen until the required load was obtained. Once this load had been set it was maintained constant since the crack lengths were comparitively short and relaxation of the load due to the specimen

bending as the crack grew did not occur to any great extent. A synchronous counter indicated the number of load cycles applied to the test piece. For any given test piece an alternating load was applied, cycling from zero to a maximum level. Since it was not within the scope of this work to determine crack initiation data, which can be extremely time consuming, the mean load was increased by small increments if a crack had not initiated after 10^5 loading cycles. Once crack initiation had occured the load was adjusted so that in general low loads were used for fatigue crack growth in order to ensure that low values of the ratio of fatigue stress intensity to fracture toughness resulted to comply with the relevent standard consulted.

3.3.3 The Test Proceedure

A test piece, which had been fatigue cracked and heat tinted, had knife edges fixed to either side of the notch with adhesive, at a predetermined distance apart, this distance falling within the linear range of operation of the particular clip guage to be used. The test piece was then placed on a three-point bending rig set on an Instron universal testing machine. During loading, the output from the clip guage was fed into the X-axis of a graph recorder and the load cell output of the testing machine was fed to the Y-axis. Adjustments to the sensitivilty of the crack opening displacement were made if necessary to ensure that the slope of the trace produced was within the specified range.

In the development of the testing proceedure, it was decided that the J-integral approach would be better suited as a measure of fracture toughness. Thus the displacement of the loading point was measured by a transducer and the output fed into an X-Y recorder

so that a load vs. load point displacement trace could be obtained. In this testing procedure it is necessary to be able to note the onset of crack extension and for this purpose the potential drop across the crack was monitored during testing the measurement being made in the manner described in Section 3.4, Crack Length Monitoring by Potential Drop Measurement.

The calculation of J was made from equation (20) . This requires the energy contributed by the uncracked ligament, or 'compliance' to be subtracted from the total energy, as measured under the load vs. LPD trace. For this purpose, beam (i.e. un-notched) specimens, at each density investigated were loaded on the testing machine. Measurement of the load vs. LPD of the beam specimens was taken, using the calibrated transducer to measure the displacement of the loading point. The slope of the resultant trace, measured from the line produced during the unloading cycle, gave a displacement/load, or compliance value.

The measurement of LPD vs. load was taken in conjunction with that of COD vs. load in order that the values of $K_Q J$ obtained could be compared with the values of K_Q obtained prior to J-integral analysis, and the test set-up is illustrated in Figure 3.6 .

After testing measurement of the fatigue crack length was made on a travelling microscope, and if the various validity criteria were met, the calculated value of K_Q was recorded as K_{IC} . Values of J and of $K_Q J$ were also calculated.

A small number of specimens which had not been fatigue pre-cracked were also tested. These test pieces had a notch depth of 12.5mm and the experimental procedure used was the same as that for fatigue pre-cracked test pieces described above.

3.4 Crack Length Monitoring by Potential Drop Measurement

3.4.1 Fatigue Pre-cracking

In early experiments the crack growth was monitored by viewing the surface of the test piece through a binocular microscope set horizontally. As an indication of the crack length, scribe lines were marked lightly, and away from the prospective crack path, on the surface of the test piece at three levels, that is, at the extreme limits of the allowed crack length (0.45W and 0.55W) and centrally between these limits. Subsequently a potential drop technique was used for the determination of crack growth since a continuous measurement of crack length could be made and crack growth data, although limited due to the overall short lengths of crack grown, could be generated.

In order to relate the potential drop vs. time trace produced by the potential drop technique to crack length, calibration of crack length vs. potential drop for test pieces of the nominal densities investigated i.e. 6.4, 6.6, 6.8 and 7.0Mgm^{-3} was required. For this purpose a specimen at each density was produced in the normal manner and scribe lines were marked at one millimeter intervals from the base of the notch. The notch was 8.5mm in depth since determination of potential drop vs. crack length was not required for fatigue cracks in specimens with notches shorter than this constant depth,as all the fatigue data was obtained from specimens to be used finally for fracture toughness testing.

Nichrome probe wires approximately 15cm long were spot welded on either side of the notch in a position which was kept constant for each specimen, as shown in Figure 3.7 . The specimen was then set in the three-point bending rig for fatigue pre-cracking as described previously. A constant current source was used to

obtain the potential drop across the notch, the cables from this source being connected to the test piece by means of a clamp at either end. The probe wires were connected to a chart recorder in parallel with a variable potential output which could be set in opposition to the potential across the notch in such a manner that the maximum sensitivity of the recorder could be used, that is, 50 microvolts full scale deflection in order to enable detection of very small changes in voltage. A schematic diagram of the equipment is shown in Figure 3.8 . The fatigue machine was then set in operation and,as a crack was produced,the potential drop increased and this was indicated on the trace from the chart recorder. By monitoring the crack visually as well as through a binocular microscope the approximate length could be judged by the scribe lines on the test piece surface. Once the crack length had reached the first scribe line i.e. was approximately one millimeter in length, the test piece was removed from the fatigue machine and placed in an air circulating furnace for approximately one hour at 220^{o}C (the exact time at temperature depended upon the density of the test piece since at lower densities oxidation of the uncracked material was possible due to interconnected porosity, and so the time was shorter than for the higher densities). The test piece was then replaced in the fatigue machine, the crack grown for another millimeter and heated again, and this process was repeated up to the final crack length required for calibration, which was just longer than the maximum required for the fracture test.

The test piece was then placed in liquid nitrogen and broken along the crack. The heat tinted portion could be seen as a series of bands of different colouration. The length of each band

was measured on a travelling microscope and for each crack length there was a corresponding potential which had been noted on the potential vs. time trace.

A graph was then plotted, which took the form Va/VoW vs. a/w where Va = potential drop across the notch plus the crack, Vo = p.d. across the notch, W = specimen width and a = crack length. Vo was measured across the notch and not on the specimen surface due to density variations which occur in sintered compacts and the possibility arises that the value of Vo taken from the surface can vary from one specimen to another despite them being the same overall density (see Section 3.6.2) .

During fatigue pre-cracking, the instrumentation and method of potential drop measurement was the same as described above for the calibration of crack length vs. potential drop.

3.4.2 Fracture Toughness Testing

To determine the onset of cracking during fracture toughness testing for the measurement of the J contour integral, potential drop measurement is also used. Calibration of the test pieces is required since it cannot be assumed that the point of increase in potential drop is the exact point at which crack extension occurs. This increase in potential drop could be caused by the separation of a few remaining points of conatct of the rough crack surfaces, despite most of the points of contact having been broken at the stage in the loading of a test piece where crack propagation will occur. Consequently this was investigated by producing a number of test piece blanks of one nominal density and testing them in slow bending with potential drop equipment for monitoring the crack extension. The set up for the measurement of potential drop was the same as that used during fatigue pre-cracking (see

Figure 3.8) . The test piece blanks were loaded up to various points on the p.d. vs. time chart, that is one up to the point of increase in potential, another up to a point 5μV after that, the next 5μV after that and finally another 5μV making a total of 15μV beyond the point of potential increase. After heat-tinting the test pieces were broken open to determine at which point crack extension had occured. Naturally, extremely small extensions of the crack were being looked for at the low levels of potential increase, but it was found that no distinction could be made between the fatigue cracked portion and extension of the crack which may have occured. This is thought to be due to the fact that the fatigue cracked portion, having been heat tinted twice and the crack extension once, does not produce a distinct difference in colouration or tone which is easily visible on the rough crack surface, which in itself makes this a difficult determination. For this reason the point of increase in potential was taken as the critical value at which crack extension occured since the corresponding load measurement taken during testing would be such that the resultant value of fracture toughness would be a conservative one rather than an overestimated one.

The instrumentation and method for potential drop measurement during the fracture toughness test was again the same as used during fatigue pre-cracking.

3.5 Mechanical Testing

3.5.1 Tensile Testing

The tensile test pieces produced from the broken fracture toughness test piece were tested on an Instron universal testing machine by using adaptors to accept Hounsfield No.14 tensile colletts in which the test piece was fixed. All tensile tests

carried out in this work employed the use of the constant crosshead speed of 0.01cm min^{-1} . The load during the tests was monitored by the built in chart recorder which allowed magnification of the crosshead movement by pre-selection of timing gears.

Elongation and percentage reduction in area were not measured from these tests since meaningful results were not expected from the small test pieces used.

No clear yield point was exhibited by this material and the yield stress was taken as the stress at the first deviation of the trace from elastic behaviour.

3.5.2 Determination of Young's Modulus

The Young's modulus of the material investigated was determined from test pieces compacted in a die of standard specifications[103] and sintered to densities of 6.4, 6.6, 6.8 and 7.0Mgm^{-3} . After fitting in the wedge grip jaws of a tensile testing machine, an extensometer, previously calibrated, was attached to the test piece such that its arms were set at a distance apart which spanned the guage length. The output from the extensometer was fed into the X-axis of a graph recorder via an amplifier and the load cell of the tensile machine to the Y-axis in order to produce a trace of the load vs. extension of the guage length. The test piece was then loaded in tension to a level which was approximately one half of the yield stress of the material at the density being investigated, the loading was halted for approximately thirty seconds to allow the trace to settle into a steady position and then unloaded. This process was repeated five times at each density investigated. The Young's modulus was then calculated from the slope of the trace produced during the unloading of the test piece, since the trace produced during

loading could contain components due to the wedge grip jaws "biting" into the test piece or the extensometer settling into position.

3.6 Metallography

3.6.1 Preparation of Metallographic Specimens

The true pore structures present in sintered materials can be difficult to examine due to flow of the metallic matrix into the pores during polishing. To overcome this, samples were ground on silicon carbide grinding discs down to the finest "grit" size, P1200 . They were then deeply etched in 4% Nitric acid in alcohol and washed thoroughly in alcohol and dried. The specimens were subsequently submerged in a cold setting resin ("Araldite 778") and placed in a dessicator which was evacuated by means of a water aspirator. This evacuation caused air to be removed from the pores and on readmitting air to the dessicator the resin was forced into the pores. The resin was then allowed to harden and the specimen re-ground lightly on the fine grinding disc to reveal the surface of the sample and finally polished on 6μ and then 1μ diamond polishing wheels. All metallographic work was carried out in this manner.

3.6.2 Measurement of Density Variation

Sections through the fracture toughness test piece, and near to the fracture face, were mounted as for metallographic examination and polished. The surface of the specimen was then viewed on the Quantimet B Image Analysing Computer. This instrument can be set to detect either black or white phases, and by adjustment of the threshold control can be used to determine the amount of any discriminated phase. The accuracy is very dependent on the ability of the operator to determine when the total area of the

phase to be measured is being detected. Once this threshold value is set, it need not be adjusted and on moving to a different field only adjustment to the focus may be needed. The measurements taken were the areas due to pores in fields of one square millimeter over the total surface of the specimen. The results of each percentage area of pores were recorded such that their positions corresponded to those on the specimen.

Area readings were converted to density (100-area %) and averaged into $4mm^2$ blocks, as shown in the simplified diagram, Figure 3.9 . The density was plotted against distance for each horizontal set of readings over the specimen surface, producing a "smoothing curve" for each row of density values, as in Figure 3.10 , the graph being divided into 2% relative density intervals as shown. The density contours were then drawn from these curves by transferring the density value read from the curve to a drawn grid which represented the specimen surface, and boundary, or contour, lines drawn to enclose areas representing one of the 2% density intervals, as in Figure 3.11 .

These density contours represent imaginary boundaries separating adjacent areas of differing density ranges. During their construction it was assumed that densities along any section must form a continuous range. This means that narrow regions beyond the resolution of the method must be drawn in between areas which do not have a common boundary. An example is shown in Figure 3.11 , by the line x-x . The narrow regions of B dividing A and C are beyond the resolution of the method, however, they must exist since A (88-90%) and C (84-86%) have no common boundary.

3.7 Microscopy

Microscopical examination of specimens, prepared as described in Section 3.6.1 , was carried out in both the etched and unetched conditions, and photomicrographs were taken using a Reicheart MeF optical microscope system. Examination of the pore morphologies and structural details was carried out at high magnification on a scanning electron microscope (SEM) . The particular instrument used had an energy dispersive X-ray analysing attachment, which allowed direct analysis of the specimen, as viewed on the screen, by detection of the X-rays emitted from the specimen surface. Additional preparation of the metallographic specimens was required prior to examination on the SEM, viz, a gold coating was deposited on the specimen surface, in a vacuum coating unit, in order to render the mounting resin conducting and to disipate the heat caused by the impingement of the electron beam.

Fracture surfaces were viewed directly on an SEM since the depth of focus afforded by this instrument made it possible to view the considerable variation in topography associated with the fracture of sintered materials. Both fatigue and fast fractures were examined in order to assess the fracture mechanism dominant in each case.

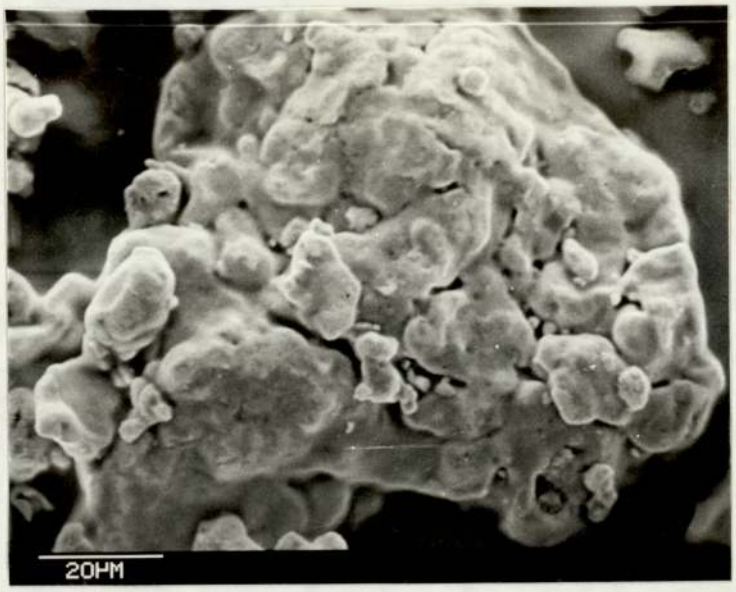

(a) Powder particle

(b) Nickel X-ray map

Figure 3.1 : Typical powder particle (continued over)

(c) Molybdenum X-ray map

(d) Copper X-ray map

Figure 3.1 : continued.

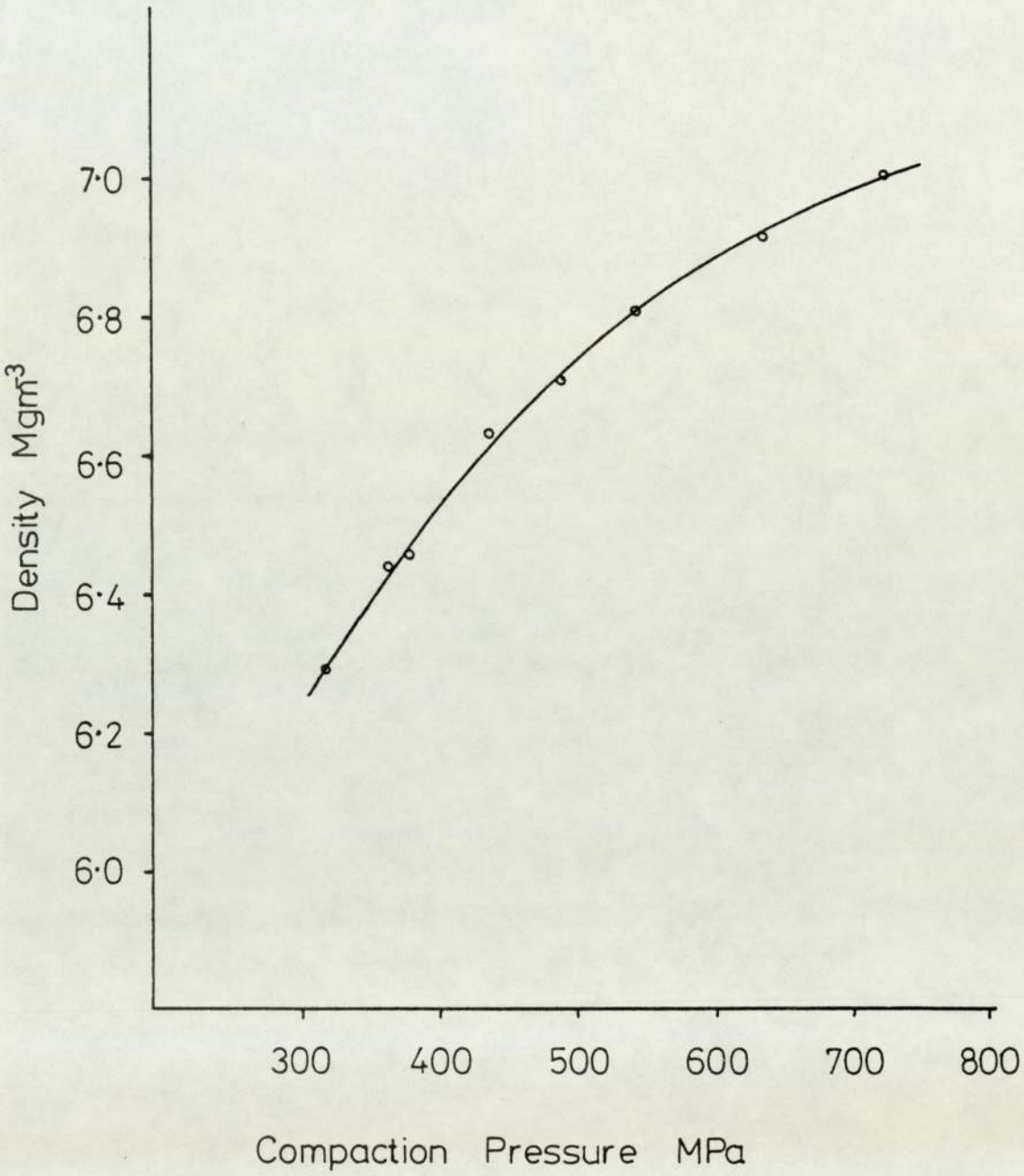

Figure 3.2 : Pressure/density curve

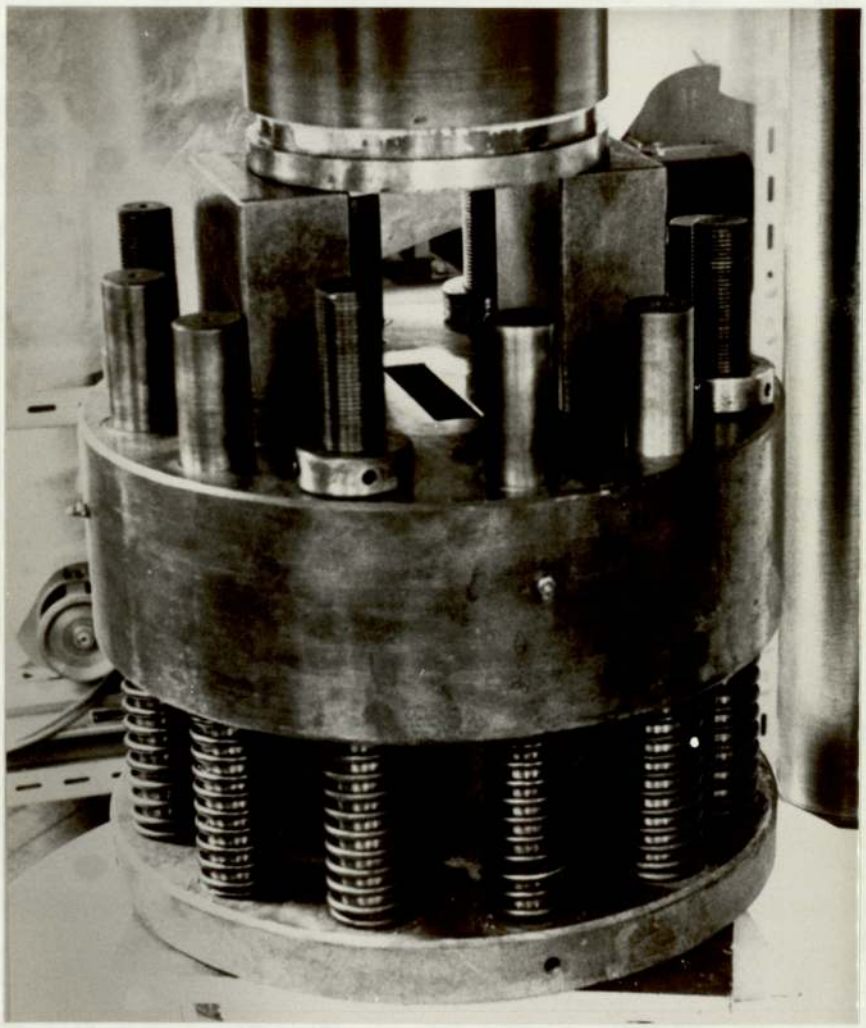

Figure 3.3 : The die set

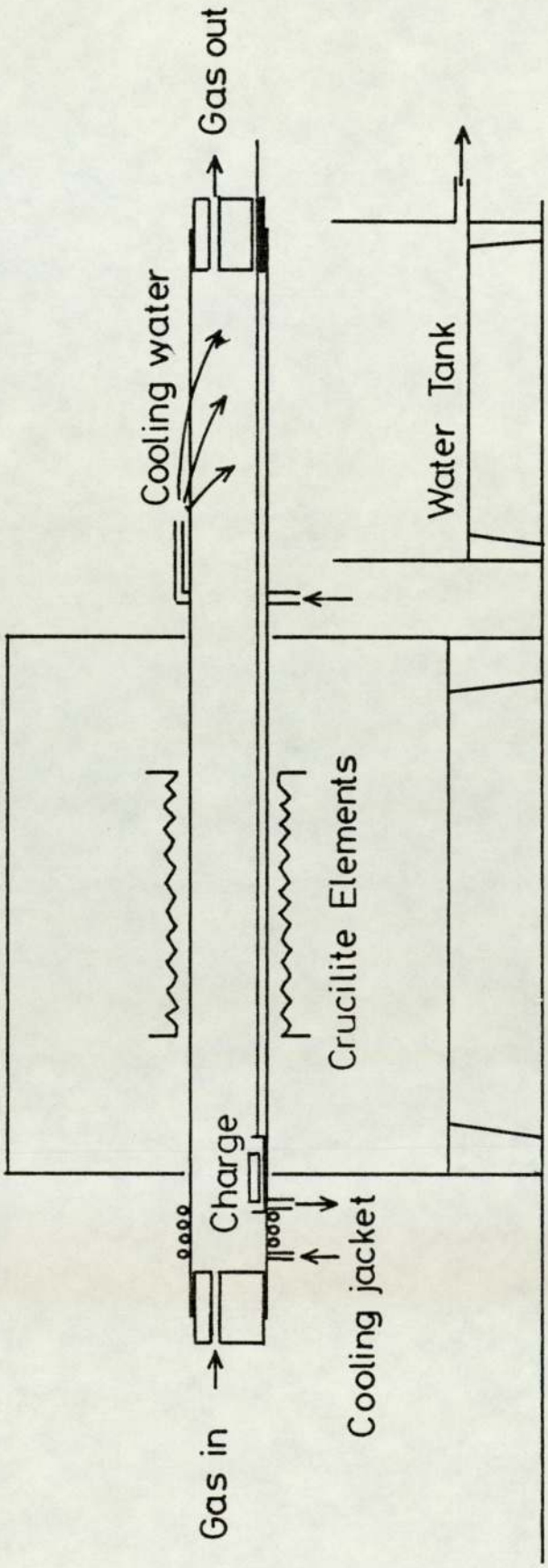

Figure 3.4 : Laboratory tube furnace

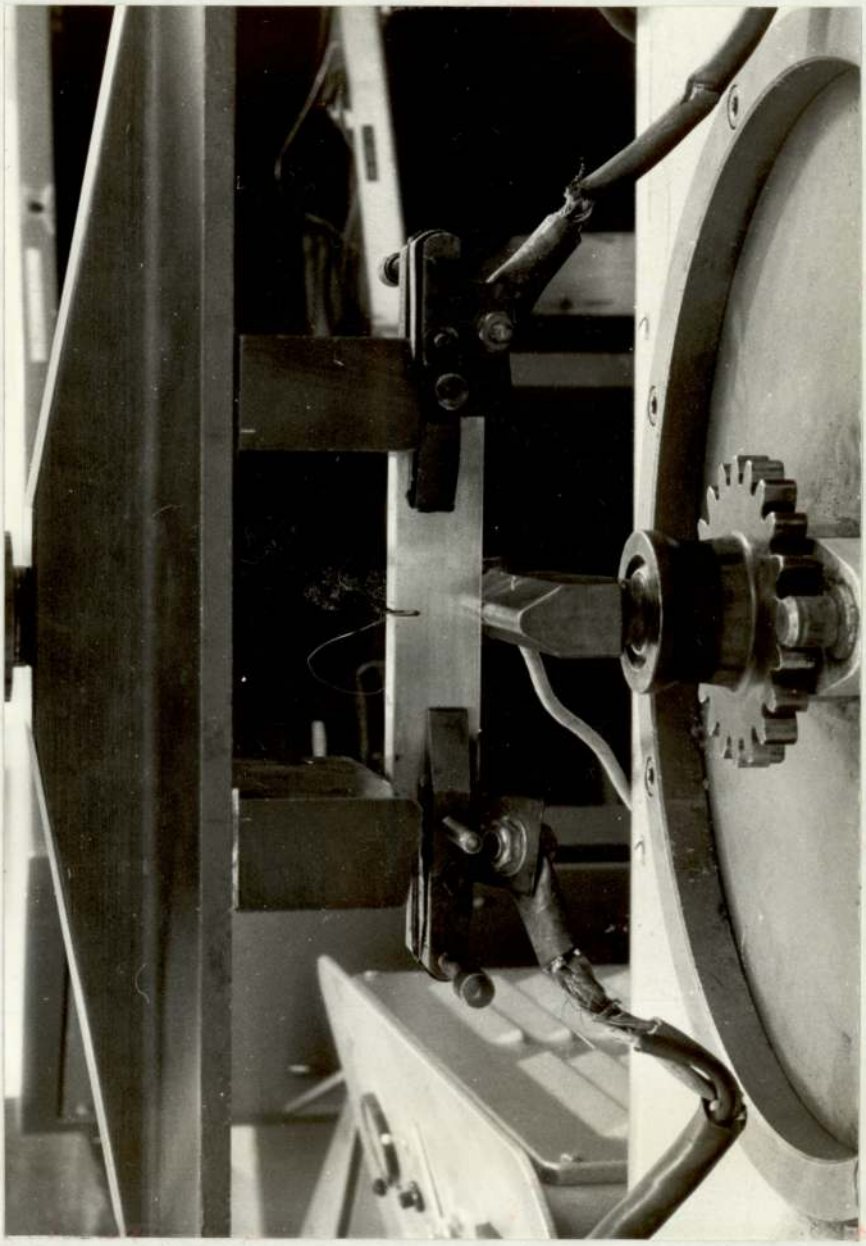

Figure 3.5 : Fatigue pre-cracking test set-up

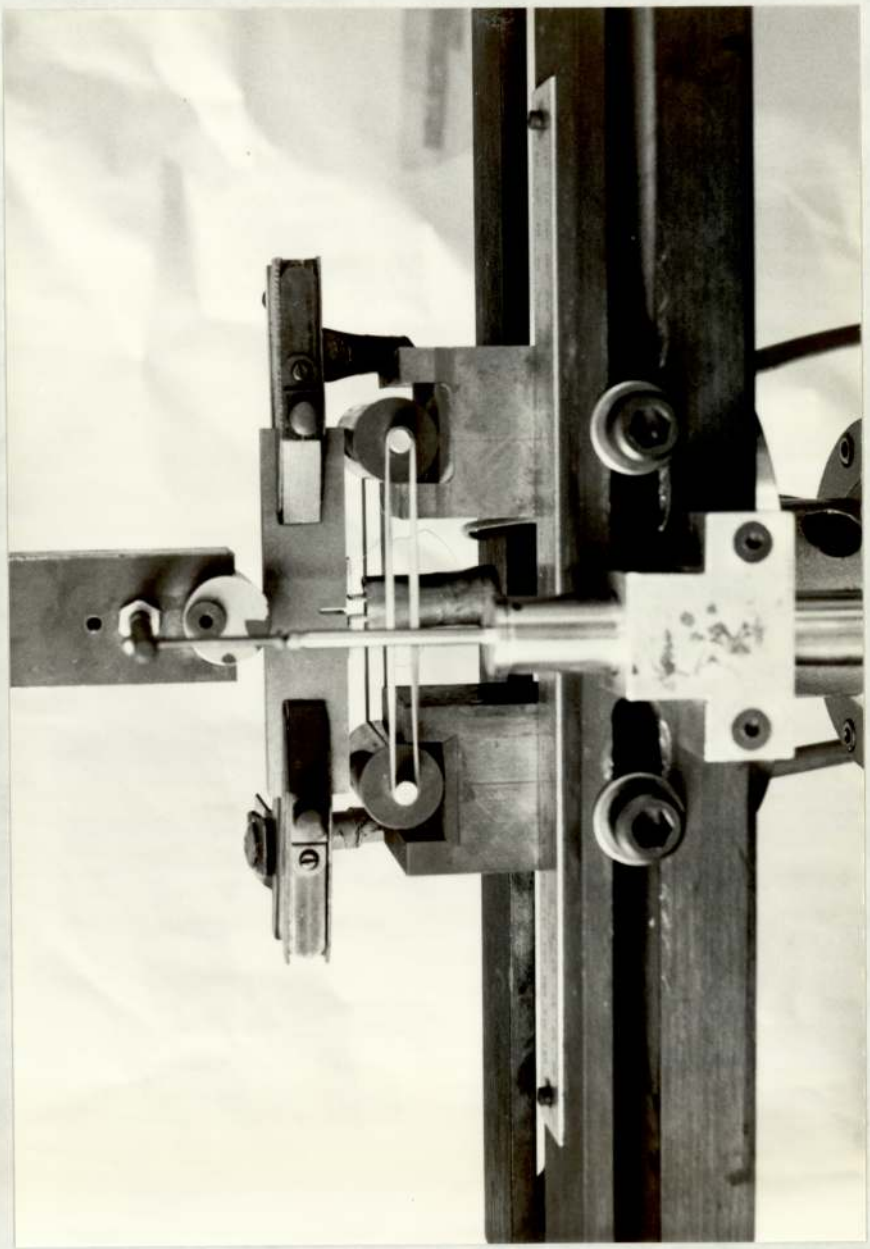

Figure 3.6 : Fracture toughness test set-up

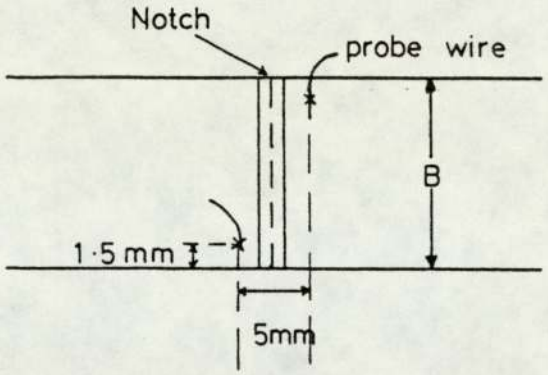

Figure 3.7 : Position of potential drop probe wires

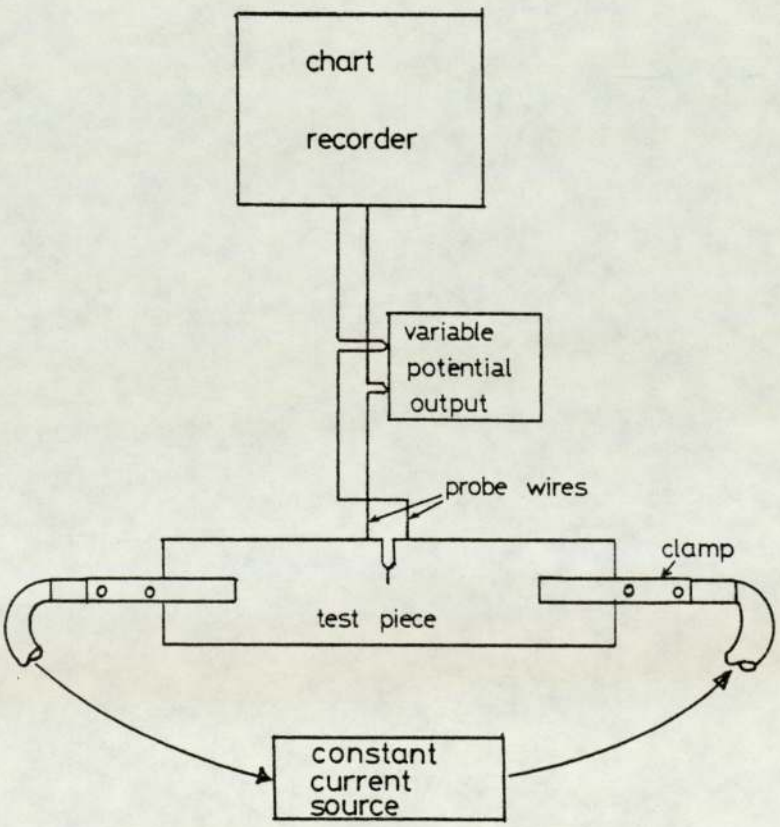

Figure 3.8 : Schematic representation of potential drop measurement

89·5	87	89	90	86	89	X
87	87	84·5	85	86	87·5	O
89	86·5	89·5	89	87	89·5	□

Figure 3.9 : Percentage density on $4mm^2$ grid

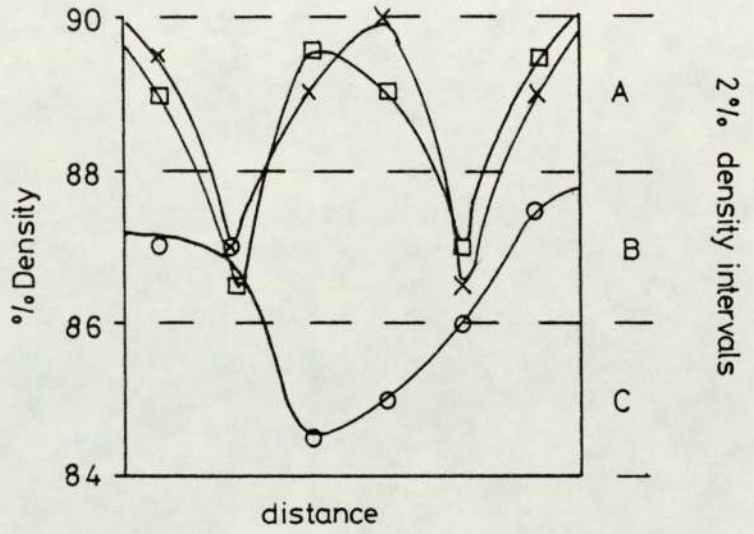

Figure 3.10 : Smoothing curve

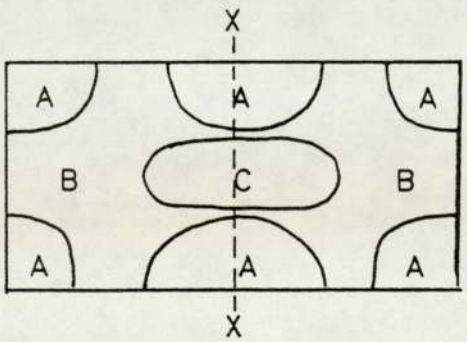

Figure 3.11 : Density contour map

4. RESULTS

4.1 Variables

The ranges of variables studied are summarised in tabular form below, Table 4.1 :

Variable	Range
Carbon content	Nominal 0.5%
Density, Mgm^{-3}	6.4; 6.6; 6.8; 7.0/7.1
Sintering treatment	Laboratory, N_2 / H_2; Laboratory, vacuum; Industry, endothermic atmosphere.
Heat-treatment	30 mins. at 850°C in argon-oil quench. Temper for 60 mins. at 200°C in air.
Notch	Milled; milled + fatigue crack.

Table 4.1 : Range of Variables Studied.

4.2 Analyses

The chemical analysis, oxygen content and hydrogen loss results are set out in Table 4.2 , with the values as quoted by the manufacturer for comparison.

Broken fracture toughness test pieces, of similar density, were selected at random from batches produced by the three different sintering treatments, and small samples cut from near the fracture faces. The oxygen contents of these samples were determined. Duplicate determinations gave the average results presented in Table 4.3.

All oxygen determinations were made with a Balzer Exhalograph apparatus.

Analysis of carbon content was carried out on a sample from each sintered batch of test pieces. A combined carbon content of 0.5% was aimed for, and all analyses gave results within the range 0.47-0.52% C .

4.3 Mechanical Properties

For convenience, results are presented mainly in graphical and pictorial form, with some tables. As discussed elsewhere, regular developments in testing techniques resulted in a move from the linear elastic (K_{IC}) to J integral approach, and coupled with difficulties in interpretation of test results at the beginning of the programme, limited the amount of useable data generated. However, each batch of test pieces was studied in considerable detail and the information recorded.

Three sintering treatments were studied, namely, reducing atmosphere in a laboratory tube furnace, reducing atmosphere in an industrial mesh belt furnace and vacuum sinter in a laboratory furnace. The time and temperature of sintering were very similar in each case, but the rate of cooling from the sintering temperature depended on the mode of operation of the particular furnace, and differed in each case. With the type of alloy being examined, cooling rate would have had an effect on the structure, and hence the mechanical properties of a compact (see Section 2.1.2) . Thus the physico-chemical effects of the different sintering treatments on, for example, fracture toughness could not necessarily be compared directly. Also, relationships between density and mechanical properties could only be compared in samples which had been sintered in a particular manner.

As expected, the hardness increased with density as shown in Figure 4.1 . The anticipated large degree of scatter, highlights the problems of obtaining reproducible values of indentation hardness from materials containing porosity. Hence, definite differences in hardness between the three sintering treatments could not be detected, and the values appear to be of the same

order at any given density. Only the heat treated samples show a definite difference, having significantly higher values.

The yield stress and maximum stress increased with increasing density for all sintering treatments investigated, including heat treatment, as shown in Figures 4.2 and 4.3 respectively.

Determination of Young's Modulus at various densities gave the results presented in Table 4.4, which includes, for comparison, a value for wrought material of the nearest equivalent composition. A plot of Young's modulus vs. fractional porosity on a logarithmic scale, including the wrought material to represent zero porosity, resulted in the linear relationship shown in Figure 4.4 . A regression analysis of the data from Table 4.4 resulted in the following equation relating Young's modulus, E , and fractional porosity, ε :

$$E = 209\ (1-\varepsilon)^{3.54} \qquad (28)$$

The relationship between toughness, K_Q and test piece density is given in Figure 4.5 . The values quoted for toughness do not precisely fit the criteria to correspond to the minmum critical value, namely K_{IC} , since in most cases the ratio P_{max} / P_Q exceeded 1.10, but was generally within the range 1.15 to 1.35. This could be viewed as reasonably close to the requirements, such that each K_Q value would be close to the critical value, K_{IC} .

The compliance of specially prepared beam specimens was measured, and from the values obtained, the dimensionless constant CEB (where C compliance, E Young's modulus and B specimen thickness) was calculated. Table 4.5 presents the compliance values at the four densities investigated, and the resultant

constant, CEB . The averaged value of CEB was then used to determine the compliance at any specimen density for calculation of the proportion of the total displacement energy contributed by the uncracked ligament. Hence, U_{crack} was evaluated from the area under the load vs. load point displacement trace and J was calculated from equation (20) .

Values of J were converted to fracture toughness, $K_Q J$, values using the expression:

$$K_Q J = \sqrt{\frac{JE}{(1-\nu^2)}} \qquad (29)$$

The relationship between fracture toughness, $K_Q J$, and density is given in Figure 4.6 . A limited number of test pieces yielded valid K_{IC} results and these values are included in Figure 4.6 . Some test pieces were tested without pre-fatigue cracking, and the fracture toughness results were found, within experimental error, to be the same as those which had been fatigue pre-cracked. Therefore, the values obtained were used to construct Figures 4.5 and 4.6, and are indicated in the diagrams.

The relationship between fracture toughness, $K_Q J$ and K_{IC} , and yield stress is given in Figure 4.7 . K_Q values were not used, since they were not comparable to the few K_{IC} values obtained (cf Figures 4.5 and 4.6).

A number of load vs. COD traces were rejected, since 'bowing' of the curve was evident, as shown scematically in Figure 4.8. This effect, when observed, was noted to occur to a greater degree in specimens of low density ($6.4 Mgm^{-3}$) than in those of high density, where the effect, if present, was barely detectable.

The data used to prepare Figures 4.1, 4.2, 4.3, 4.5, 4.6 and 4.7 from specimens sintered in laboratory, sintered in laboratory and heat treated, sintered in industry and vacuum sintered in laboratory, is given in detail in Tables 4.6 to 4.9 respectively, the results being grouped in order of ascending density.

4.4 Fatigue crack Propagation

The length of a crack, grown from the machined notch in a test piece, was related to the potential drop by the method described in Section 3.4.1 . The data obtained from the 'calibration' specimens is given in Table 4.10 . From this data the calibration curve, shown in Figure 4.9 , was plotted.

Values of potential were taken at set intervals from the traces of p.d./time obtained during fatigue pre-cracking. Since the number of cycles is noted during the test, the time scale can be converted into the number of cycles of fatigue loading relating to a given increase in p.d., that is, the crack length. A computer programme, which incorporated the calibration curve expressed as an exponential function, was available to calculate the change in crack length for a change in the number of fatigue cycles, da/dN . The corresponding change in stress intensity, ΔK , for each change in crack length, was calculated from the applied load using the equation:

$$\Delta K = \frac{PL}{BW^{3/2}} f(a/w) \qquad (29)$$

where P is the applied load and f(a/w) is given in Table 2.3 . Fatigue crack propagation data was plotted, on a logarithmic scale, from the resulting values of da/dN vs. ΔK . Regression analysis of the data produced the results shown in Figure 4.10 . These

straight lines can be represented by the Paris-Erdogan equation (see equation (25)), from which the constants, C , and growth exponents, n , were determined and these are given in Table 4.11.

A minimum of forty plotted points were used to represent the fatigue crack propagation results, with the exception of the heat treated samples at a density of $6.4 Mgm^{-3}$, for which only twenty seven points were used.

4.5 Density Variations

The variations in density across sections cut from near the notch of several test pieces, were studied, using a Quantimet instrument. The distributions in test pieces of a certain Archemedian density were similar, and 'averaged' maps are presented in Figure 4.11 .

4.6 Metallographic Observations

The main observation from microscopical examinations is to acknowledge the pore morphologies and the complexity of the structures in the sintered low alloy steel. It was decided to record, in as much detail as possible, the pore morphologies and structures observed, to allow possible interpretation at a later stage, when more information was available. There was no immediately apparent differences between the pore morphologies and structures produced by the various processing schedules at a given final density. Thus the pore morphologies, Figure 4.12 , and structures, 4.13 , indicated on these micrographs are typical. The structure of the heat treated material is shown in Figure 4.14 .

The pore morphologies were examined in greater detail, on a scanning electron microscope (SEM) . Of particular interest were the minimum radii present in the corners of irregularly shaped pores. Again, specimens produced by the various processing schedules were

examined, and no differences were apparent at the resolution available. The micrographs presented in Figure 4.15 show typical pore morphologies. The structure of the matrix surrounding the pores can be seen in detail in these micrographs. High resolution micrographs of particular structural features were taken on the SEM, and are shown in Figure 4.16 . It was realised that an "in depth" analysis of the structures and attempted linking with mechanical properties was outside the scope of this present work.

4.7 Fractography

Numerous fracture faces were examined in detail by scanning electron microscopy. At the resolution available, there was a basic similarity between the fracture faces produced either by fatigue pre-cracking or during fracture toughness testing (fast fracture) , in test pieces with various processing histories. A fractured test piece is shown in Figure 4.17, and Figure 4.18 illustrates the typical features of the fracture faces from various test pieces.

Again, it was not feasible, in the time available, to make a detailed study of the fracture faces.

Source	Chemical analysis %			Hydrogen loss %	Oxygen content %
	Ni	Mo	Cu		
Laboratory determination	1.53	0.46	1.62	0.18	0.35
Hoganas[43]	1.75	0.50	1.50	0.10	-

Table 4.2 : Analysis of Distaloy SA powder.

Sintering treatment	Oxygen %
Industry, endothermic atmosphere.	0.35
Laboratory, N_2 / H_2	0.25
Laboratory, vacuum	0.22

Table 4.3 : Oxygen contents of sintered test pieces.

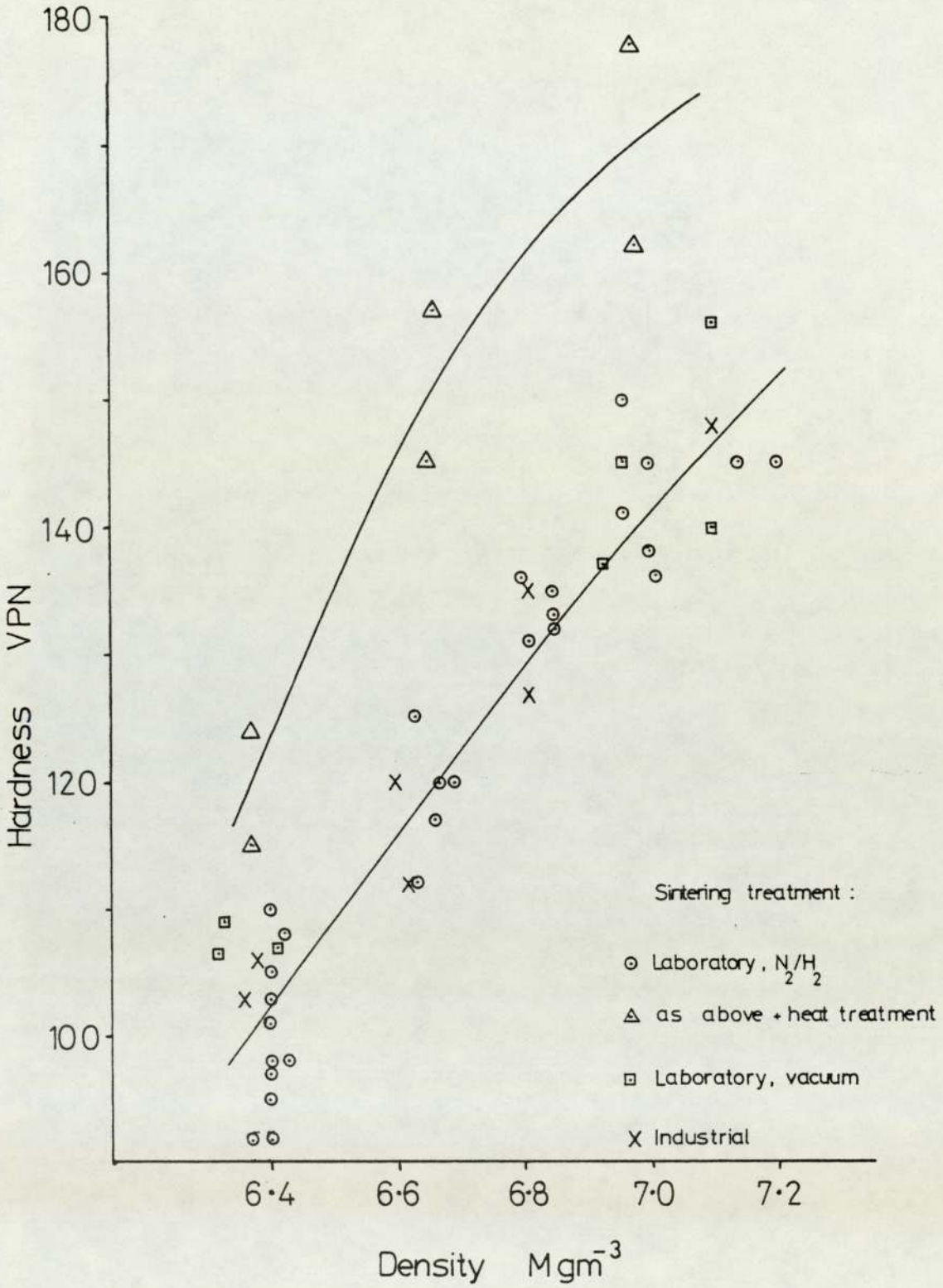

Figure 4.1 : Relationships between hardness and density

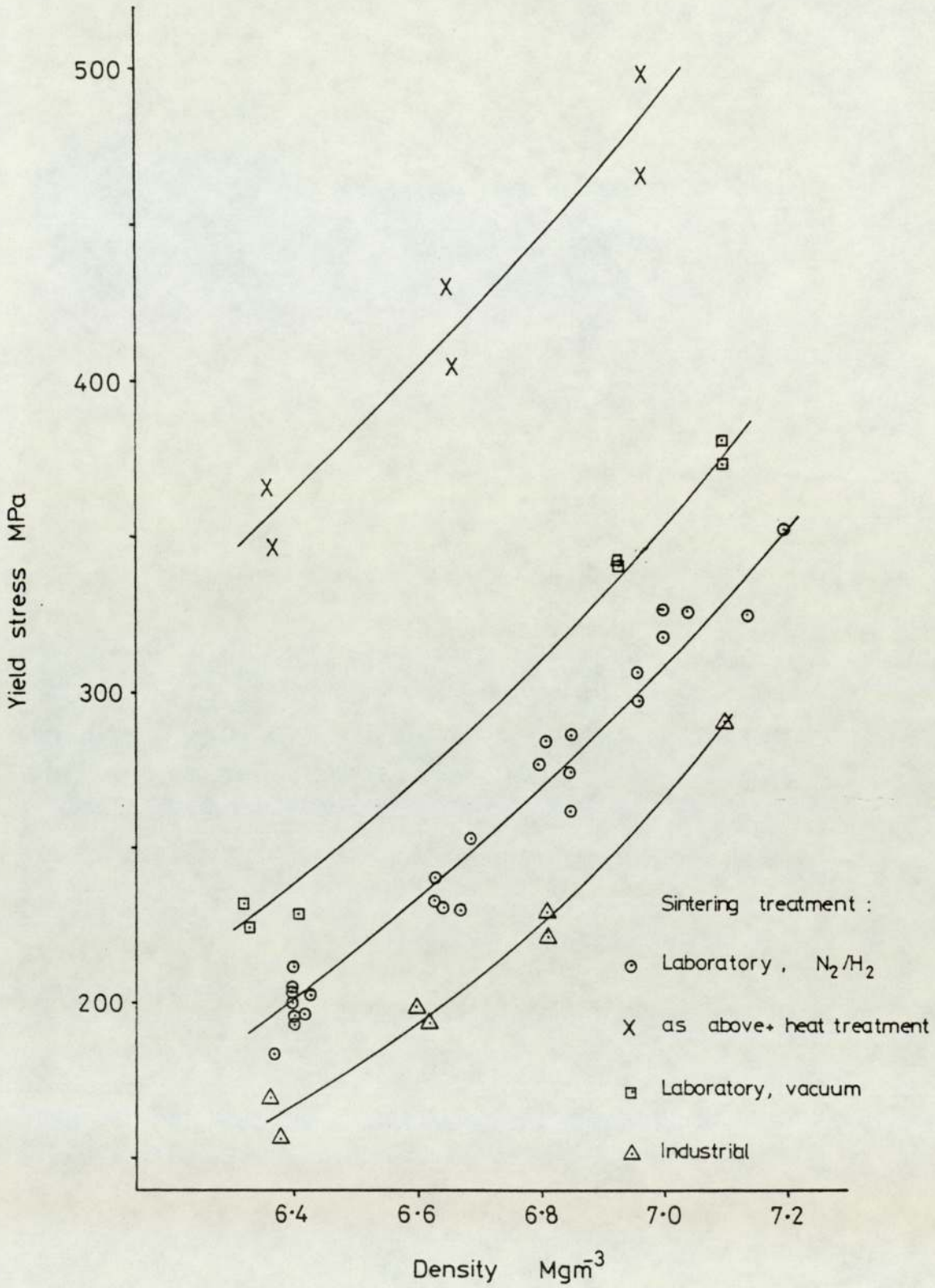

Figure 4.2 : Relationships between yield stress and density

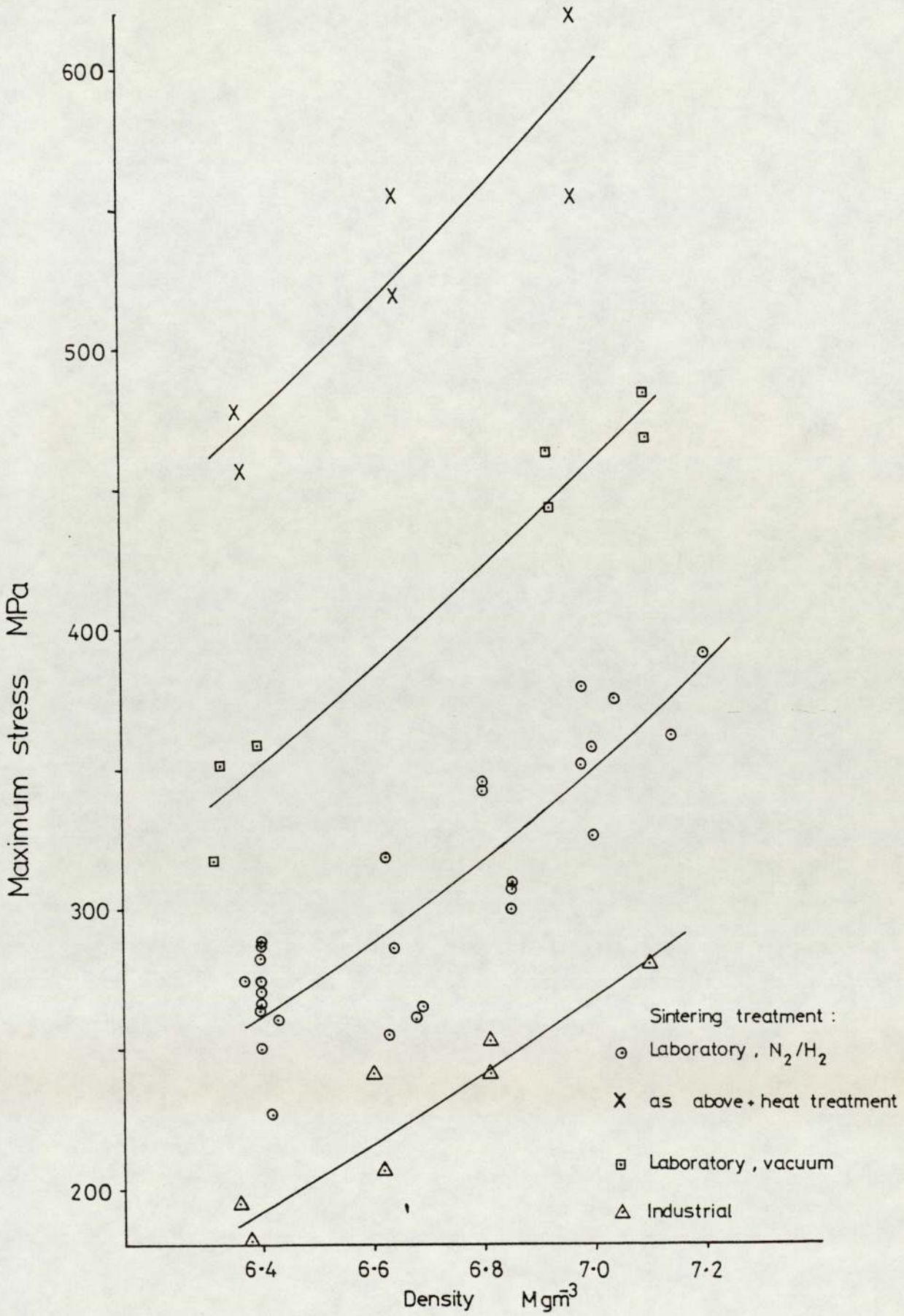

Figure 4.3 : Relationships between maximum stress and density

Density Mgm^{-3}	6.4	6.48	6.57	6.65	6.71	7.01	7.87
Fractional porosity	0.191	0.181	0.170	0.160	0.146	0.114	0
Young's Modulus GPa	94	101	108	118	120	136	207

Table 4.4 : Effect of density on Young's Modulus.

Density Mgm^{-3}	Compliance,C $mN^{-1} \times 10^{8}$	Young's Modulus,E GPa	Thickness,B m	C.E.B.
6.43	2.429	100	0.01201	29.17
6.65	2.159	113	0.01220	29.76
6.81	1.933	123	0.01220	29.01
6.99	1.863	135	0.01215	29.98
			Averaged value of C.E.B. =	29.48

Table 4.5 : Effect of density on compliance, C .

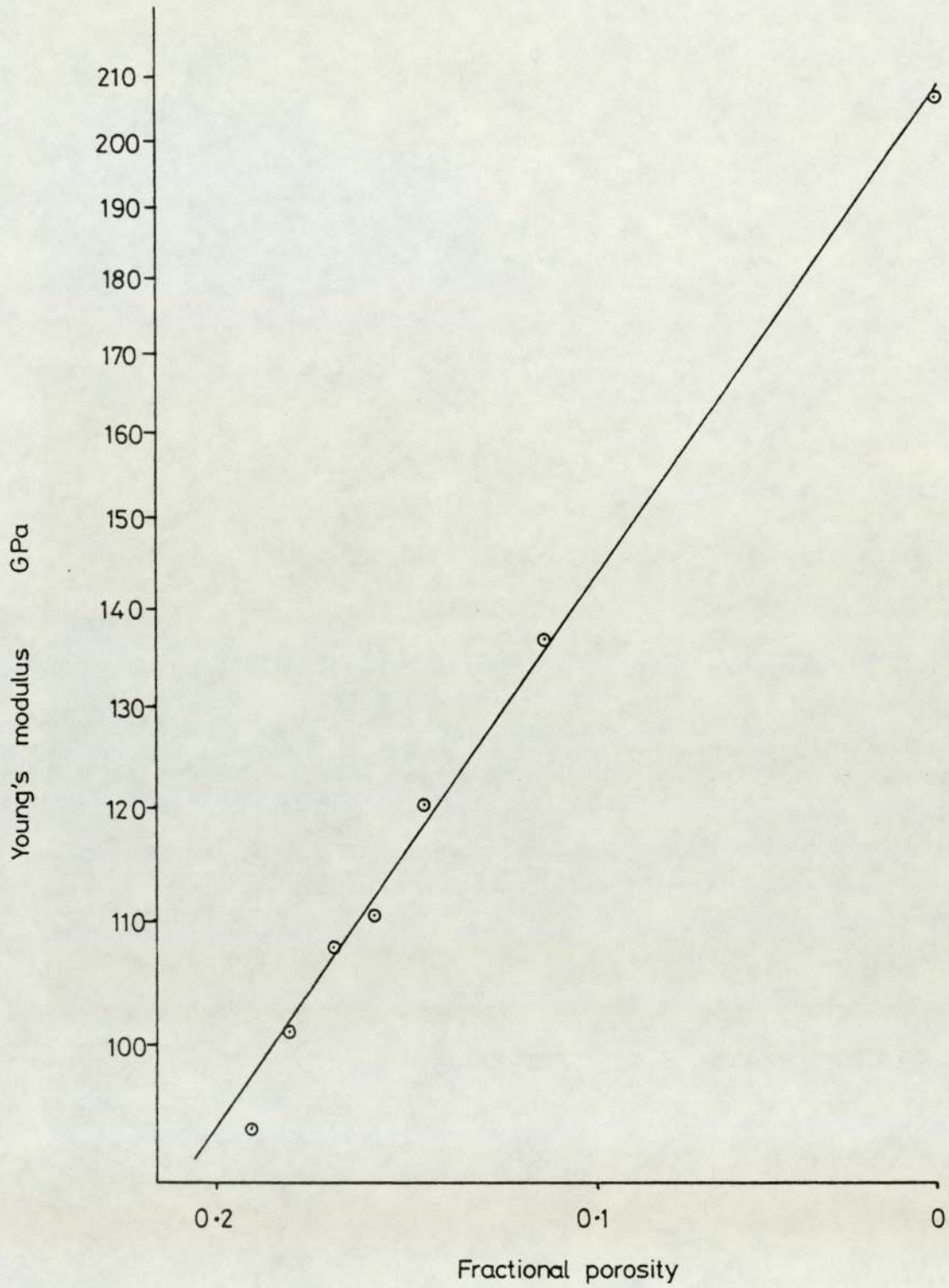

Figure 4.4 : Relationship between Young's modulus and fractional porosity

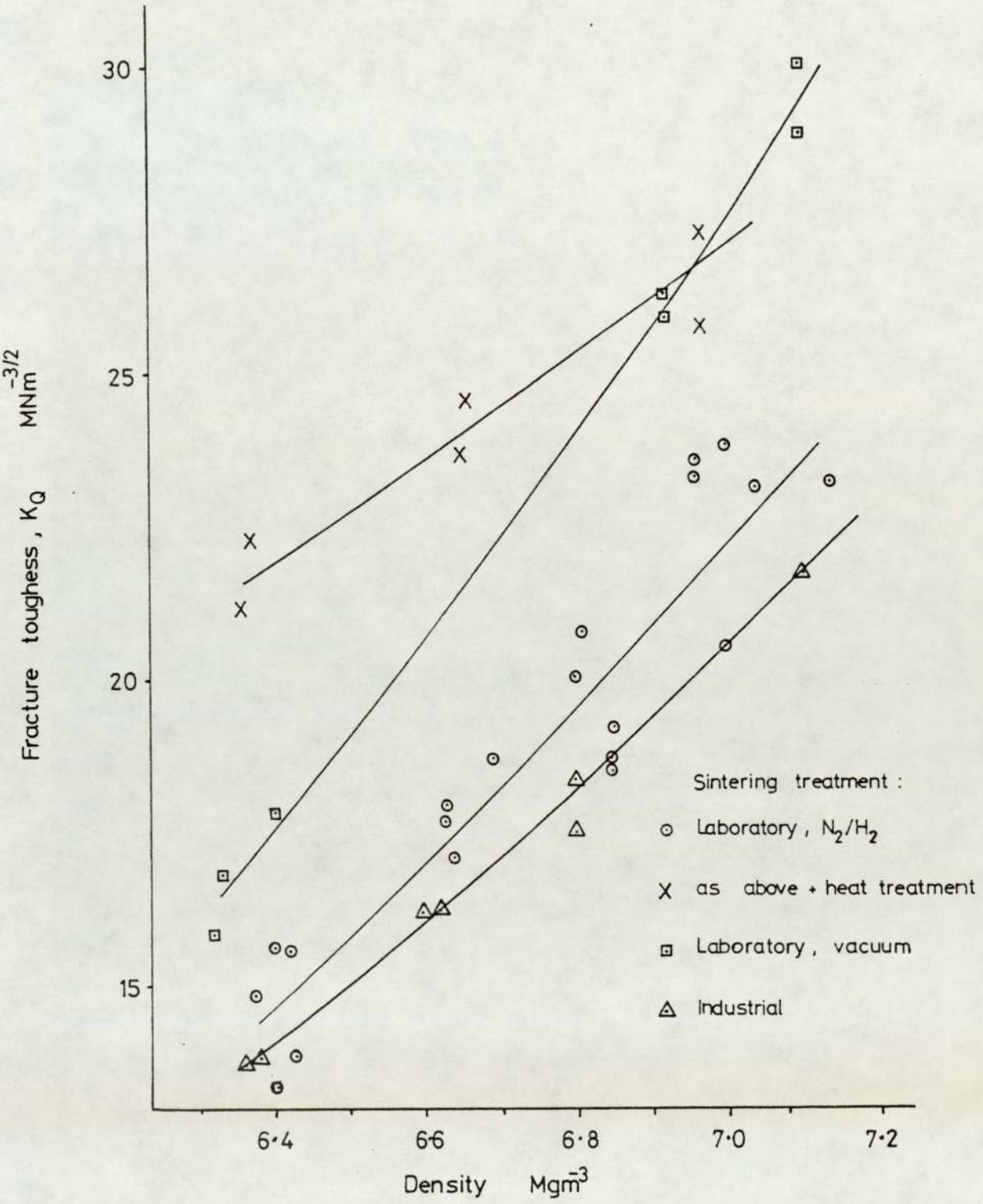

Figure 4.5 : Relationships between fracture toughness, K_Q , and density

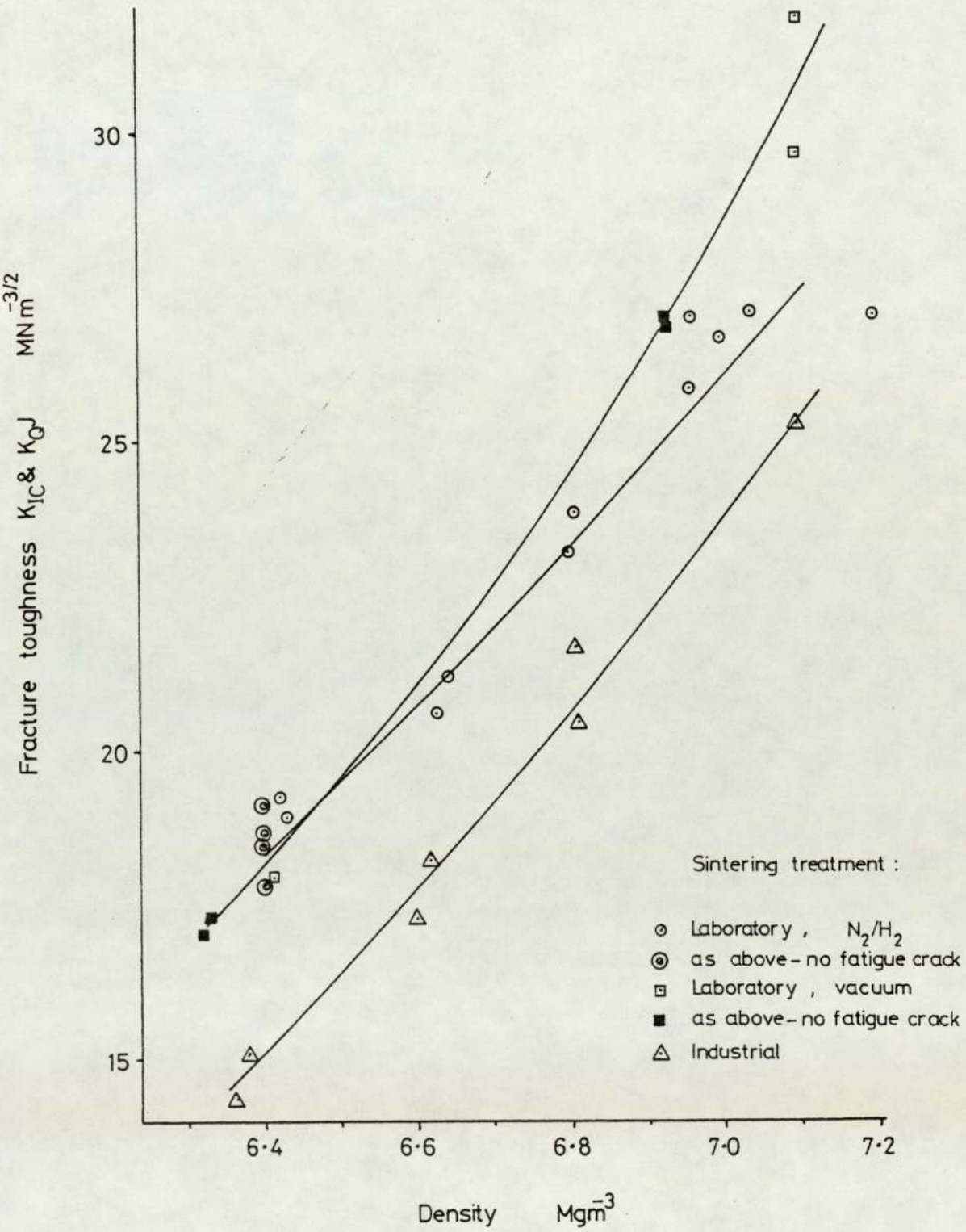

Figure 4.6 : Relationships between fracture toughness, K_{IC} and $K_Q J$, and density

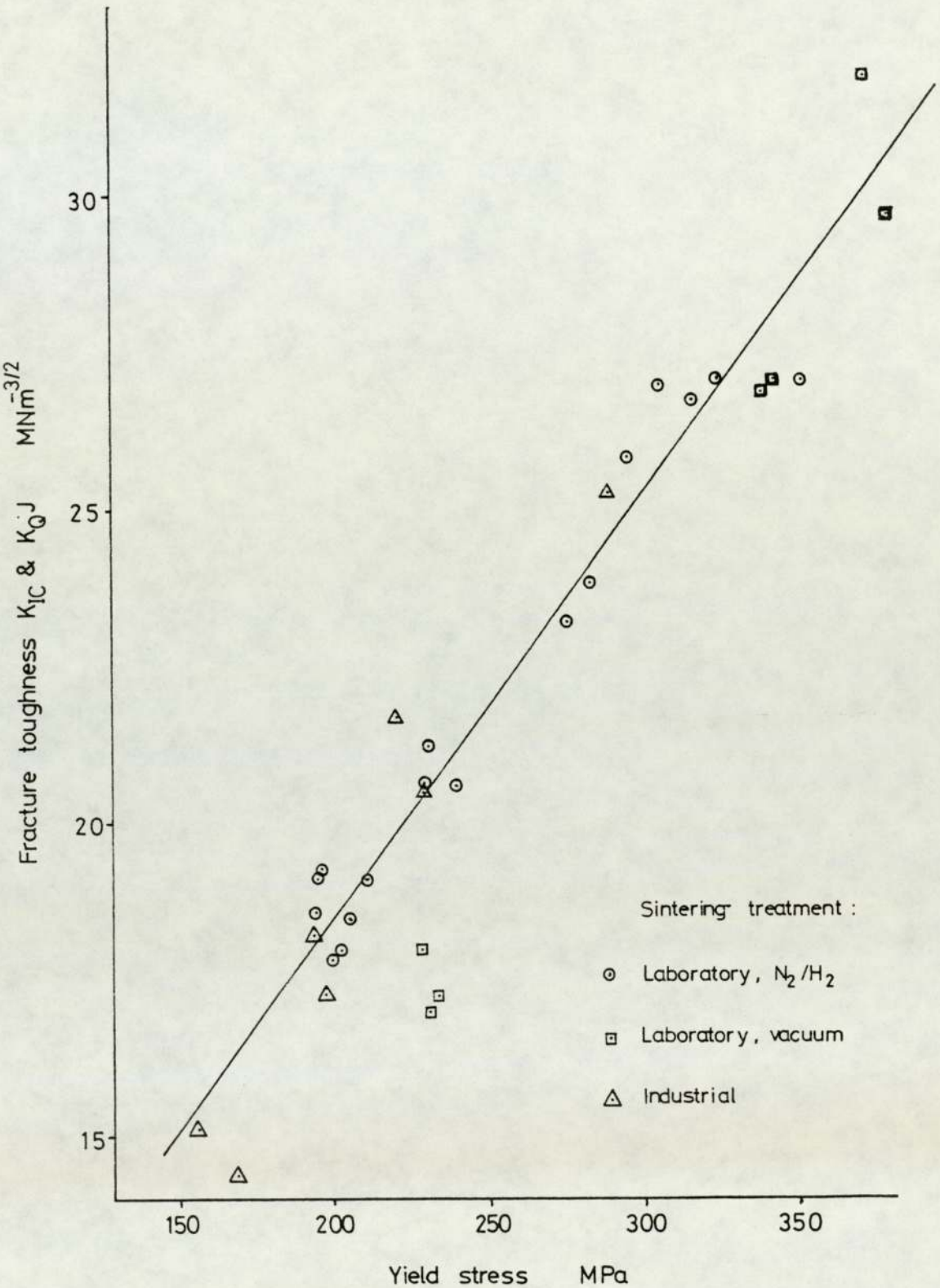

Figure 4.7 : Relationship between fracture toughness, K_{IC} and $K_Q J$, and yield stress

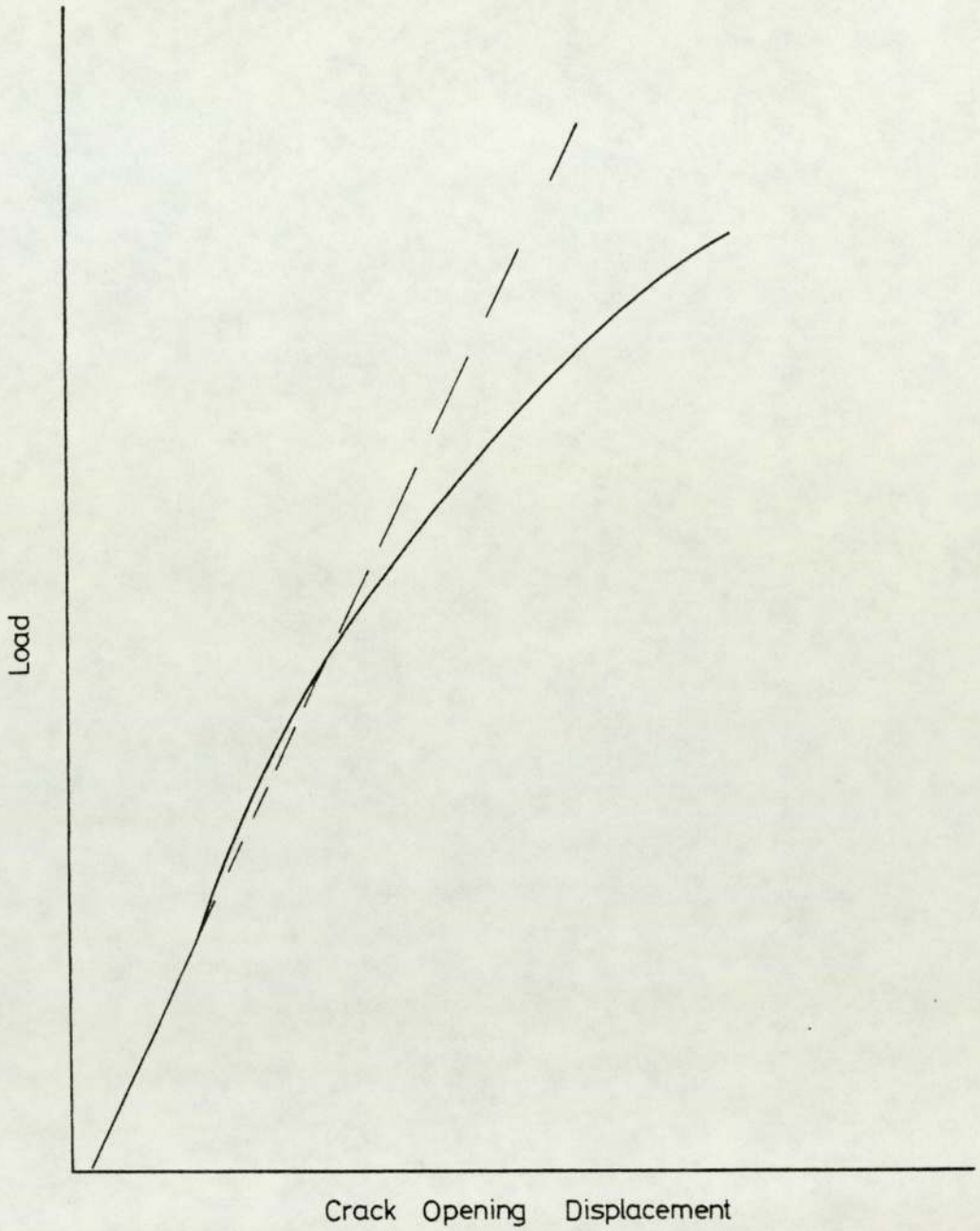

Figure 4.8 : Schematic bowing of load/crack opening displacement trace

Test piece number	Density	Fracture Toughness			Yield Stress	Maximum Stress	Hardness
		K_Q	K_QJ	K_{IC}			
	Mgm^{-3}	$MNm^{-3/2}$	$MNm^{-3/2}$	$MNm^{-3/2}$	MPa	MPa	VPN
40	6.37	14.78	-	-	184	274	92
12	6.40	15.63	-	-	203	267	97
13	6.40	13.31	-	-	212	289	103
43	6.63	17.91	-	-	233	255	112
55	6.69	18.72	-	-	252	265	120
1	6.85	19.17	-	-	261	299	132
2	6.85	18.69	-	-	274	309	135
4	6.85	18.53	-	-	285	307	133
5	7.00	20.41	-	-	326	346	138
36	7.14	23.14	-	-	324	362	145
19	6.40	-	-	19.10	211	271	98
23	6.40*	-	-	17.80	200	282	101
25	6.40*	-	-	19.12	195	250	95
28	6.40*	-	-	18.43	205	263	105
27	6.40*	-	-	18.64	194	287	110
44	6.67	-	-	20.57	230	261	120
35	7.20	-	-	27.00	352	391	145
79	6.42	15.53	19.24	-	197	227	108
80	6.43	13.82	17.94	-	203	260	98
83	6.63	17.68	20.60	-	240	318	125
82	6.64	17.07	21.21	-	231	286	117
85	6.80	20.01	23.18	-	276	342	136
86	6.81	20.75	23.80	-	284	345	131
76	6.96	23.32	25.78	-	296	379	150
77	6.96	23.59	26.94	-	306	351	141
88	7.00	23.78	26.70	-	317	357	145
89	7.04	23.13	27.06	-	325	375	136

* No fatigue crack

Table 4.6 : Mechanical Property data for test pieces sintered in Laboratory, N_2 / H_2 .

Test piece number	Density Mgm^{-3}	Fracture Toughness $K_Q MNm^{-3/2}$	Yield Stress MPa	MS MPa	Hardness VPN
41	6.36	21.17	366	478	115
39	6.37	22.33	347	459	124
47	6.65	23.63	430	520	145
45	6.66	24.65	405	555	157
46	6.97	27.34	498	555	162
51	6.97	25.74	466	621	178

Table 4.7 : Mechanical Property data for test pieces sintered in Laboratory, N_2 / H_2 and heat treated.

Test piece number	Density Mgm^{-3}	Fracture Toughness K_Q $MNm^{-3/2}$	Fracture Toughness $K_Q J$ $MNm^{-3/2}$	Yield Stress MPa	MS MPa	Hardness VPN
60	6.36	13.69	14.34	169	194	103
61	6.38	13.82	15.10	156	181	106
62	6.60	16.17	17.26	198	240	120
63	6.62	16.23	18.20	194	206	112
64	6.81	18.35	21.66	221	252	135
65	6.81	17.51	20.45	229	241	127
67	7.10	21.66	25.26	290	280	148

Table 4.8 : Mechanical Property data for test pieces sintered in Industry, endothermic atmosphere.

Test piece number	Density Mgm^{-3}	Fracture Toughness K_Q $MNm^{-3/2}$	Fracture Toughness $K_Q J$ $MNm^{-3/2}$	Yield Stress MPa	MS MPa	Hardness VPN
73	6.32*	15.84	16.97	232	318	106
72	6.33*	16.78	17.22	224	352	109
57	6.41	17.83	17.98	229	359	107
74	6.93*	26.34	26.86	340	443	137
75	6.93*	25.96	27.00	343	463	145
58	7.10	28.98	29.65	380	484	156
59	7.10	29.99	31.86	373	468	140

* No fatigue crack

Table 4.9 : Mechanical Property data for test pieces sintered in Laboratory, vacuum.

Specimen density, ρ Mgm^{-3} and width, W mm	P.d. across notch V_a uV	Notch + crack length(mm)	$V_a / V_o W$ mm^{-1}	a/W
	346(V_o)	8.5(notch only)	25.08	0.339
ρ = 6.37	363	9.42	26.31	0.376
	406	10.61	29.43	0.423
W = 25.08	452	11.73	32.76	0.468
	498	12.84	36.10	0.512
	521	13.41	37.76	0.535
	318(V_o)	8.5(notch only)	25.07	0.339
ρ = 6.64	332	9.49	26.17	0.379
	370	10.61	29.18	0.423
W = 25.07	422	11.79	33.27	0.470
	464	12.90	36.58	0.515
	517	14.22	40.76	0.567
	301(V_o)	8.5(notch only)	25.10	0.339
ρ = 6.81	311	9.38	25.93	0.374
	345	10.52	28.77	0.419
W = 25.10	390	11.63	32.52	0.463
	423	12.49	35.27	0.498
	475	13.77	39.61	0.549
	274(V_o)	8.55(notch only)	25.12	0.338
ρ = 7.01	286	9.32	26.23	0.371
	303	10.21	27.78	0.406
W = 25.12	351	11.45	32.18	0.455
	391	12.55	35.85	0.499
	440	13.88	40.34	0.552

Table 4.10 : Potential drop calibration data

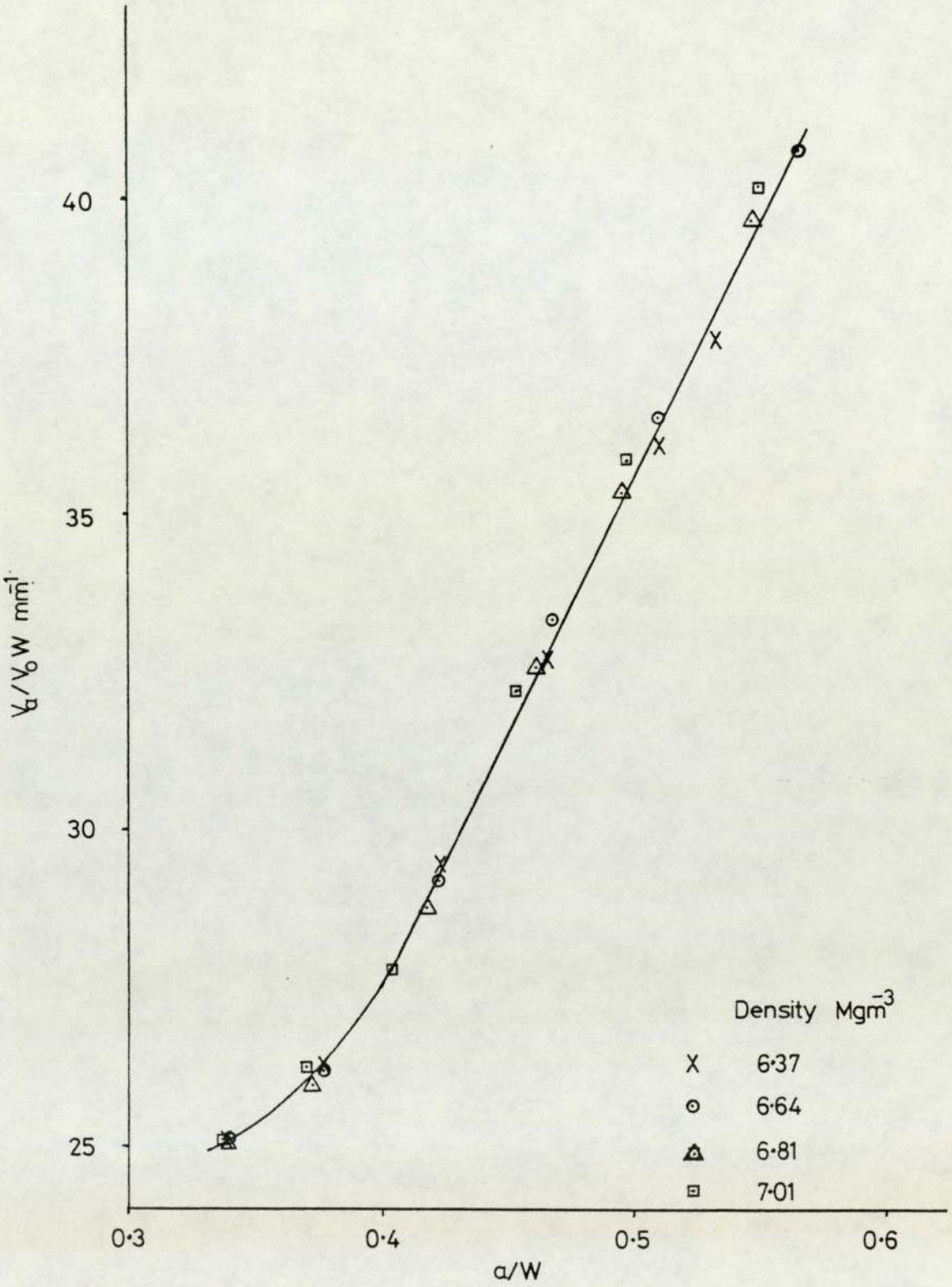

Figure 4.9 : Potential drop calibration curve

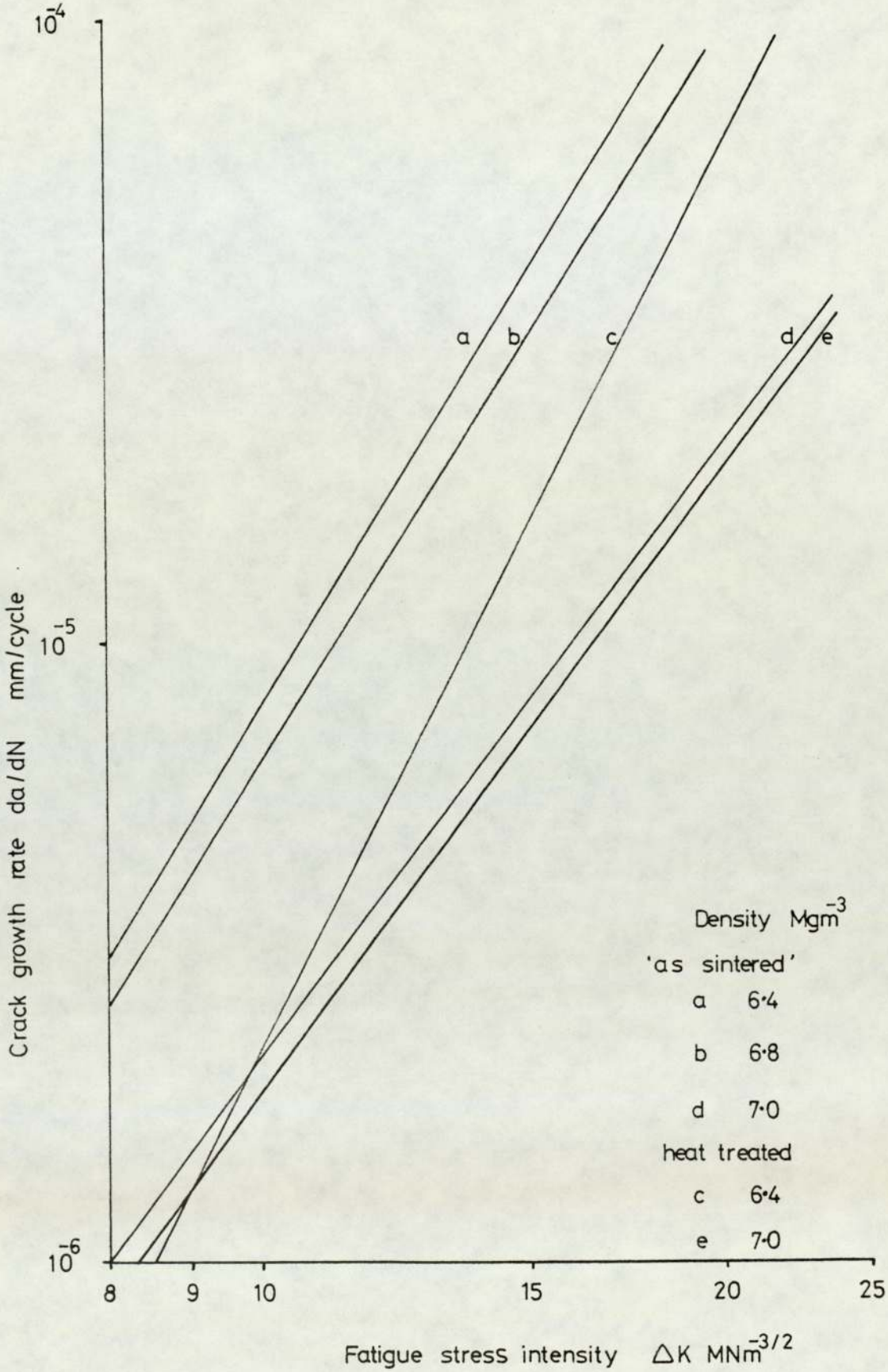

Figure 4.10 : Fatigue crack growth rate vs. fatigue stress intensity

Specimen density Mgm^{-3}	Treatment	Constant, C	Growth exponent, n
6.4	Laboratory, N_2 / H_2	$10^{-9.07}$	3.97
6.8		$10^{-9.04}$	3.86
7.0		$10^{-8.92}$	3.25
6.4	Laboratory N_2 / H_2 + heat treatment	$10^{-10.44}$	4.79
6.97		$10^{-9.08}$	3.35

Table 4.11 : Fatigue crack propagation constants, C , and growth exponents, n .

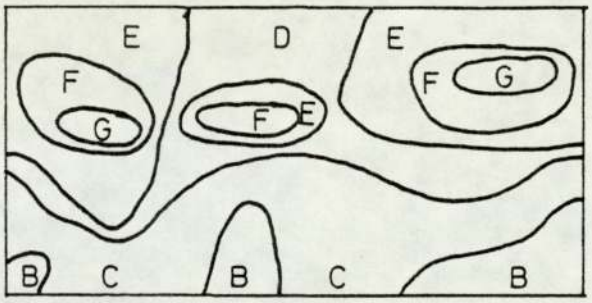

1

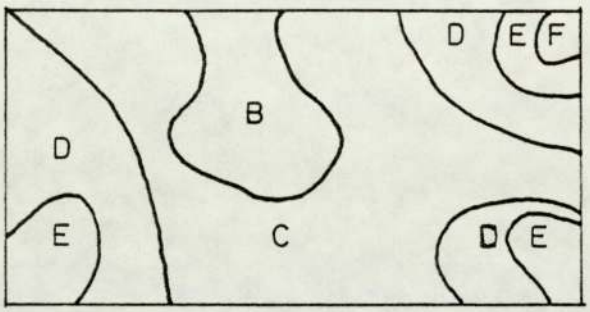

2

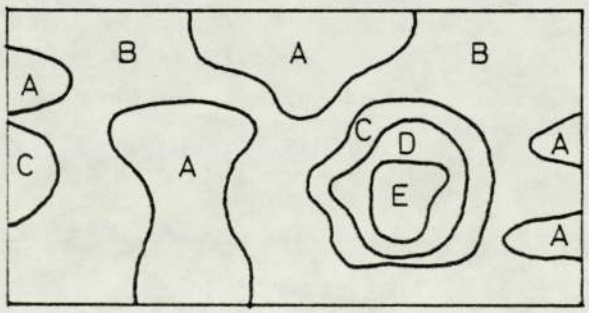

3

Density interval

A	88 - 90	%
B	86 - 88	%
C	84 - 86	%
D	82 -84	%
E	80 - 82	%
F	78 - 80	%
G	76 - 78	%

Compact density:

1. 80%
2. 84%
3. 88%

Figure 4.11 : Density variation contour maps

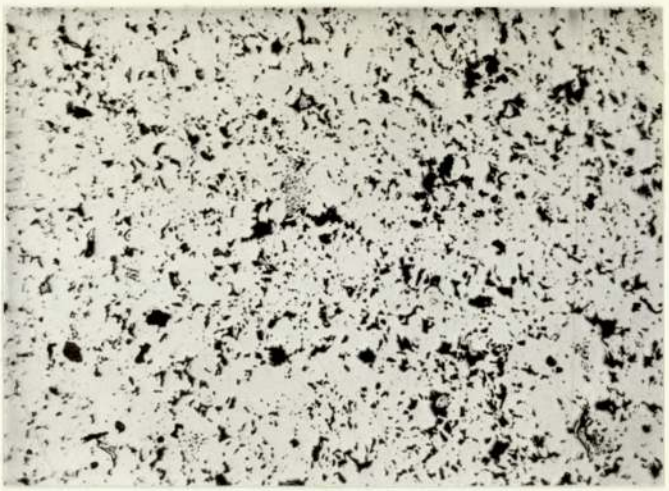

(a) 6.4 Mgm^{-3} Mag.X50

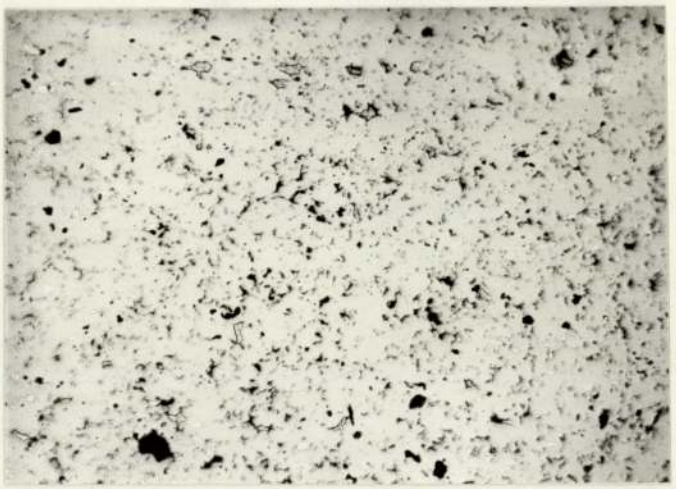

(b) 6.7 Mgm^{-3} Mag.X50

(c) 7.0 Mgm^{-3} Mag.X50

Figure 4.12 : Typical pore morphologies (continued over)

(d) 6.4 Mgm^{-3} Mag.X375

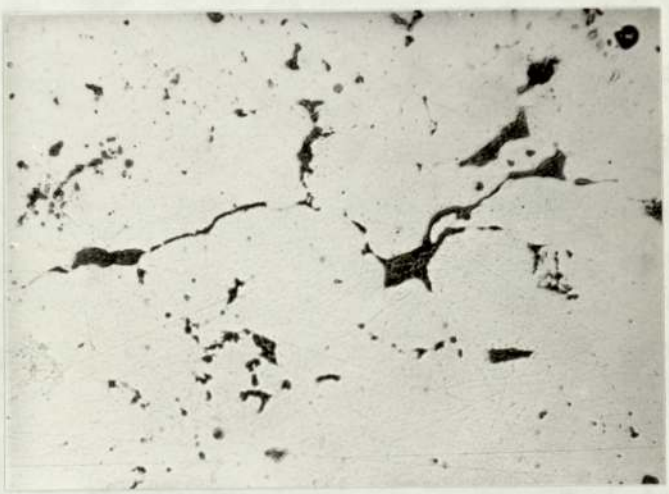

(e) 6.7 Mgm^{-3} Mag.X375

(f) 7.0 Mgm^{-3} Mag.X375

Figure 4.12 : continued.

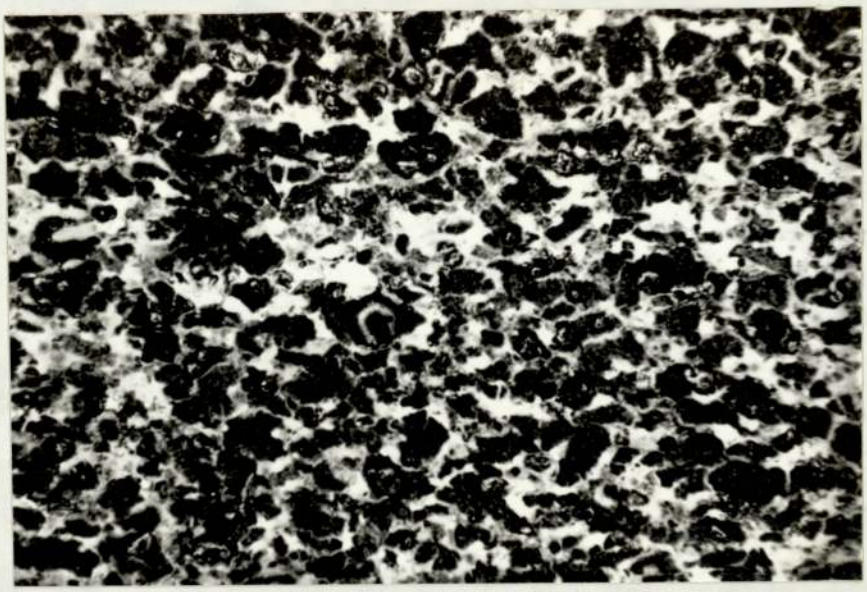

(a) Mag.X100

(b) Mag.X210

Figure 4.13 : Typical microstructures of sintered material (continued over).

(c) Mag.X570

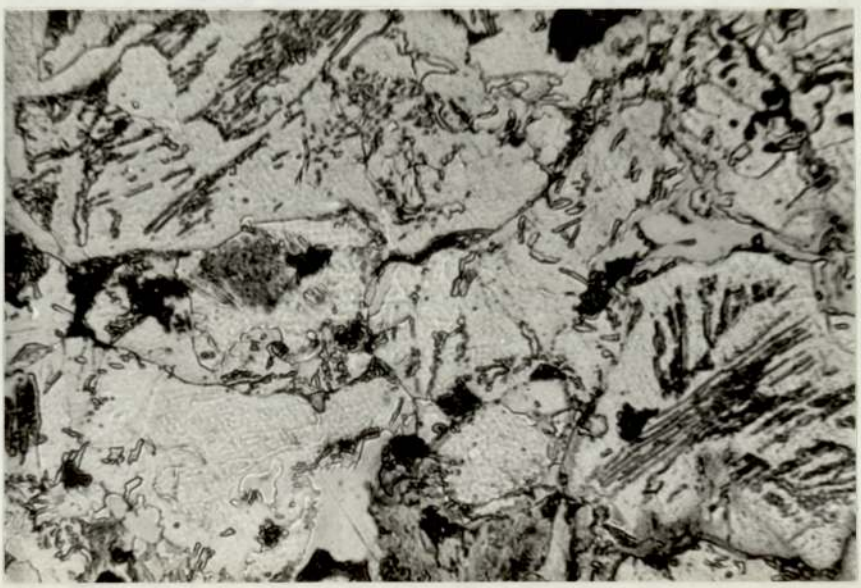

(d) Mag.X720

Figure 4.13 : continued

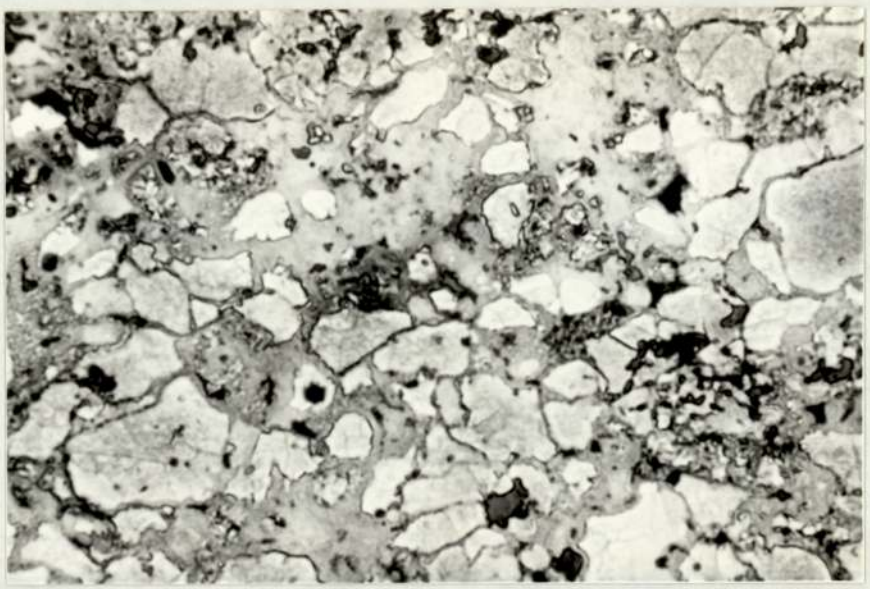

(a) Mag.X350

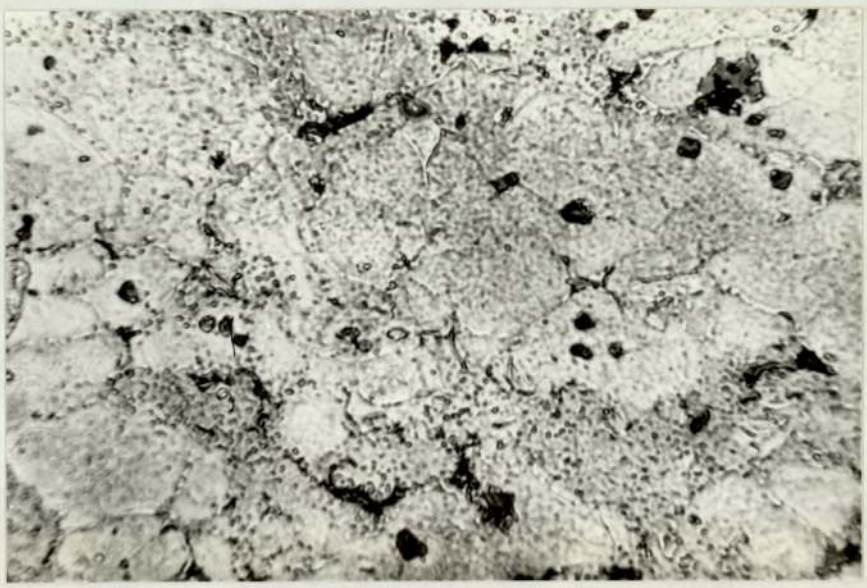

(b) Mag.X720

Figure 4.14 : Microstructure of heat treated material

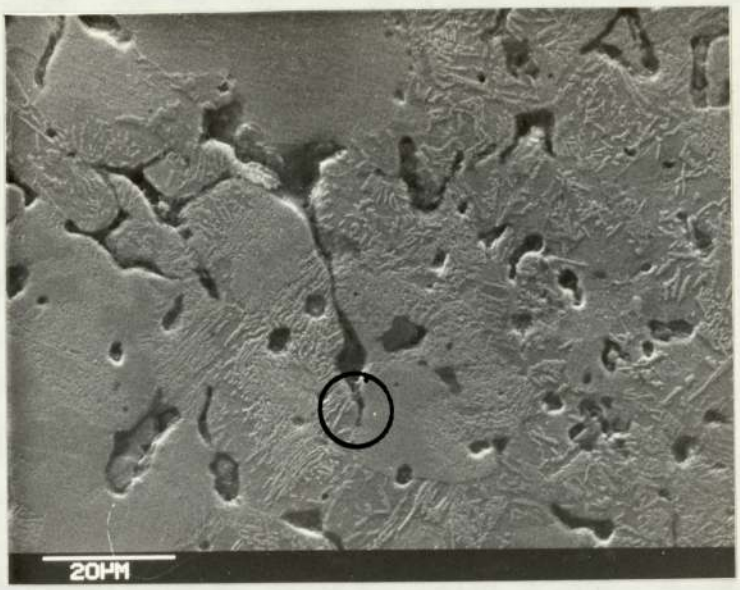

(a) General

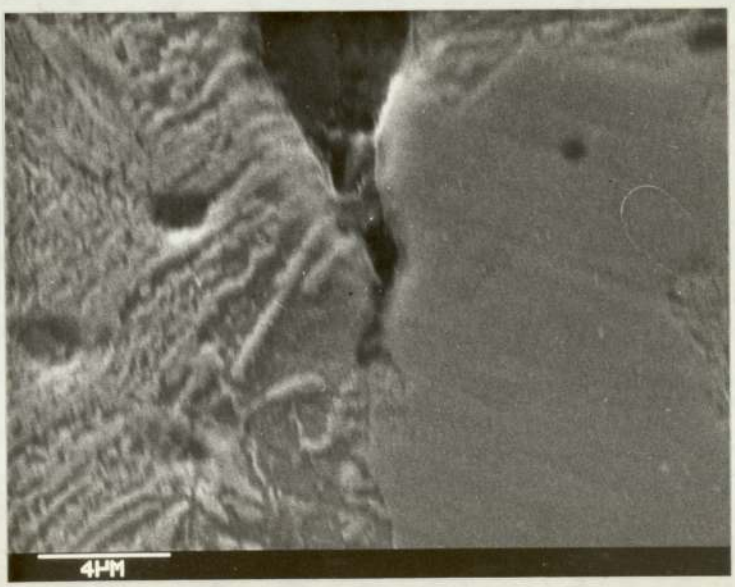

(b) Minimum radius of pore from (a) (circled)

Figure 4.15 : Typical pore morphologies showing minimum radii present in the corners of irregularly shaped pores (continued over).

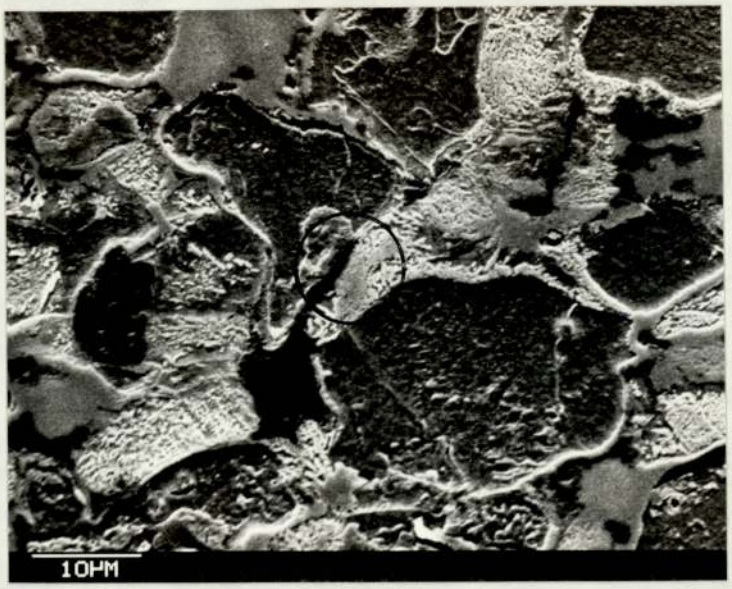

(c) General

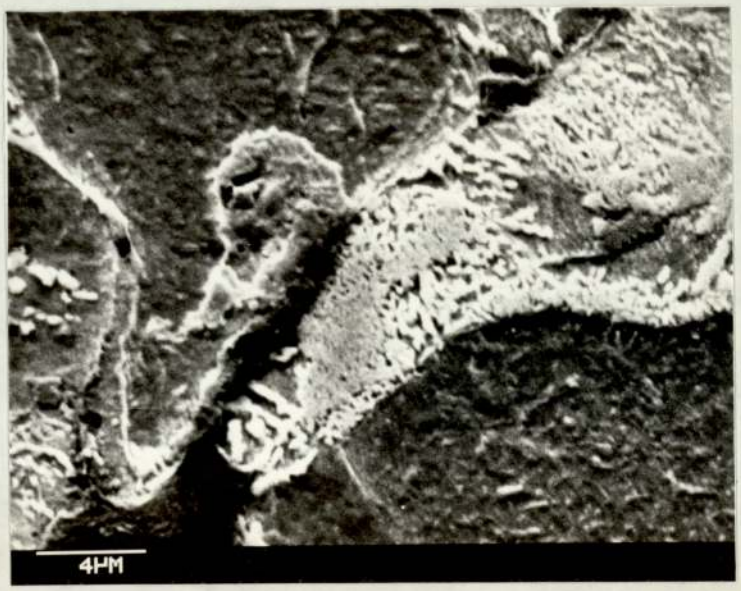

(d) Minimum radius of pore from (c) (circled)

Figure 4.15 : continued

(continued over)

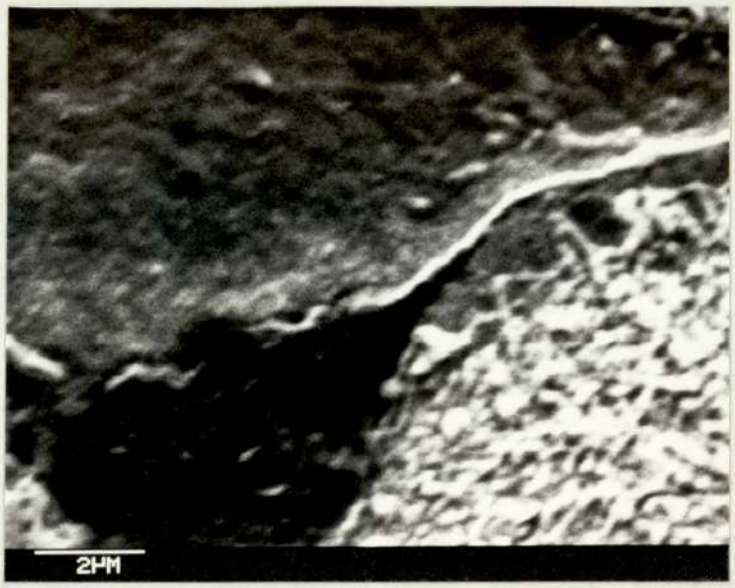

(e) Typical minimum radius

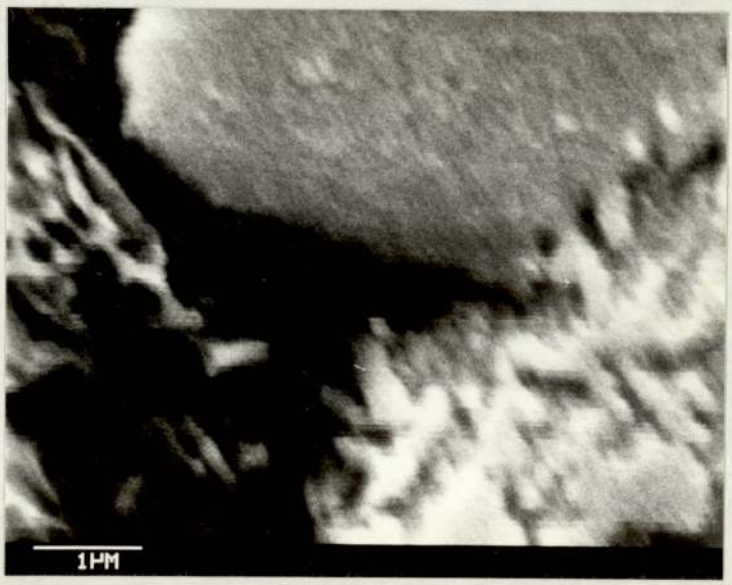

(f) Typical minimum radius

Figure 4.15 : continued

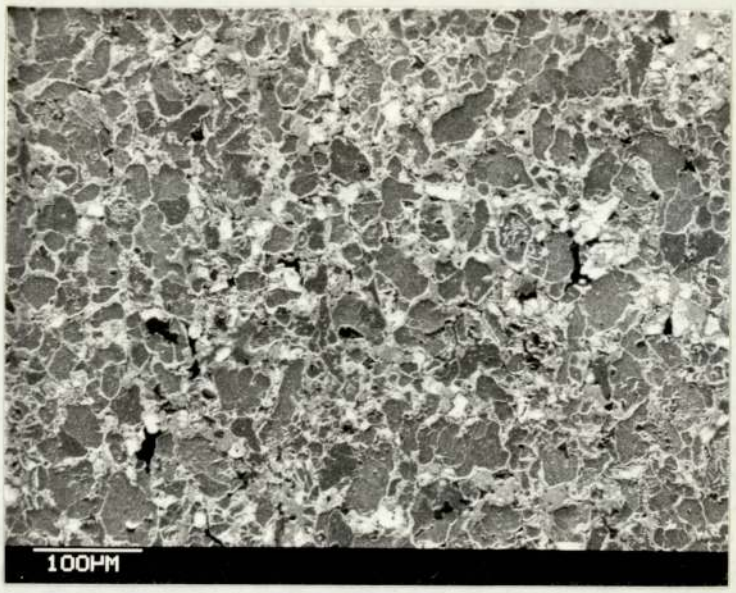

(a) General

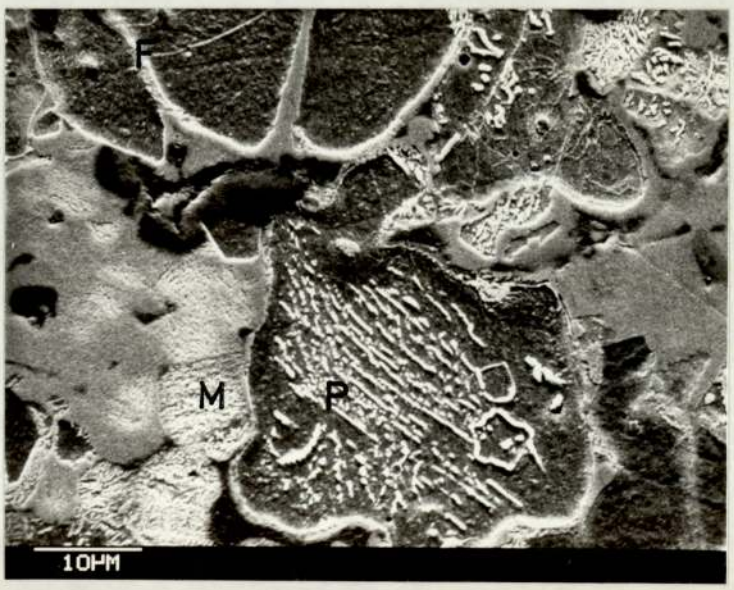

(b) Micrograph showing pearlite (P), martensite (M), and ferrite (F)

Figure 4.16 : Scanning electron micrographs of structural features (continued over)

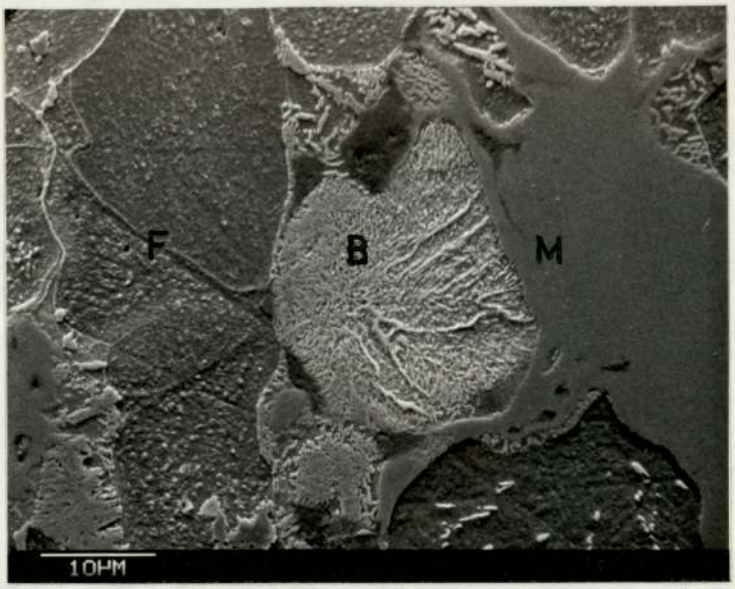

(c) Micrograph showing ferrite (F), bainite (B) and martensite (M).

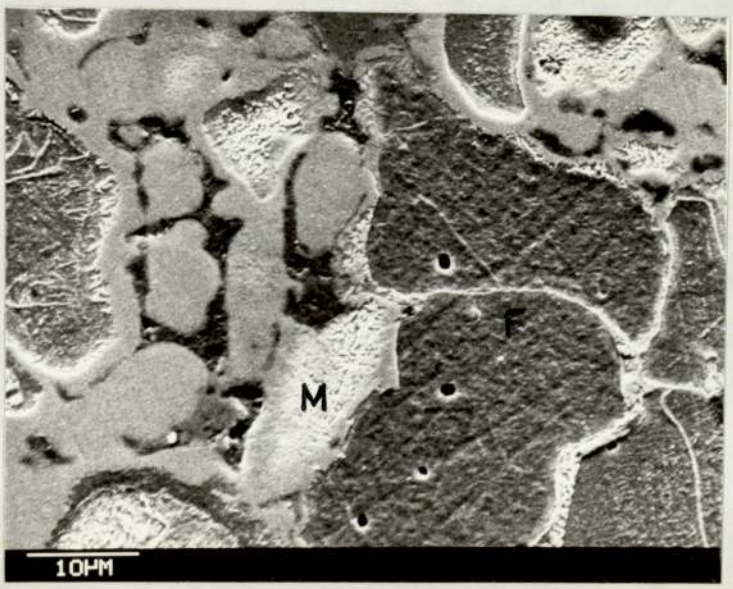

(d) Micrograph showing ferrite (F) and martensite (M).

Figure 4.16 : continued

(a) General view

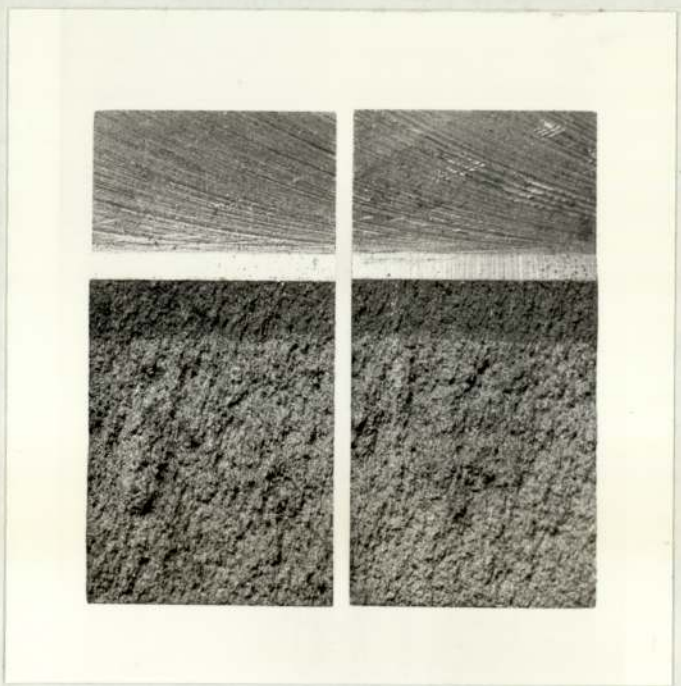

(b) Fracture faces showing heat-tinted fatigue crack

Figure 4.17 : Fractured test piece.

(a) Fast fracture, laboratory N_2/H_2 sinter — Mag.X600

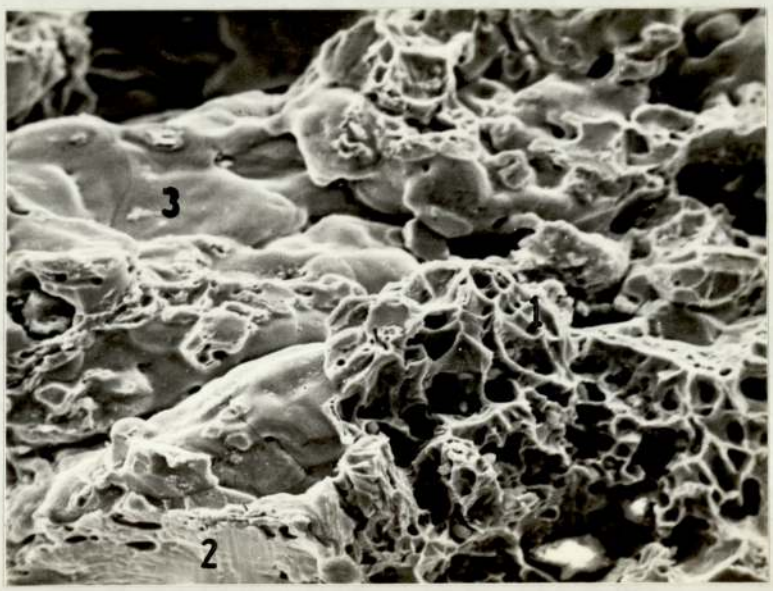

(b) Fast fracture, laboratory N_2/H_2 sinter — Mag.X1.1K

Figure 4.18 : Typical fracture faces (continued over)

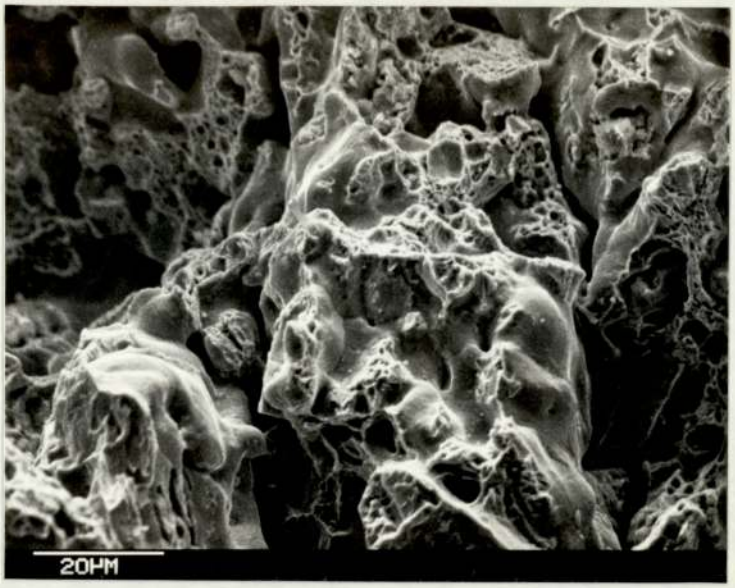

(c) Fast fracture, vacuum sinter

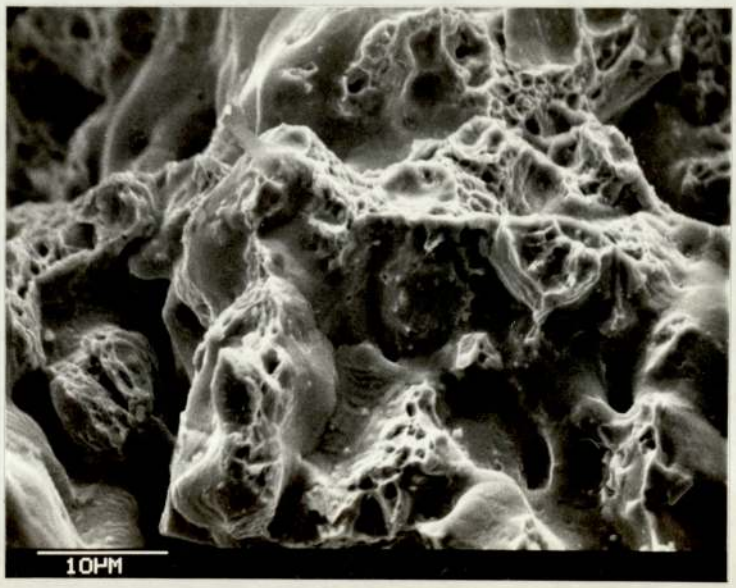

(d) Fatigue fracture, vacuum sinter

Figure 4.18 : continued

(continued over)

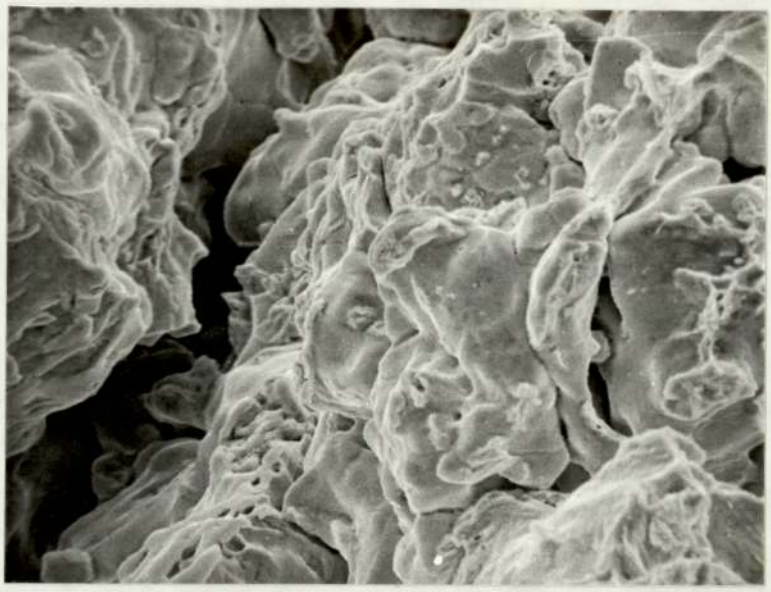

(e) Fatigue fracture, laboratory N_2/H_2 sinter — Mag.X1.1K

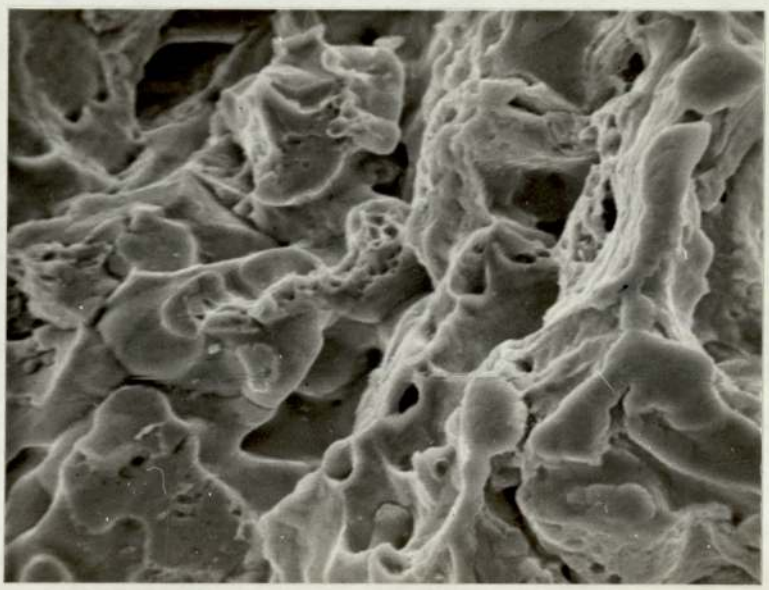

(f) Fatigue fracture, laboratory N_2/H_2 sinter — Mag.X2.2K

Figure 4.18 : continued.

5. DISCUSSION

5.1 Mechanical Properties

5.1.1 Hardness

Porosity and matrix heterogeneity inevitably cause considerable scatter in hardness measurements, especially when using a pointed indentor. However, it was not intended to attempt to include hardness in any correlations, and was measured for interest. Hardness measurements are used by the P/M industry for quality control, but only on a 'broad'basis, for example, to check that components have been heat treated after sintering to a set minimum hardness. The hardness of sintered Distaloy SA compacts increased with increasing density in the expected manner. Wide scatter in the results from the three sintering treatments prevents determination of any difference between treatments, but it can be said that the hardness, at a particular density, are of the same order, irrespective of the sintering treatment. The heat treated samples showed a definite difference, being harder by approximately 25 points at a given density.

5.1.2 Tensile Properties

The yield stress of the material increases with increasing density for all sintering treatments, including heat treatments, the rate of increase becoming slightly greater at higher density levels, as seen in Figure 4.2 . The'yield' loads of duplicate test pieces were of similar value, differing in most cases by no more than 10 MPa . However, the ensuing fracture loads were often markedly different. The averaged maximum stress values were plotted in Figure 4.3 , which shows a much wider scatter of results than that exhibited by the yield stresses, Figure 4.2 . However, the results do indicate a trend of increasing maximum stress with increasing density. The similarity in the slopes of all the curves indicates that the strength is predominately controlled by the

percentage porosity, the level of strength being controlled by the resistance to deformation and fracture of the ligaments between the pores.

It has been shown[29] that, in tensile loading, crack formation occurs within sintered iron test pieces, at and below the macroscopic yield point, the first cracks observed being at the surface edges, at load values barely above half the 0.2% proof stress. These workers state that, the cracks continue to form during loading and propagate quickly to a certain length and then stop, but open up further with increasing load. Metallographic evidence is presented to support this argument. The extension of the test piece due to crack opening retracts during unloading, because plastic deformation at the crack tips is not very pronounced due to the multi-axial state of stress. After the attainment of the yield point, cracks occur that propagate continuously and combine with other cracks. The crack formation eventually weakens the cross section to such an extent that fracture ensues. The deviation from linearity can be taken as being the point at which extensive crack propagation begins to occur, leading to eventual fracture. This point can therefore be taken as the 'yield point' in a porous material which does not exhibit a macroscopic yield point.

The crack formation has been shown to vary over the cross section of the test piece, being considerably higher at the perimeter than at the centre. Surface defects, such as machining marks, will greatly assist the higher proportion of cracks at the perimeter to propagate catastrophically in test pieces of small diameter. Thus, it is considered that the use of small machined test pieces in this work was the cause of the wide scatter of maximum stress results. Small test pieces were used in order to satisfy the fracture

toughness requirement that yield stress values should represent the material through which the crack was being extended. Results from 'dog-bone' test pieces would not necessarily have been representative since the density variations in the fracture toughness test pieces would be difficult to simulate.

At any one density, the lowest yield stress was found in the samples sintered in industry, about 20% higher values in laboratory, N_2 / H_2 sintered samples, and about 40% higher values in samples sintered under vacuum. As stated previously, the cooling rate from the sintering temperature will affect the strength. The vacuum sintering treatment had the slowest cooling rate since a 'furnace cool' was used. In both the laboratory atmosphere and industrial treatments, the samples were moved to a cooling zone after sintering which resulted in a degree of enforced cooling. This, coupled with the somewhat shorter industrial sintering times, is considered to be the reason for the differences in yield stress values between laboratory atmosphere and industrially sintered samples. One hour was chosen as the sintering time. This was aimed at in the industrial sinter, but on the particular furnace run, the time at temperature was estimated as being 5-10 minutes less than this. However, the high yield stresses of vacuum sintered samples cannot be explained by the thermal cycle, and a structural feature must be controlling the strength level in these samples. Further discussion of this point will be deferred until the other mechanical property results have been examined.

5.1.3 Young's Modulus

The derived relationship between fractional porosity and Young's Modulus, equation (28) , was used throughout this work. A degree of scatter due to experimental error was to be expected,

as discussed earlier, using test pieces with a small guage length (25mm) . As a consequence, very small extensions were being measured with the extensometer. Hence it was necessary to include a value of Young's modulus which represented zero porosity, to extend the comparitively small range of fractional porosity over which this determination was made. The published value[104] of Young's modulus of En34 was used, since this wrought material has the nearest equivalent composition to Distaloy SA.

The values of Young's modulus calculated from the derived relationship are in accord with those from equation (2) , after the work of McAdam[33], differing by a maximum of 2% over the range of densities investigated. Any relationship between modulus and density must depend upon pore shape, size, spacing and orientation with respect to the applied stress. Therefore, there will be differences when applying a general relationship to a particular system.

The Youngs modulus of a sintered material shows an exponential relationship which increases with increasing density. At low densities (high porosity) the elastic strain will be related to the volume of pores which effectively allows large elastic displacements of the matrix. As the density increases, the interaction of particles will progressively inhibit elastic displacement, resulting in a disproportionate 'stiffening' of the material, as indicated by the exponential relationship.

5.1.4 Compliance

The value of the dimensionless constant CEB, taken as the averaged value from four determinations, was used in subsequent calculations for the determination of U_{crack} in equation (20) . The value of CEB for a beam in three point loading can be derived

theoretically thus:

$$\text{displacement, } d = \frac{PL^3}{48EI} \qquad (29)$$

where P= load, L= loading span, E = Youngs modulus and I = moment of inertia.

$$\text{Moment of Inertia, } I = \frac{BW^3}{12} \qquad (30)$$

substituting in equation (29)

$$d = \frac{PL^3}{4EBW^3} \qquad (31)$$

The geometry of the fracture toughness and beam test pieces is such that L = 4W, and since compliance, C, = d/P, by substituting in equation (31) and rearranging:

$$CEB = 16 \qquad (32)$$

The calculated value of CEB was 29.48 and is high because the measured compliance value reflects additional displacement due to the rollers 'sinking' into the test piece during loading. During fracture toughness testing, the rollers will also 'sink' in and hence calculation of the portion of the energy contributed by the uncracked ligament will account for this additional displacement of the loading point.

As with Young's modulus, an exponential relationship between compliance and density would be expected, for the same reasons.

The gradual 'stiffening' of the material with increasing density results in decreasing values of compliance.

5.1.5 Fracture Toughness

To test for the plane strain fracture toughness, the thickness of the specimen is of prime importance, and the limiting thickness must be ascertained. With wrought and cast materials, in most cases, a suitable size test piece may be machined from a blank. It is not difficult to change the dimensions if considered necessary after initial testing. When dealing with metal powders, the specimen size is governed by the tool sets available, so there is little flexibility. The tool set available for this work had been designed for earlier studies of fracture toughness, and measured 110 x 25mm, the other dimension being controlled by depth of fill, which is limited by powder compressibility. Thus the thickness, B , of the test piece was chosen as 12.5mm, since the 50mm requirement, to conform with the dimensions stated in the document initially consulted[103], would lead to unacceptable density variations in the pressing direction. The subsequent standard[53] allows a range of thicknesses, should an alternative be required, of $B = 0.25\text{-}1.0W$ (W = width) . To have taken advantage of this, however, would have introduced problems of interpretation of results, when compared to those already obtained, due to variations in density within specimens of different dimensions, but the same Archemedian density.

The initial tests resulted in very few valid K_{IC} results being obtained, due to non-linearity of the load/COD trace as determined from the validity checks for linearity (see Section 2.2.2) . The ratio P_{max} / P_Q was greater than 1.1, and the distance V_1 was greater than $\frac{1}{4}V$ (see Figure 2.7), in nearly all cases. However,

discrepancies were relatively small and it is likely that the K_Q values were very near to the K_{IC} requirements. Non-linearity of the trace was a constant problem. This finding was in apparent contrast to those of Ghosh[12] and Andrews[7], who obtained valid K_{IC} results throughout with this material using the same specimen dimensions. The latter worker stated that the load/COD trace was "linear almost up to fracture".

The 'bowing' of the load/COD trace observed in a number of cases indicates a disproportionate increase in resistance to crack opening. Exhaustive checks on all the test equipment, and the experimental procedure, revealed no reason for this observation. The occurence must, therefore, be associated with a change in material properties, during loading. There are two possibilities. Any retained austenite in the structure would transform to martensite if deformed. Retained austenite was not seen during metallographic examination, but small regions would be very difficult to detect, even by special techniques. This occurence, naturally, leads to considerable stiffening of the structure, in effect, rapid work hardening. The other possibility is that pore closure occurs in the region ahead of the crack tip, giving a localised increase in stiffness. No reference has been made to this bowing in Load/COD curves in publications relating to sinter forged (nil porosity) material of similar composition. The region ahead of the crack tip is one of large micro-structural damage and deformation[6]. If pore closure was to occur, the points of particle contact would be increased and pressure welding may take place. This would then effectively increase the density, and hence compliance, in this region. The increased degree of 'bowing' in specimens of low density could then be explained since there is more scope for this effect

where there is a greater amount of porosity present. It was noticed that, following the introduction of the potential drop equipment to test procedure, a very small but definite decrease in p.d. occurred at the point of initial bowing of the trace. This observation supports the pore closure theory, the very small change in conductivity due to the possible phase change, would not be detected. However, this occurrence of bowing was not observed in all cases and at the present time precise reasons for this are unclear.

A condition for a valid test is that the fatigue stress intensity must not exceed 70% of the provisional fracture toughness value during the final stages of fatigue crack growth (i.e. the last 1.25mm or 2.5%W, whichever is the greater) . There has been an easing of the limitations since the inception of fracture toughness testing as a standard test, perhaps a reflection of the difficulties encountered as more and more materials and alloys become the subject of investigation. The American standard for plane strain fracture toughness testing of 1968 (ASTM E399-68) stated that the fatigue stress intensity, K_f , should not exceed $0.5K_Q$ (where K_Q is the provisional value of fracture toughness) but this has been relaxed so that the limits are now $0.6K_Q$ (ASTM E399-78a) . The current British Standard specification states that the limit should be $0.7K_Q$, this figure having been $0.67K_Q$ in the draft stage. The object of these recommendations is to ensure the growth of a 'sharp' crack. In establishing the limits for fatigue pre-cracking, experiences vary. For example, May[105] reported that the value of K_f could be $0.9K_Q$, when investigating maraging steel, without having any effect on the final K_{IC} value, whereas Brown and Srawley[106] reported that this value should not exceed $0.6K_Q$ for the same material. The latter investigators also published data

for aluminium alloys which stated that K_f values of $0.6K_Q$ had no effect on the final K_{IC} value. Kaufman and Schilling[107] suggested that the limit should be $0.8K_Q$ for the aluminium alloys investigated by them, but that additional data should be generated for other metals to determine whether this is generally true. It appears that the acceptable levels of K_f depend upon the material under investigation and thus requires individual determination.

During this investigation, the fatigue ratio was kept as low as possible, to conform with the standard. Difficulty was encountered with specimens of low density (6.4 Mgm^{-3}) during the final stages of crack growth, when the load was reduced. Often, no crack growth could be detected at these loads, and the load had to be increased until the crack started to grow again. The loads required for crack initiation in these specimens are of the same order as those required for higher densities (up to 7.1 Mgm^{-3}), but to comply with the standard, the propagation loads must then be reduced to a lower value than that for higher density samples(because of the lower K_Q value in the fracture toughness test which follows) . The tensile loading at the crack produces residual compressive stresses at the crack tip and subsequent lowering of the load would reduce the rate of growth or even halt it completely for a time. Thus, certain specimens required long periods of load cycling at low loads. Barnby et al[6] encountered the same problem, but stated that, with reference to the standard test method employed (BS DD3[102]), the fatigue crack propagation rate was slow enough to ensure a sharp fatigue crack. During the initial tests, the ratio K_f / K_Q used by the author was sometimes as high as 0.9, since the subsequent value of K_Q had not previously been determined. The indication from the results was that this had no effect on the

final K_Q value, although no limiting value was determined.

The fracture toughness, K_{IC} , values quoted (Table 4.6) show that most valid results were obatined from specimens with no fatigue crack. It has been demonstrated[108] that no decrease in toughness occurs as the notch root radius is reduced below a certain value, depending upon the material investigated. This critical notch root radius was not investigated, but, although only one value is available for comparison, the K_{IC} values obtained are certainly no higher than that obtained with a fatigue crack present, at the same density. The notch root radius for the specimens was of the order of 0.1mm (in the range 0.08-0.11mm) . Using this root radius, Barnby et al[6] determined that the fracture toughness values were the same as those for fatigue cracked specimens. From Figure 4.15, it can be seen that the minimum radii present in the corners of irregularly shaped pores are of the order of 0.4μm or less. Where the intrusion of a pore continues as two particles in intimate contact, but not bonded, it would be equivalent to a crack, as indicated by Figure 4.15e . At the point where the particle contact transforms to particle bonding, the 'radius' would be of atomic proportions, and equivalent to a fatigue crack. Pores of this type, at the base of a machined notch, would therefore have the effect of sharpening the notch to such an extent that a fatigue crack itself is unnecessary. The final machining operation was carried out carefully to avoid any heavily deformed region being produced below the cutting tool. It is by no means certain that crack initiation takes place at a free surface, since pores act as sites of stress concentrators. Microcrack formation, as stated previously, has been observed[100] at sharp corners of sub-surface pores. "Smearing" or a small degree of work hardening caused by

the cutting tool is, then, probably quite acceptable since crack initiation may well take place outside these regions. The specimen thickness, selected by the writer, for the test pieces was somewhat less than that required by equation (14) . Since the criterion for a valid K_{IC} is more than sufficient to ensure a minimum plateau, it is considered that the measurements made here are in fact valid K_{IC} values. This view is endorsed by the fact that all the fracture faces were flat and in no cases were shear lips observed.

The relationship between toughness, K_Q and density (Figure 4,5) was that, for any given treatment, toughness increases with increasing density. Subsequent use of the J integral approach showed that, for a given density, the K_QJ value obtained was, within experimental error, the same as the K_{IC} value. The relationship between toughness, K_{IC} and K_QJ, and density, shown in Figure 4.6, shows the same trends as those in Figure 4.5, with the exception of results from heat treated samples for which J integral analysis was not performed. A simple analysis of the situation would expect this relationship, since it implies that toughness is directly related to the number and volume of angular discontinuities in the structure. Likewise, tensile properties would be expected to increase with an increase in the effective cross section, therefore one would expect yield stress to directly correlate with fracture toughness. The toughness in the range of treatments tested is clearly dominated by the yield stress, since toughness increases with yield stress, with the exception of laboratory vacuum sintered samples at low density (6.4 Mgm^{-3}), as shown in Figure 4.7 . This trend is the opposite to that which normally occurs in, say, high strength steels, aluminium alloys, or titanium alloys. As discussed earlier, cracks develop in a tensile test piece below the yield point, and propagate to a certain

length and then stop. At the 'yield point' these cracks propagate continuously, that is, a critical value of stress is reached which causes the cracks to extend. Therefore, it seems possible that the apparent yield stress corresponds to a fracture test, with simply a different test piece geometry to that used for fracture toughness testing. This would, then, explain why toughness rises with increasing yield stress.

The thermal history and density of a compact determines the yield strength and hence the fracture toughness of Distaloy SA, with the exception of vacuum sintered samples. As stated previously, vacuum sintering produced a disproportionately high yield stress, with a corresponding increase in toughness at the higher densities only. When a powder is compacted, particles are cold welded together to form necks. Around the necks there will be a region of intimate contact, but no bonding. During sintering, the neck consolidates and increases in size. One factor restricting neck growth is the presence of surface impurities on the particles. It would appear that, because of the enhanced removal of surface impurities, due to the "scavenging" effect, during vacuum sintering, interparticle bonding could be improved beyond that achieved by reducing atmosphere sintering. The improved interparticle bonding would tend to delay the initiation and propagation of microcracks during tensile loading, in effect giving a higher yield stress. Although no evidence could be found from the micrographs studied, it is proposed that the increase in toughness at the higher densities only is due to an increase in the interparticle bond region, as illustrated in Figure 5.1 . The unbonded interparticle contact region, which represents a sharp crack, would therefore be smaller. At lower densities, there would be much less scope for this effect

to occur due to the overall smaller area of particle contact after compaction. Thus, after sintering, particle contact regions could be of the same size as those in samples sintered in a reducing atmosphere. Increasing the compaction pressure, and hence density, would increase the size of contact regions and, after sintering, increase the interparticle bond region. The result would be to effectively increase the net section of material, hence raising the toughness. Figure 4.6 shows a gradual increase in toughness for vacuum sintered samples away from the toughness of reducing atmosphere sintered samples with increasing density. Careful experimental techniques, probably involving both Auger and scanning electron microscopy would need to be developed to further explore this postulation.

In recent years, a great deal of attention has been given to producing powders of low oxygen content. There is evidence that the mechanical properties of sintered steels, especially at the higher densities, are directly related to oxygen content[109,110]. In this investigation, the oxygen content of test pieces sintered in a reducing atmosphere in industry remained the same as that of the powder (0.35%) . The oxygen content of laboratory, N_2 / H_2 sintered test pieces was considerably less than the powder, (0.25%) and vacuum sintered test pieces, lower still (0.22%) . This gives support to the postulation that vacuum sintering enhances the removal of oxide impurities when compared to atmosphere sintering. Although the oxygen content of vacuum sintered samples is not very low, it is possible that the oxides are preferentially removed from the particle contact regions, since they are likely to be 'broken up' in these regions during compaction. Although, as discussed elsewhere, the fracture toughness is likely to be affected by other

differences between the three sintering treatments, the levels of fracture toughness do relate directly to oxygen content of the test pieces. Increased oxygen content has been proposed as being the cause of low fracture toughness values in earlier work[8,9].

The foregoing discussion demonstrates that the differences in mechanical properties between laboratory atmosphere and industrially sintered test pieces was due to the thermal cycles employed in each case, and that there was no evidence of physico-chemical differences between these sintering treatments. This infers that the laboratory atmosphere sinter simulated industrial practice. Pore geometry is much discussed in the literature, in the sense of whether they are rounded or angular, and the resultant stress concentration effects. However, it is now proposed that the interparticle boundaries are critical regions, due to their sharp, crack-like nature. The general level of toughness of the material discussed here is about one fifth of that of a wrought steel of similar composition. It is noticeable that the fracture toughness of an alloy steel powder, sinter forged to full theoretical density, is higher than, but still of the same order as its sintered counterpart containing about 10% porosity[8]. Although the forging operation will reduce the total porosity to a very low level, the weakly bonded particle contact areas could remain, to act as sharp defects.

Recent research in the field of fracture mechanics has led to the development of new specimen geometries which could be particularly suited to testing sintered materials. Ritchie et al[111] have proposed a simple method for measuring valid J_{IC} fracture toughness in small (Charpy-size) specimens, where failure occurs beyond general yield by a mechanism of ductile rupture (microvoid coalescence). Briefly, the method entailed the introduction of side grooves along

the edge of the test piece after fatigue pre-cracking. It was condidered that this would reduce or eliminate regions of through-thickness deformation (i.e. plane stress regions). It appeared that, with a 30% side groove depth, J_{IC} (or $K_Q J$) could be determined simply by measurement of the test piece dimensions and maximum load (i.e. there is no need to detect crack initiation). Another testing method which has been developed[112], is that known as the short bar testing method, which uses small scale test pieces. The constraint required to give valid K_{IC} results is developed by virtue of the geometry of the chevron notch rather than by the test piece thickness. This method does not require a fatigue crack, because the required pre-crack is obtained prior to maximum load as a result of initial stable crack growth inherent in the specimen design. Since it has been demonstrated that fatigue pre-cracking is not necessary where irregularly shaped pores are present, the former method, outlined above, could be simplified further in the case of sintered materials by having a machined notch only. Being in a position to use a small tool-set or to compact a relatively large blank to be cut into several test pieces would be very attractive to the powder metallurgist. Again, the established technique used by the writer to obtain fracture toughness data proved very time consuming. These newly proposed techniques would enable much more data to be obtained in a given time.

5.2 Fatigue Crack Propagation

As stated previously, no special tests were made to study the fatigue behaviour of sintered compacts. During fatigue pre-cracking of the fracture toughness test pieces, data was recorded. However, the data should be treated with some caution, for the following reasons:

1. The fatigue crack was grown over a small distance only. A standard notch depth of 8.5mm was used for all specimens, and grown only to a length which meets the conditions for fracture toughness testing, i.e. 0.45-0.55W (11.25-13.75mm). Thus the maximum crack length is 5.25mm, or ~20% of the total specimen width at most.

2. The crack was grown for very short distances at any one load. The load was reduced 2-3 times during fatigue pre-cracking in order to keep the fatigue stress intensity as low as possible. After the load was reduced, the crack growth rate was reduced, presumably until it had grown through the plastic zone formed by the crack at a higher load. This means that the first few values of da/dN at any load are dubious and should perhaps be ignored, although from graphs of da/dN vs. ΔK it is not clear where the results become valid, due to general scatter.

3. Inaccuracies are expected in the final graph since the specimen densities to produce the line for, say, a nominal density of 6.4 Mgm^{-3} are in fact in the range 6.38-6.45 Mgm^{-3}. This variation would cause a degree of scatter in the results.

4. The frequency of the vibrophore changes with load, and at any one load it also changes with crack length. The makers state that the frequency changes by ±2%, and calculations of frequency at various loads for the type of test piece used confirms this, and the values ranged from 95-99Hz . During testing, the number of cycles is noted at intervals which are larger than the time intervals at which measurement of p.d. (for crack length) are taken, since it would require almost continuous monitoring of the number of cycles for values to be assigned to these time intervals, which is not practical. Hence the total number of

cycles was measured and was assumed to be constant for constant time intervals (i.e. frequency is taken as being constant at any one load over the range of crack lengths at that load).

5. The data, for any one nominal density, was only obtained from a compararatively small number of specimens (in general, at least three specimens) which is not normally considered to be enough to allow reliable interpolation[86].

A combination of the above factors influences the fatigue crack growth data, resulting in a large amount of scatter. The graph in Figure 4.10 was deduced by regression analysis. Because of the reservations held regarding the data obtained, discussion is limited to the general trends indicated by Figure 4.10 and Table 4.11 .

Data was obtained for laboratory, N_2 / H_2 , sintered material at nominal densities of 6.4, 6.8 and 7.0 Mgm^{-3} and heat treated material at nominal densities of 6.4 and 7.00 Mgm^{-3} . The small number of specimens from other processing schedules prohibited any usable data being generated. As seen in Figure 4.10, the rate of crack growth, at any particular stress intensity, decreases with increasing density. This relationship is to be expected, since increasing the density effectively increases the cross section through which a crack has to propagate. Heat treatment increases the resistance of the matrix to crack propagation by virtue of the improved mechanical properties and this is indicated in Figure 4.10, the heat treated material showing a decrease in growth rate when compared to 'as sintered' material of the same density.

The growth exponent, n , shows the rate of increase in crack growth rate. From Table 4.11, for 'as sintered' and high density heat treated test pieces, the growth exponent was similar, but did increase slightly with a decrease in density. For the low density

heat treated test pieces, the growth exponent was about 20% higher. As mentioned previously, propagation behaviour gives rise to a fatigue crack growth curve which is sigmoidal in shape, Figure 2.13 . Where the testing range is close to the transition between growth regions 2 and 3, higher growth exponents,n , are to be expected due to the contribution from monotonic failure modes. The difficulties encountered with specimens of low density meant that a high fatigue stress intensity was required in order to propagate a crack, and was particularly the case with heat treated material. The result from the heat treated material at a density of 6.4 Mgm^{-3}, having a high growth exponent, possibly corresponds to region 3 and is not comparable to the other results per se. The amount of data for this particular condition of test piece was also limited, and hence would contribute to the overall incompatability of this result. The crack growth rate of low density (6.4 Mgm^{-3}) 'as sintered' material increases with an increase in stress intensity to a larger degree than the high density material (7.0 Mgm^{-3}), as reflected by the growth exponent value. The values of the growth exponent, Table 4.11, are comparable with published values[88,113] for mild and low alloy steels. Hardened steels show a growth exponent which is in general less than the normalised wrought steels, and it would be expected that the heat treated material used in this work would show a similar trend. However, the growth exponent is higher when compared to 'as sintered' material of the same density. As previously discussed, the results from low density heat treated material possibly correspond to region 3 of the fatigue crack growth curve, and it is quite possible that this is again the case with the high density material. Investigation of the fatigue behaviour of Distaloy SA compacts[7] has shown a reduction in the growth exponent of heat treated material

when compared to their sintered counterparts. It can be inferred from the results obtained from the as sintered material that an increase in fracture toughness results in an increase in resistance to fatigue crack propagation. Hence, it would be expected that the vacuum sintered material has a lower fatigue crack growth rate than reducing atmosphere sintered material.

From the discussion above, it is clear that fatigue crack growth data must be generated from specific experimentation, but a useful 'broad picture' can be obtained from fatigue pre-cracking of fracture toughness test pieces.

5.3 Fractography

The typical features of fracture faces are shown in Figure 4.18. All fractures examined, whatever the means of propagation, showed regions of a ductile dimpled type of propagation (Region 1 in Figure 4.18b) from pore to pore. There were also relatively flat, featureless areas (region 2) between the pores (region 3), presumably representing unbonded inter-particle contact.

The mechanisms of ductile fracture is one of enlargement and coalescence of voids, which are often associated with inclusions. During compaction, any impurities on the surface of a powder particle, will be broken up, but trapped, between adjacent particles which have been cold welded together. These inclusions then become prime sites for the dimpled type of mechanism to occur. Because pores act as stress concentrators, local shear stresses are high due to the relaxation of strict plane strain conditions on a micro-scale, which results in ductile dimple failure. Fatigue fractures, Figure 4.18d, e, and f, also showed this type of failure mechanism, with no evidence of striations. This is normally associated with high rates of fatigue crack growth. In the case of sintered materials

under cyclic loading, Franklin and Davies[97] demonstrated that where the pore radii are sufficiently small, cracks propagate rapidly through the ligaments between pores due to stress intensification. When the crack encounters a pore in which the effective notch is insufficiently sharp for crack initiation, it becomes 'pinned' at this point, but will pass through other pores on either side. The macrocrack length is now increased, and the displacement experienced by the remaining neck increases. The stress intensity reaches a critical value for cracking to occur, as in sharp pores, and then propagates rapidly through the neck. A mixed mode of striations associated with ductile dimples was observed by these workers. It may be that the fatigue process in a sintered steel is a series of fast fractures through necks between pores when the fatigue stress intensity is at a relatively high level, the macrocrack growth being retarded where it encounters a 'blunt' pore. The attainment of a critical stress intensity at such a pore causes fast fracture to occur through these necks also, resulting in an overall ductile dimpled fracture at all necks.

The research project was based on a commercially available alloy steel powder, processed in a variety of ways, broadly based on a typical industrial schedule. The fracture toughness and fatigue data compares with the small amount already published and can be understood from a scientific basis. The observed effects of pore geometry and interparticle characteristics encourage further research to seek ways of improving fracture toughness, perhaps by liquid phase and vacuum sintering. It is apparent from the work carried

out here that a wide variety of properties can be obtained from Distaloy SA. Whilst only a limited amount of data has been accrued, it serves as a guide for assessing the influence of a number of variables, and indicates that this material is still open to further investigation. The direct application of fracture mechanics as a design parameter in the P/M industry cannot be foreseen in the immediate future. However, it is becoming increasingly used throughout various branches of engineering, and future development may well justify design techniques, based upon fracture mechanics, being applied to sintered materials. In such an event, it is hoped that the information in this work may be usefully added to the pool of knowledge available at this present time.

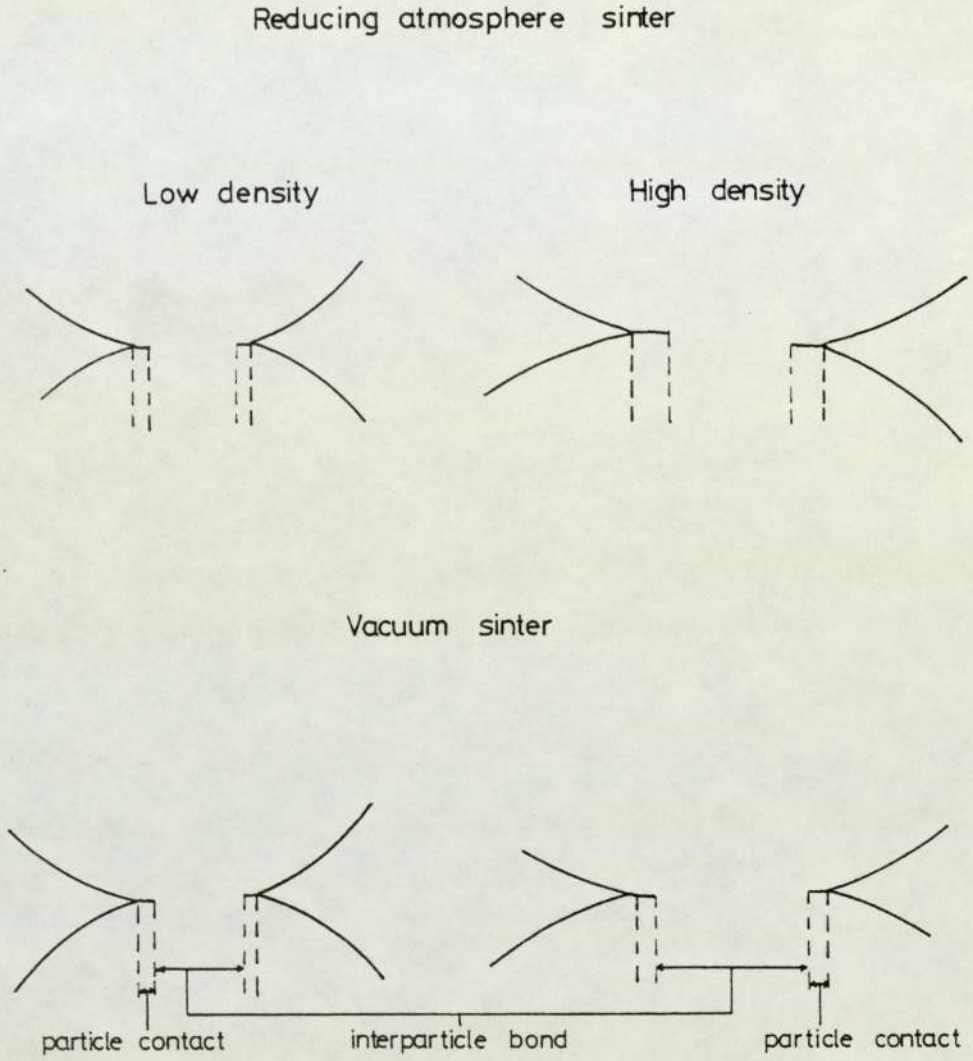

Figure 5.1 : Proposed regions of particle contact and inter-particle bonding

6. CONCLUSIONS

1. K_{IC} validity problems arise at sintered densities of 7.1 Mgm^{-3} and below when applying LEFM techniques to three point bend test pieces of section size 25 x 12mm . Reliable minimum fracture toughness values ($K_Q J$) were obtained by applying the J integral approach.
2. Compacts of densities ranging from 6.36-7.10 Mgm^{-3}, given a variety of sintering treatments, had fracture toughness values ranging from 14.5 to 32$MNm^{-3/2}$, which are of the same order as flake graphite cast iron.
3. For a given processing schedule, yield stress and fracture toughness were directly related to density.
4. With the exception of vacuum sintered samples of low density (6.4 Mgm^{-3}), the fracture toughness was directly related to yield stress, irrespective of processing schedule.
5. There was no evidence of differences in physico-chemical effects between laboratory and industrial reducing atmosphere sintering treatments. It appeared that the mechanical properties of a compact at a given density were determined by the sintering thermal cycle.
6. Sintering in vacuum significantly reduced the oxygen content of compacts and there was some evidence, from tensile properties, of enhanced interparticle bonding, but fracture toughness was only improved at the higher densities (7.0-7.1 Mgm^{-3}) .
7. The industrial sinter did not affect the oxygen content of test pieces, which remained at 0.35% . The laboratory sinter gave a reduction to 0.25% and the vacuum sinter a reduction to 0.22% .
8. Fracture toughness values from notched test pieces with a machined root radius of 0.1mm were, within experimental error,

the same as values from the fatigue pre-cracked test pieces.

9. Fatigue crack propagation data was of limited value, but indicated a trend of decreasing growth rate with increasing density. Heat treated test pieces had lower rates of crack growth than their as sintered counterparts.

7. RECOMMENDATIONS FOR FURTHER WORK

The evidence that vacuum sintering increases particle bonding needs further investigation to determine whether the particle contact area is increased, or if the improved properties result from better bonding. Special techniques, such as Auger electron microscopy, which allow determination of oxygen content, would need to be employed to study the particle interfaces, in conjunction with scanning electron microscopy. It may be possible to further this effect by using powders of extremely low oxygen content. Investigation of the mechanical properties of such sintered powders would therefore be of considerable interest. The cost of industrial sintering treatments is reducing with the introduction of new types of furnace, so studies related to 'low cost' sintered steels will become more relevent.

It would be of considerable interest to explore the effects of large differences in pore morphology within a material of known level of toughness, since it is apparent that the sharp corners of irregularly shaped pores control the toughness of the material under investigation. Hence, the methods of sealing these sharp corners, and the interparticle regions, should also be examined, possibly by combining liquid phase sintering or infiltration with vacuum sintering. The development of the new testing geometries for assessing fracture toughness would greatly simplify the overall testing procedure if they can be applied to sintered materials. Qualitative assessment of these techniques is needed, and if applicable, will make it possible to carry out in depth studies of effects such as distribution of pores and microconstituents on fracture toughness, as opposed to fracture toughness measurement being a task in itself.

Fatigue data should be obtained from studies set out for this

special purpose where adequate crack lengths are grown. As with fracture toughness, examination is required to determine the effects of pore morphology on crack growth rates, and studies on vacuum sintered materials would also be of great interest.

8. REFERENCES

1. BROWN, G.T. : Int.J. of Powder Metall., 1976, 12, 191-197

2. BARROW, D.A. : Int.J. of Powder Metall., 1980, 16, (3), 231-236

3. MATTY, M.T. : Powder Metall., 1978, 21, 93-103

4. HAYNES, R. : The Metallurgist and Materials Technologist, 1981, 13, (7), 355-360

5. WASTENSON, G. : Powder Metall., 1975, 18, 124-149

6. BARNBY, J.T., GHOSH, D.C. and DINSDALE, K. : Powder Metall., 1973, 16, 55-71

7. ANDREWS, G. : Ph.D. Thesis, University of Aston in Birmingham, May 1976

8. INGELSTROM, N. and NORDBERG, H. : Scandinavian J. of Metall., 1975, 4, 189-192

9. INGELSTROM, N. and USTIMENKO, V. : Powder Metall., 1975, 18, 303-322

10. TRUNICK, L. and QUEENEY, A. : Int.J. of Powder Metall., 1979, 15, (3), 245-251

11. BASTIAN, F.L. and CHARLES, J.A. : Powder Metall., 1979, 21, 199-208

12. GHOSH, D.C. : Ph.D. Thesis, University of Aston in Birmingham, Dec. 1976

13. DIXON, R.H.T. and CLAYTON, A. : "Powder Metallurgy for Engineers" Machinery Publishing Co. Ltd., Brighton. pub. 1971

14. BALSHIN, M.J. : Poroshkovoye metalloregyeniye. Metallurgizdat. Moscow 1948

15. RYSHKEWITCH, E. : J. Amer. Cer. Soc., 1953, 36, 65-68

16. DUCKWORTH, W. : J. Amer. Cer. Soc., 1953, 36, 68

17. PINES, B.Ya., SIRENKO, A.F. and SUCHININ, I.N. : Issledovaniya po zharoprotschnym splavam. Izdat. AK. Nauk UdSSR 1958

18. UDIER, M. : Powder Metall., 1962, No.9, 278-290

19. KNUDSEN, F.P. : J. Amer. Cer. Soc., 1959, 42, 376-387

20. McADAM, G.D. : Powder Metall., 1967, 10, 307-317

21. UDIER, M. : Second European Symposium on Powder Metallurgy. Stuttgart 1968, Vol.1.

22. POHL, D. : Second European Symposium on Powder Metallurgy. Stuttgart 1968, Vol.2.

23. GALLINA, V. and MANNONE, G. : Powder Metall., 1968, 11, 73-82

24. HAYNES, R. : Powder Metall., 1971, 14, 64-70

25. HAYNES, R. : Powder Metall., 1971, 14, 70-77

26. GESSINGER, G.H., METZLER, H., ESPER, F. and EXNER, H.E. : Powder Metall., 1971, Conference supplements to 14, 289-310

27. SQUIRE, A. : Trans. AIME, 1971, 171, 485

28. SALAK, A., MISKOVIK, V., DUDROVA, E. and RUDNAYOVA, E. : Powder Metall. Int., 1974, 6, 128-132

29. EXNER, H.E. and POHL, D. : Powder Metall. Int., 1978, 10, 193-196

30. NAKAMURA, N. and TSUYA, K. : Powder Metall., 1979, 22, (3), 101-108

31. GRIFFITHS, T.J., DAVIES, R. and BASSETT, M.B. : Powder Metall., 1979, 22, (3), 119-123

32. POHL, D. : Powder Metall. Int., 1969, 1, 26-28

33. McADAM, G.D. : JISI, 1951, 168, 346-358

34. LEHUP, E.R. and MOON, J.R. : Powder Metall., 1978, 21, (1), 1-6

35. KAPUTO, J.W. and PELS, A.R. : Int.J. of Powder Metall., 1967, 3, (2), 17-23

36. MORGAN, V.T. : Powder Metall., 1961, No.7, 44-65

37. MEYERSBERG, G. : Iron and Steel, 1944, 17, 243-247

38. THUM, A. and UDE, H. : Die Giesserei, 1929, 16, 501-515

39. THUM, A. : Die Giesserei, 1929, 16, 1164-1174

40. SCHWARTZ, H.A. and JUNGE, C.H. : Proc.A.S.T.M., 1941, 41, 816-824

41. GILBERT, G.N.J. : B.C.I.R.A. Journal of R.and D., 1957, 6, 546-587

42. GILBERT, G.N.J. : B.C.I.R.A. Journal of R.and D., 1959, 7, 745-789

43. HOGANAS A.B., Sweden : Data sheets 100-121

44. LINDSKOG, P. and THORNBLAD, O. : Powder Metall. Int., 1979, 11, (1), 10-11

45. TUNSTALL, J. and HAYNES, R. : Int.J. Powder Metall., 1980, 16, (1), 69-85

46. GRIFFITH, A.A. : Phil. Trans. Roy. Soc., 1920, 221, 163-198

47. IRWIN, G.R. : "Fracture dynamics" in Fracturing of Metals, ASM, Cleveland 1948

48. OROWAN, E. : Rep. Prog. Phys., 1949, 12, 185-232

49. IRWIN, G.R. : J.App. Mech., 1957, 24, 361-364

50. SNEDDON, I.N. : Proc. Roy. Soc. of London, 1946, 187, 229-260

51. WESTERGAARD, H.M. : J.App. Mech. 1939, 61, A49-A53

52. Standard Method for "Plane-Strain Fracture Toughness of Metallic Materials" ASTM E399-78a, American National Standards Institute

53. British Standard Methods of test for "Plane-strain fracture toughness (K_{IC}) of metallic materials" BS5447:1977, British Standards Institution

54. "Plain Strain Crack Toughness Testing of High Strength Metallic Materials" ASTM STP 410, Am.Soc. Testing Mats., Philadelphia, 1966

55. "Review of Developments in Plane Strain Fracture Toughness Testing" ASTM STP 463, Am.Soc. Testing Mats., Philadelphia, 1970

56. "Progress in Flaw Growth and Fracture Toughness Testing" ASTM STP 536, Am.Soc. Testing Mats., Philadelphia, 1973

57. "Developments in Fracture Mechanics Test Methods Standardisation" ASTM STP 632, Am.Soc. Testing Mats., Philadelphia, 1977

58. WILSON, W.K. : ASTM STP 410, Am.Soc. Testing Mats., 1966,75-76

59. KAUFMANN, J.G. : ASTM STP 632, Am.Soc. Testing Mats., 1977

60. EFTIS, J. and LIEBOWITZ, H. : Eng. Fracture Mech., 1975, 7, 101-135

61. RICE, J.R. : J.Appl. Mech., 1968, (June), 379-386

62. RICE, J.R. and ROSENGREN, G.F. : J.Mech. Phys. Solids, 1968, 16, 1-12

63. HUTCHINSON, J.W. : J.Mech. Phys. Solids, 1968, 16, 13-31

64. Mc.CLINTOCK, F. : "Fracture, An Advanced Treatise" Volume 3, Academic Press, New York, 1971, Chapter 2

65. BEGLEY, J.A. and LANDES, J.D. : ASTM STP 514, Am.Soc. Testing Mats., 1972, 1-20

66. LANDES, J.D. and BEGLEY, J.A. : ibid(65), 24-40

67. BUCCI, R.J., PARIS, P.C., LANDES, J.D. and RICE, J.R. : ibid(65) 40-69

68. RICE, J.R., PARIS, P.C. and MERKLE, J.G. : ASTM STP 536, Am.Soc. Testing Mats., 1973, 231-245

69. SUMPTER, J.D.G. and TURNER, C.E. : ASTM STP 601, Am.Soc. Testing Mats., 1976, 3-18

70. LANDES, J.D. and BEGLEY, J.A. : ASTM STP 632, Am.Soc. Testing Mats., 1977, 57-81

71. TURNER, C.E. : J.of Strain Analysis, 10, (4), 207-216

72. PRIEST, A.H. : ibid(71), 225-232

73. CHELL, C.G. : "Developments in Fracture Mechanics-1" Applied Science Publishers Ltd., 1979, 67-105

74. ASTM Task Group E24.01.09, Proc.ASTM, Amer.Soc. Testing Mats., 1977, 77, 451

75. ASTM Task Group E24.01.09, "The determination of the Elastic-Plastic Fracture Toughness J_{IC}", 1979

76. SCARLIN, R.B. and SHAKESHAFT, M. : Metals Technology, 1981, (Jan), 1-9

77. GLOVER, A. and POLLARD, G. : ISI Publication 120 "Fracture toughness of high strength materials-Theory and Practice" 90-94

78. EWING, J.A. and HUMPHREY, J.W.C. : Phil. Trans. Roy. Soc., 1903, 200, 241-250

79. FORSYTH, P.J.E. : "The Physical Basis of Metal Fatigue" pub. Blackie and Sons Ltd., 1969

80. LAIRD, C. : ASTM STP 415, Am.Soc. Testing Mats., 1967, 131-169

81. FORSYTH, P.J.E., STUBBING, C. and CLARK, D. : J.Inst. Metals, 1961, 90, 238-239

82. CARTWRIGHT, D.J. : "Developments in Fracture Mechanics-1" Applied Science Publishers Ltd., 1979, 29-66

83. BROWN, W.F. and SCRAWLEY, J.E. : ASTM STP 381, Am.Soc. Testing Mats., 1965, 133-198

84. PARIS, P.C. and SIH, G.C. : ibid(83), 30-83

85. FROST, N.E., POOK, L.P. and DENTON, K. : Eng. Fract. Mech. 1971, 3, 109-126

86. PARIS, P.C. and ERDOGAN, F. : Trans. ASME, 1963, 85, 528-534

87. Mc.CLINTOCK, F.A. : 'Fracture of Solids' AIMME, Interscience, New York, 1963, 65

88. IRVING, P.E. and McCARTNEY, L.N. : Metal Science, 1977, (Aug/Sept), 351-361

89. FORMAN, R., KEARNEY, V. and ENGLE, R. : Trans ASME, 1967, 89, 459-464

90. PEARSON, S. : Royal Aircraft Establishment Technical Report 68297, 1968, (Dec).

91. MADDOX, S.J. : Int.J. of Fract., 1975, 11, (3), 389

92. GOETZEL, C.G. and SEELIG, R.P. : Proc. ASTM, 1940, 40, 746-761

93. RADOMYSEL'SKII, I.D., GRYAZNOR, B.A. and SEMASHKO, V.G. : Sov. Powder Metall. and Met. Ceram., 1968, 64, 313-316

94. WHEATLEY, J.M. and SMITH, C.G. : Powder Metall., 1963, No.12, 141-158

95. HAYNES, R. : Powder Metall., 1970, 13, 465-510

96. WILLIAMS, S.H. and HAYNES, R. : Powder Metall., 1973, 16, 387-404

97. FRANKLIN, P. and DAVIES, B.L. : Powder Metall., 1978, 21, (1), 7-12

98. RODZINAK, D. and SLESAR, M. : Powder Metall. Int., 1980, 12, (3), 127-130

99. KRAVIC, A.F. and PASQUINE, D.L. : Int.J. Powder Metall., 1969, 5, 45-55

100. BANKOWSKI, R.S. and FIELBACH, W.H. : Int.J. Powder Metall., 1970 6, 23-37

101. WARD, M. : Ph.D. Thesis, University of Aston in Birmingham, April, 1977

102. British Standards Institution Draft for Development Methods for Plane strain fracture toughness (K_{IC}) testing of metallic materials, DD3

103. British Standard Specification for Powder Metallurgical Products (P.M. Products) BS 2590 : Part 1 : 1969, British Standards Institution

104. WOOLMAN, J. and MOTTRAM, R.A. : "The Mechanical Properties of British Standard En Steels" Volume 2, Pergamon Press, 1966 340-365

105. MAY, M.J. : ASTM STP 463, Am.Soc. Testing Mats., 1970, 42-62

106. BROWN, W.F. and SRAWLEY, J.E. ibid (105), 216-248

107. KAUFMAN, J.G. and SCHILLING, P.E. : ASTM STP 536, Am.Soc. Testing Mats., 1973, 312-319

108. TETELMAN, A.S., WILSHAW, T.R. and RAU, C.A. : Int.J. Fracture Mechs., 1968, 4, 147-158

109. LINDSKOG, P. : Powder Metall. 1973, 16, 374-386

110. BORLAND, W., EVANS, J.P., MARDON, P.G., SUTCLIFFE, P.W., and WALDRON, M.B. : Powder Metall., 1980, 23, (3), 145-152

111. RITCHIE, R.O., SERVER, W.L. and WULLAERT, R.A. : Int.J. of Fracture, 1978, 14, R329-R335

112. BARKER, L.M. : ASTM STP 678, Am.Soc. Testing Mats., 1979, 73-82

113. POOK, L.P. : J. of Strain Analysis, 1975, 10, (4), 242-250